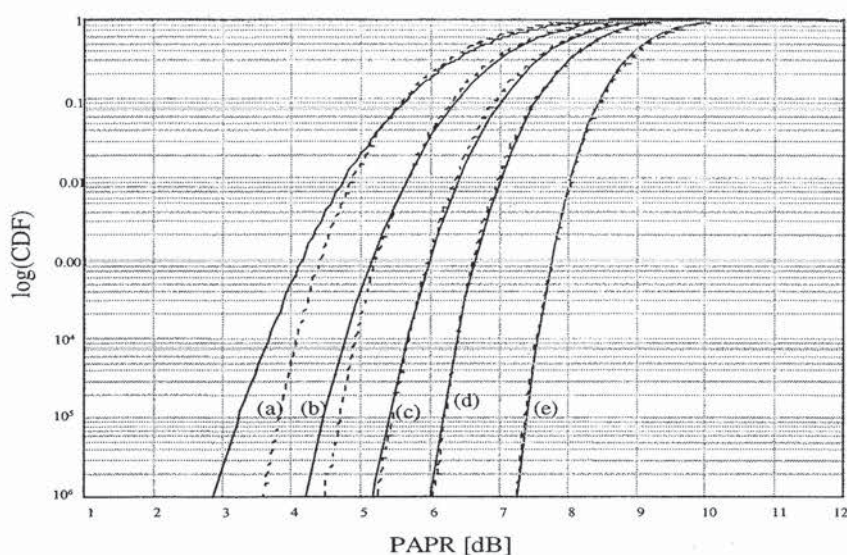


reasonable error correcting properties. Section 6.5 describes a solution to this problem.

A different approach to the PAP problem is to use the fact that because large PAP ratios occur only infrequently, it is possible to remove these peaks at the cost of a slight amount of self-interference. Now, the challenge is to keep the spectral pollution of this self-interference as small as possible. Clipping is one example of a PAP reduction technique creating self interference. In the next sections, two other techniques are described which have better spectral properties than clipping.



**Figure 6.4** Cumulative distribution function of the PAPR for a number of subcarriers of (a) 32, (b) 64, (c) 128, (d) 256, and (e) 1,024. Solid lines are calculated; dotted lines are simulated.

### 6.3 CLIPPING AND PEAK WINDOWING

The simplest way to reduce the PAP ratio is to clip the signal, such that the peak amplitude becomes limited to some desired maximum level. Although clipping is definitely the simplest solution, there are a few problems associated with it. First, by distorting the OFDM signal amplitude, a kind of self-interference is introduced that degrades the BER. Second, the nonlinear distortion of the OFDM signal significantly increases the level of the out-of-band radiation. The latter effect can be understood easily by viewing the clipping operation as a multiplication of the OFDM signal by a rectangular window function that is 1 if the OFDM amplitude is below a threshold and smaller than 1 if the amplitude needs to be clipped. The spectrum of the clipped OFDM signal is found as the input OFDM spectrum convolved with the spectrum of the window function. The out-of-band spectral properties are mainly determined by the

wider spectrum of the two, which is the spectrum of the rectangular window function. This spectrum has a very slow rolloff that is inversely proportional to the frequency.

To remedy the out-of-band problem of clipping, a different approach is to multiply large signal peaks with a certain nonrectangular window. In [1], a Gaussian shaped window is proposed for this, but in fact any window can be used, provided it has good spectral properties. To minimize the out-of-band interference, ideally the window should be as narrowband as possible. On the other hand, the window should not be too long in the time domain, because that implies that many signal samples are affected, which increases the BER. Examples of suitable window functions are the cosine, Kaiser, and Hamming windows. Figure 6.5 gives an example of reducing the large peaks in OFDM with the use of windowing.

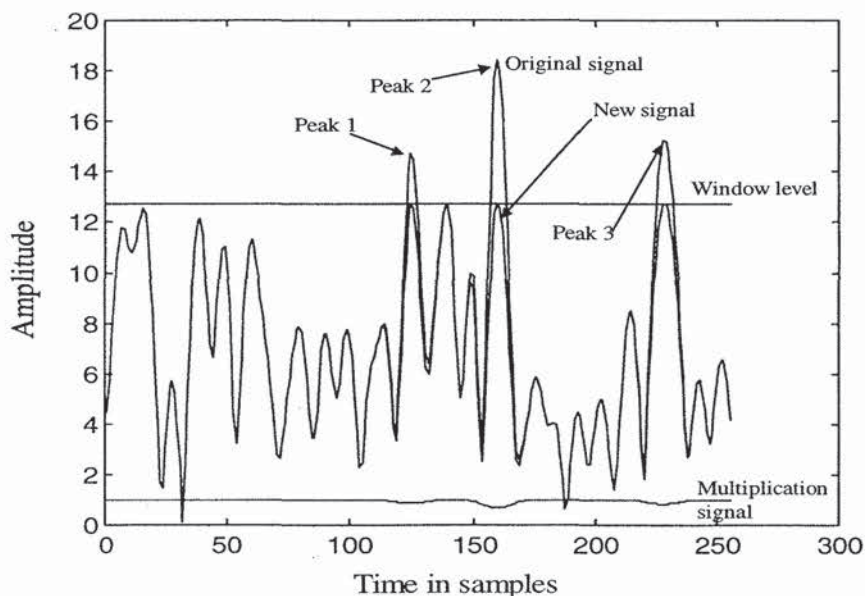


**Figure 6.5** Windowing an OFDM time signal.

In Figure 6.6, the difference between clipping the signal and windowing the signal can be seen. Figure 6.7 shows how the spectral distortion can be decreased by increasing the window width.

Figure 6.8 shows PER curves with and without clipping, using a rate 1/2 convolutional code with constraint length 7. The simulated OFDM signal used 48 subcarriers with 16-QAM. The plots demonstrate that nonlinear distortion only has a minor effect on the PER; the loss in SNR is about 0.25 dB when the PAP ratio is decreased to 6 dB. When peak windowing is applied, the results are slightly worse; see Figure 6.9. This is caused by the fact that peak windowing distorts a larger part of the signal than clipping for the same PAP ratio.

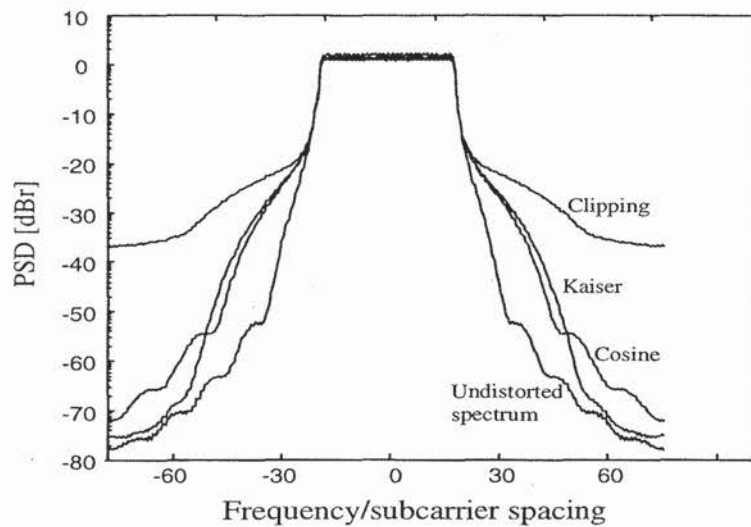


**Figure 6.6** Frequency spectrum of an OFDM signal with 32 subcarriers with clipping and peak windowing at a threshold level of 3 dB above the rms amplitude.

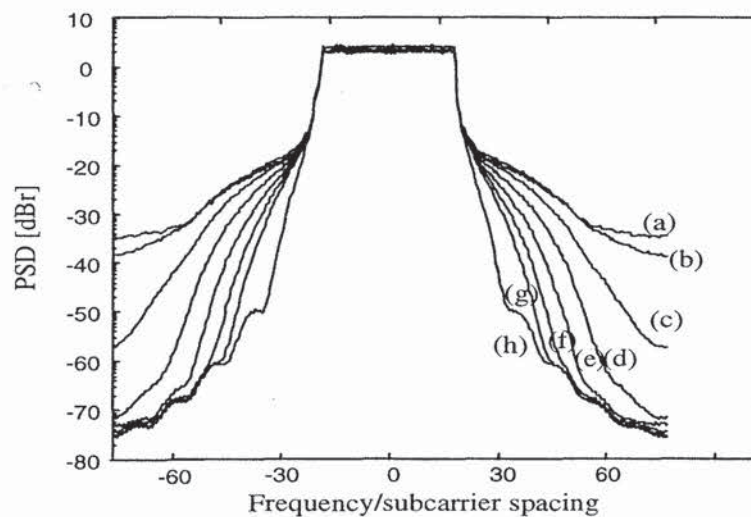


**Figure 6.7** Frequency spectrum of an OFDM signal with 32 subcarriers with peak windowing at a threshold level of 3 dB above the rms amplitude. Symbol length is 128 samples (4 times oversampled) and window length is (a) 3, (b) 5, (c) 7, (d) 9, (e) 11, (f) 13, and (g) 15 samples. Curve (h) is the ideal OFDM spectrum.

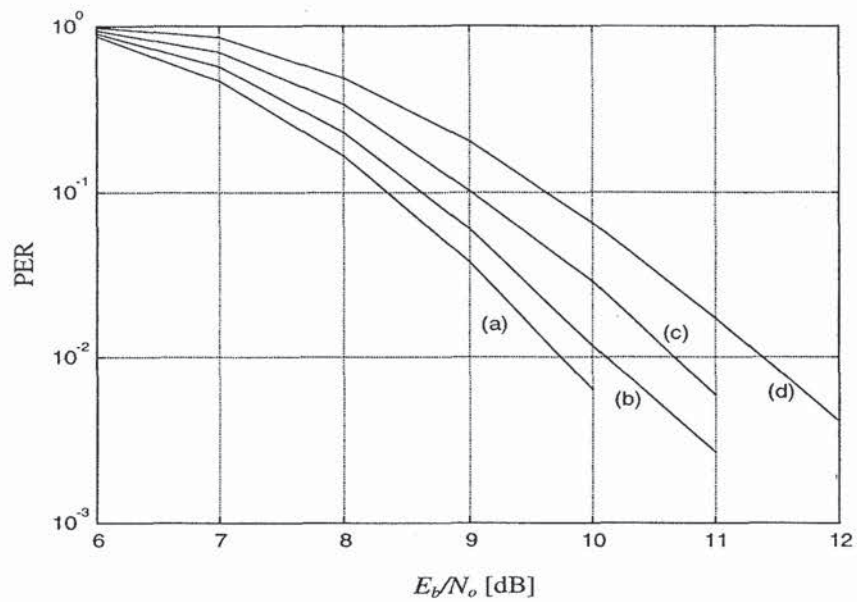


**Figure 6.8** Packet error ratio versus  $E_b/N_o$  for 64 byte packets in AWGN. OFDM signal is clipped to a PAP ratio of (a) 16 (= no distortion), (b) 6, (c) 5, and (d) 4 dB.

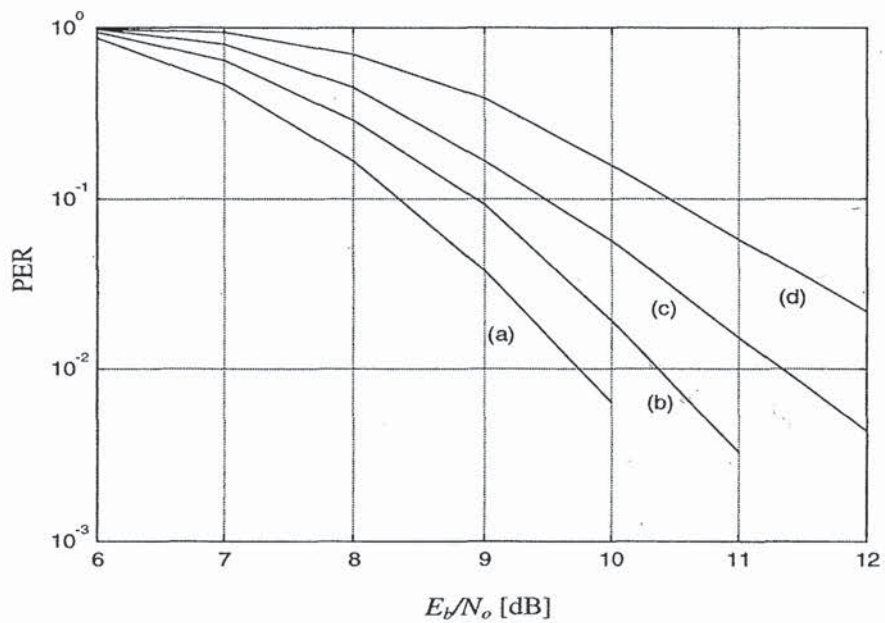


**Figure 6.9** PER versus  $E_b/N_o$  for 64-byte packets in AWGN. Peak windowing is applied with a window width of 1/16 of the FFT duration. The PAP ratio is reduced to (a) 16 (= no distortion), (b) 6, (c) 5, and (d) 4 dB.

### 6.3.1 Required Backoff with a Non-Ideal Power Amplifier

The previous section demonstrated that peak windowing is very effective in reducing the PAP ratio. This does not immediately tell us, however, what backoff is required for a practical power amplifier to attain an acceptable level of out-of-band radiation. The backoff is defined here as the ratio of the output power and the maximum output power (saturation power) with a sinusoidal input signal. Another definition that is frequently used in the literature uses the power at the 1-dB compression point instead of the saturation power. Because the 1-dB compression point is typically 1 to 3 dB lower than the maximum power level, depending on the amplifier transfer function, the backoff values according to the latter definition are 1 to 3 dB smaller than the values mentioned in this section.

To simulate a power amplifier, the following model is used for the AM/AM conversion [2]:

$$g(A) = \frac{A}{(1 + A^{2p})^{\frac{1}{2p}}} \quad (6.5)$$

The AM/PM conversion of a solid-state power amplifier is small enough to be neglected. Figure 6.10 gives some examples of the transfer function for various values of  $p$ . A good approximation of existing amplifiers is obtained by choosing  $p$  in the range of 2 to 3 [2]. For large values of  $p$ , the model converges to a clipping amplifier that is perfectly linear until it reaches its maximum output level.

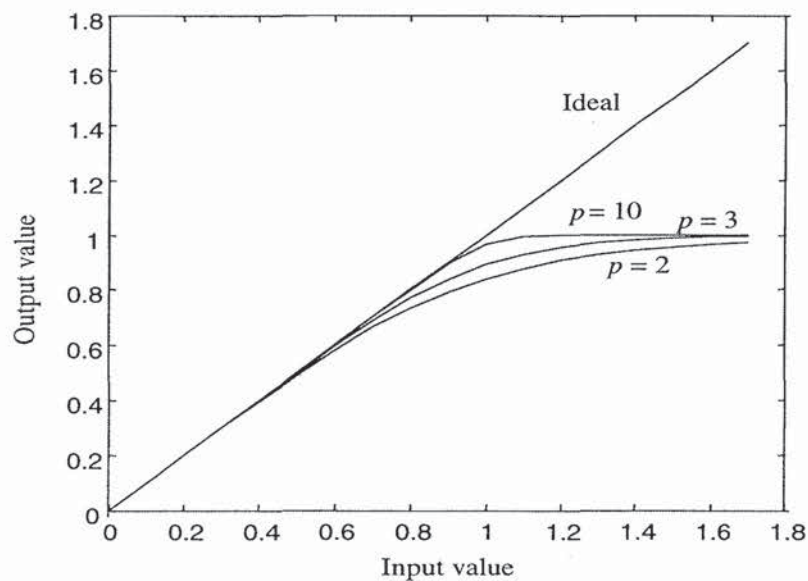
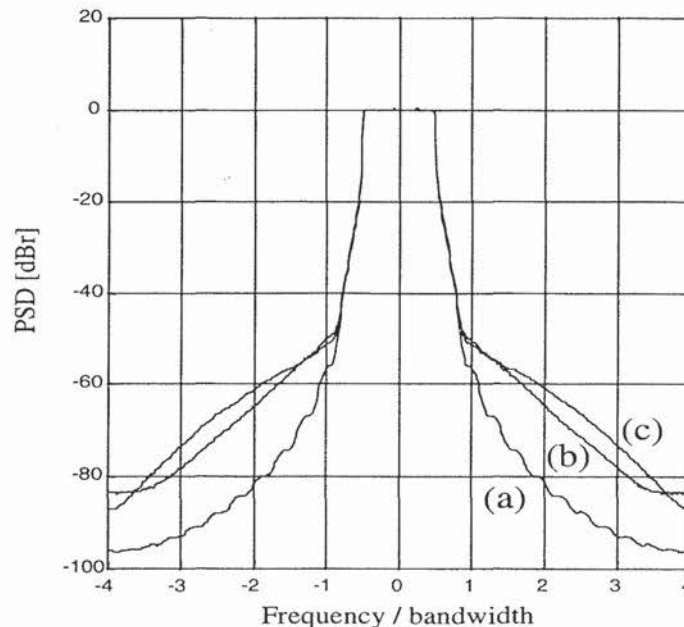


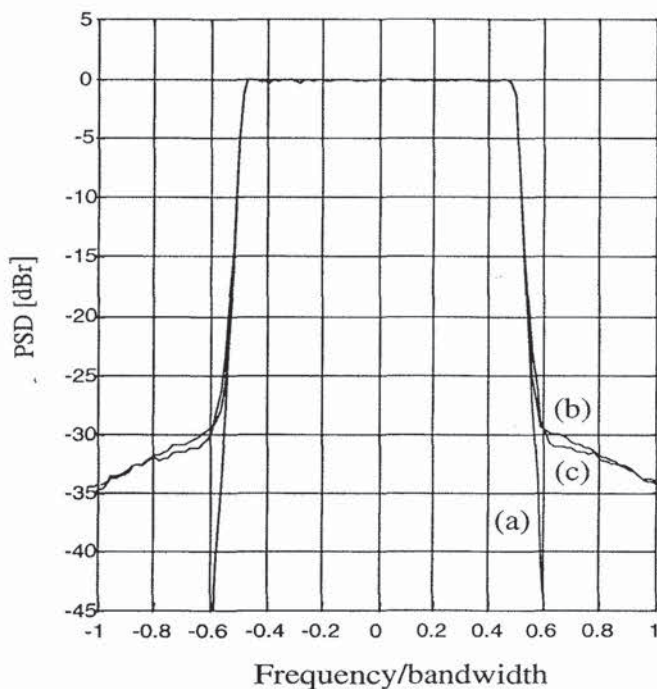
Figure 6.10 Rapp's model of AM/AM conversion.

Figure 6.11 shows the output spectra of an undistorted OFDM signal and the spectra of two distorted signals, assuming a highly linear amplifier model ( $p = 10$  in (6.5)). The backoff relative to the maximum output power was determined such that any significant distortion of the spectrum is at least 50 dB below the in-band spectral density. In this case, peak windowing gives a gain of almost 3 dB in the required backoff relative to clipping. This difference in backoff is much less than the difference in PAP ratio at the input of the power amplifier; without peak windowing, the PAP ratio is about 18 dB for the OFDM signal with 64 subcarriers. With peak windowing, this PAP ratio is reduced to approximately 5 dB. Hence, for the latter case, it is clear that the backoff of a highly linear amplifier must be slightly above this 5 dB to achieve a minimal spectral distortion. It is not true, however, that without peak windowing, the backoff must be in the order of 18 dB for the same amount of distortion as with peak windowing. The reason is that there is little energy in the signal parts that have a relatively large PAP ratio, so it does not affect the spectrum that much if those parts are distorted. After peak windowing or any other PAP reduction technique, however, a significant part of the signal samples are close to the maximum PAP ratio (e.g., 5 dB); in this case, any distortion of samples that is a dB or so below this maximum produces more spectral distortion than clipping the original OFDM signal at 10 dB below its maximum PAP level, simply because for the latter, a much smaller fraction of the signal is affected. Thus, the lower the PAP ratio is made by PAP-reduction techniques, the less tolerant the signal becomes against nonlinearities in the area of its maximum PAP ratio.



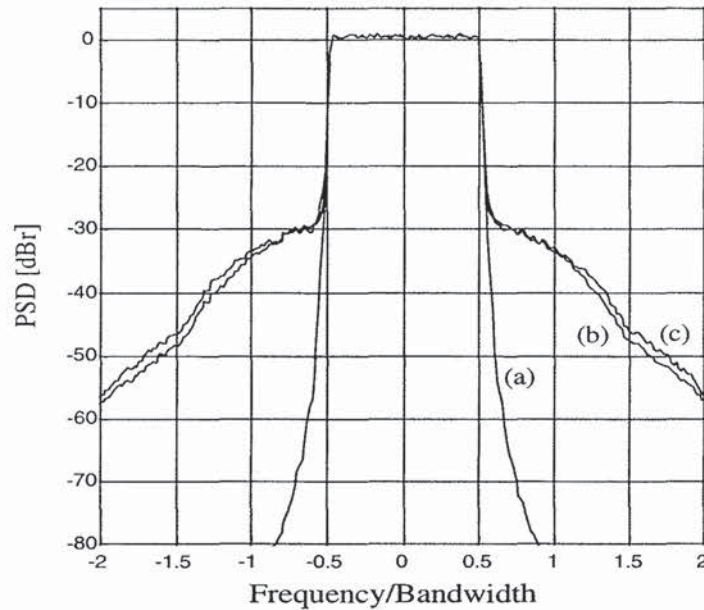
**Figure 6.11** (a) Ideal OFDM spectrum for 64 subcarriers, (b) spectrum after highly linear amplifier (Rapp's parameter  $p = 10$ ) with 8.7-dB backoff, (c) spectrum using peak windowing with 5.9-dB backoff.

Figure 6.12 shows OFDM spectra for a more realistic amplifier model with  $p = 3$ . The target for undesired spectrum distortion has now been set to a less stringent level of 30 dB below the in-band density. The difference in backoff with and without peak windowing is now reduced to 1 dB. This demonstrates that the more spectral pollution can be tolerated, the less gain can be achieved with PAP reduction techniques.



**Figure 6.12** (a) Ideal OFDM spectrum for 64 subcarriers, (b) plain OFDM with 6.3-dB backoff and Rapp's parameter  $p = 3$ , (c) peak windowing with 5.3-dB backoff.

Figure 6.13 shows similar plots as Figure 6.12, but now for 256 subcarriers. This demonstrates that the required backoff with or without peak windowing is almost independent from the number of subcarriers, as long as this number is large compared with 1. In fact, the difference in backoff with and without peak windowing reduced slightly to 0.8 dB by going from 64 to 256 subcarriers.



**Figure 6.13** (a) Ideal OFDM spectrum for 256 subcarriers, (b) plain OFDM with 6.3-dB backoff and Rapp's parameter  $p = 3$ , and (c) peak windowing with 5.5-dB backoff.

### 6.3.2 Coding and Scrambling

A disadvantage of distortion techniques is that symbols with a large PAP ratio suffer more degradation, so they are more vulnerable to errors. To reduce this effect, forward-error correction coding can be applied across several OFDM symbols. By doing so, errors caused by symbols with a large degradation can be corrected by the surrounding symbols. In a coded OFDM system, the error probability is no longer dependent on the power of individual symbols, but rather on the power of a number of consecutive symbols. As an example, assume that the forward-error correction code produces an error if more than 4 out of every 10 symbols have a PAP ratio exceeding 10 dB<sup>1</sup>. Further, assume that the probability of a PAP ratio larger than 10 dB is  $10^{-3}$ . Then, the error probability of the peak cancellation technique is  $1 - \sum_{i=0}^3 \binom{10}{i} (10^{-3})^i (1 - 10^{-3})^{10-i} \cong 2 \cdot 10^{-10}$ , which is much less than the  $10^{-3}$  in case no forward-error correction coding is used.

Although such a low symbol error probability may be good enough for real-time circuit-switched traffic, such as voice, it may still cause problems for packet data. A packet with too many large PAP ratio symbols will have a large probability of error. Such packets occur only very infrequently, as shown above, but when they occur, they

<sup>1</sup> The simplifying assumption is made here that 4 symbols with reduced power always result in an error, while in reality there is always a certain error probability  $< 1$ , depending on the SNR.



may never come through, because every retransmission of the packet has the same large error probability. To solve this problem, standard scrambling techniques can be used to ensure that the transmitted data between initial transmission and retransmissions are uncorrelated. To achieve this, the scrambler has to use a different seed for every transmission, which can be realized for instance by simply adding one to the seed after every transmission. Further, the length of the scrambling sequence has to be in the order of the number of bits per OFDM symbol to guarantee uncorrelated PAP ratios for different seeds. Different scrambling in every transmission will then guarantee independent PAP ratios for the OFDM symbols in retransmissions and hence, independent error probabilities. For example, if the probability of a worst case packet is  $10^{-6}$ , the probability that it does not come through within two transmissions is  $10^{-12}$ .

#### 6.4 PEAK CANCELLATION

The key element of all distortion techniques is to reduce the amplitude of samples whose power exceeds a certain threshold. In the case of clipping and peak windowing, this was done by a nonlinear distortion of the OFDM signal, which resulted in a certain amount of out-of-band radiation. This undesirable effect can be avoided by doing a linear peak cancellation technique, whereby a time-shifted and scaled reference function is subtracted from the signal, such that each subtracted reference function reduces the peak power of at least one signal sample. By selecting an appropriate reference function with approximately the same bandwidth as the transmitted signal, it can be assured that the peak power reduction does not cause any out-of-band interference. One example of a suitable reference signal is a *sinc function*. A disadvantage of a sinc function is that it has an infinite support. Hence, for practical use, it has to be time-limited in some way. One way to do this without creating unnecessary out-of-band interference is multiplication by a windowing function; for instance, a raised cosine window. Figure 6.14 shows an example of a reference function, obtained by multiplication of a sinc function and a raised cosine window. If the windowing function is the same as used for windowing of the OFDM symbols, then it is assured that the reference function has the same bandwidth as the regular OFDM signals. Hence, peak cancellation will not degrade the out-of-band spectrum properties. By making the reference signal window narrower, a tradeoff can be made between less complexity of the peak cancellation calculations and some increase of the out-of-band power. The peak cancellation method was first published in [3], while later it was independently described in [4].

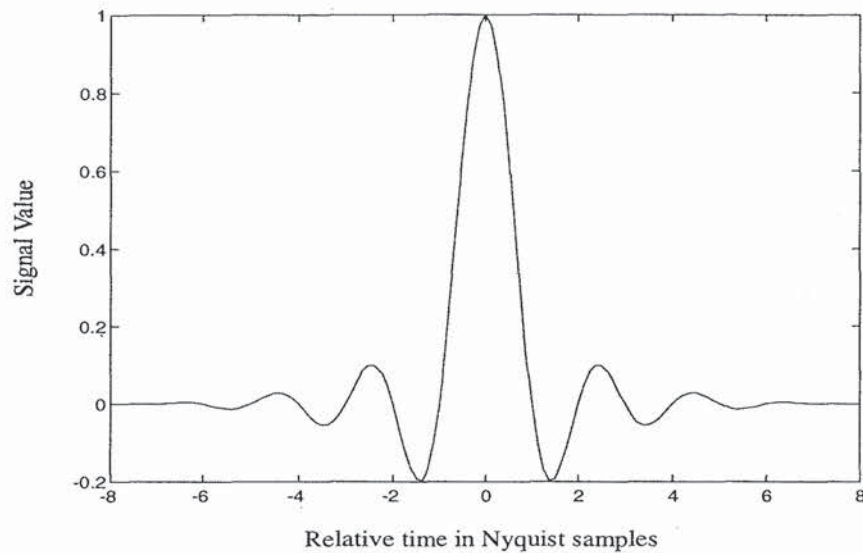


**Figure 6.14** Sinc reference function, windowed with a raised cosine window.

Peak cancellation can be done digitally after generation of the digital OFDM symbols. It involves a peak power (or peak amplitude) detector, a comparator to see if the peak power exceeds some threshold, and a scaling of the peak and surrounding samples. Figure 6.15 shows the block diagram of an OFDM transmitter with peak cancellation. Incoming data are first coded and converted from a serial bit stream to blocks of  $N$  complex signal samples. On each of these blocks, an IFFT is performed. Then, a cyclic prefix is added, extending the symbol size to  $N + N_G$  samples. After parallel-to-serial conversion, the peak cancellation procedure is applied to reduce the PAP ratio. It is also possible to do peak cancellation immediately after the IFFT and before the cyclic prefix and windowing. Except for the peak cancellation block, there is further no difference with a standard OFDM transmitter. For the receiver, there is no difference at all, so any standard OFDM receiver can be used.

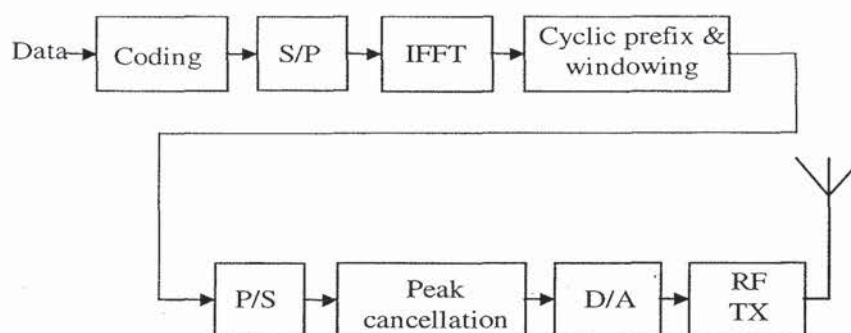


Figure 6.15 OFDM transmitter with peak cancellation.

In the previous figures, the peak cancellation was done after parallel-to-serial conversion of the signal. It is also possible to do the cancellation immediately after the IFFT, as depicted in Figure 6.16. In this case, the cancellation is done on a symbol-by-symbol basis. An efficient way to generate the cancellation signal without using a stored reference function is to use a lowpass filter in the frequency domain. In Figure 6.16, for each OFDM symbol, it is detected which samples exceed some predefined amplitude. Then, for each signal peak, an impulse is generated whose phase is equal to the peak phase and whose amplitude is equal to the peak amplitude minus the desired maximum amplitude. The impulses are then lowpass filtered on a symbol-by-symbol basis. Lowpass filtering is achieved in the frequency domain by taking the FFT, setting all outputs to zero whose frequencies exceed the frequency of the highest subcarrier, and then transforming the signal back by an IFFT.

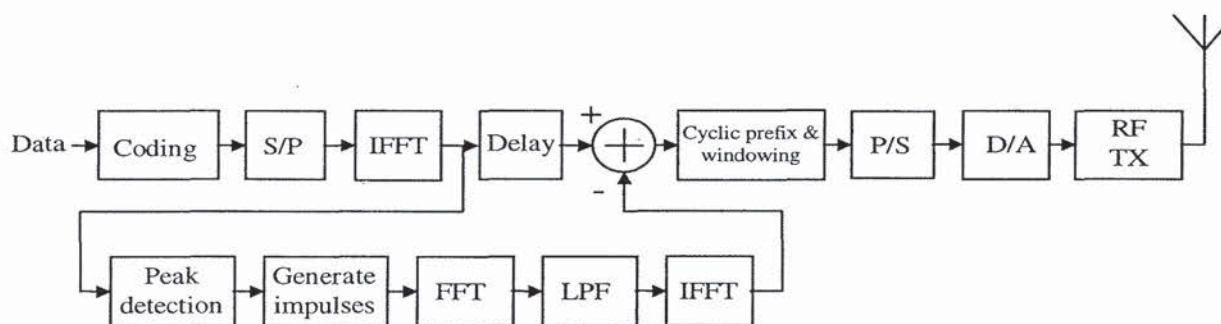
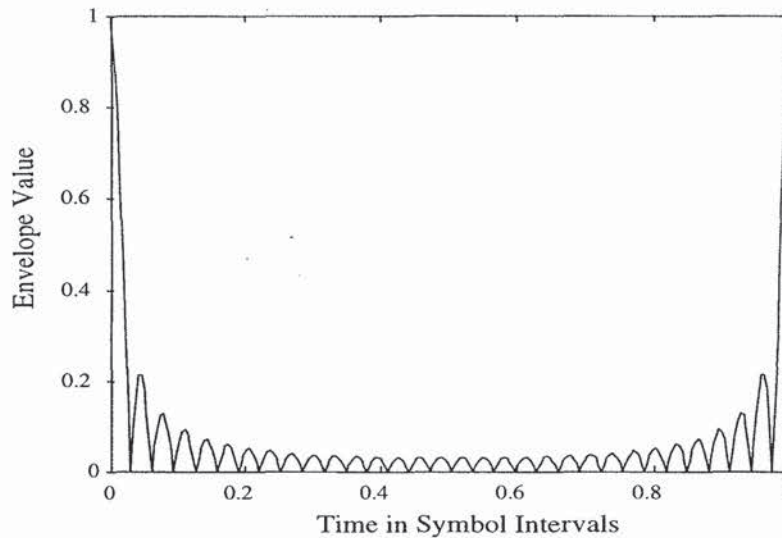


Figure 6.16 Peak Cancellation using FFT/IFFT to generate cancellation signal.

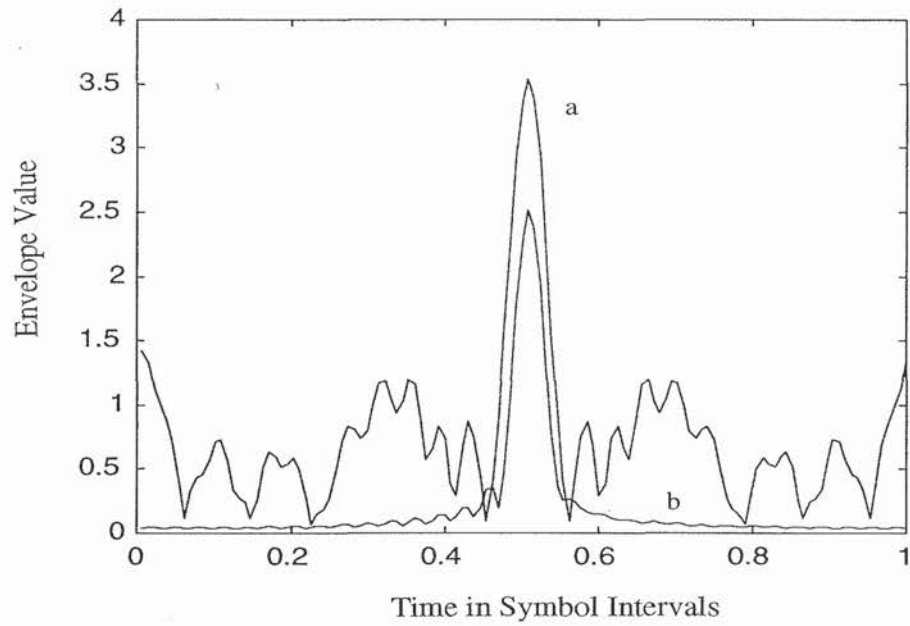
Figure 6.17 shows an example of the cyclic reference function that is used in all methods that apply cancellation *before* adding the cyclic prefix and windowing. In fact, this reference signal itself is a valid OFDM signal, which is obtained in the case of an all-ones input to the IFFT.



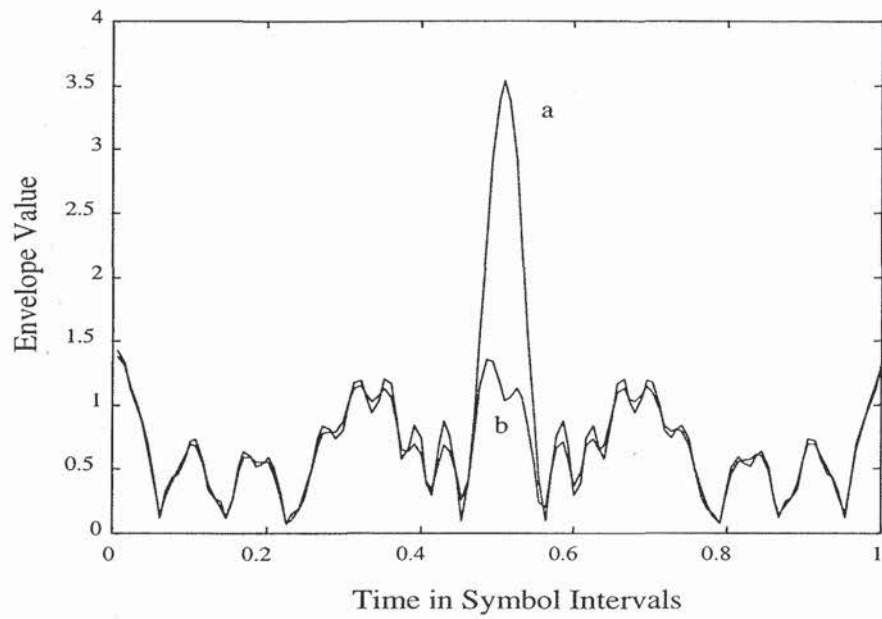
**Figure 6.17** Envelope of cyclic reference function.

Figure 6.18 shows an example of the signal envelopes of one arbitrary OFDM symbol and the corresponding cancellation signal. In this particular case, the cancellation signal actually consists of two separate sinc functions, because one sinc function is not wide enough to reduce the peak in this example. After subtraction, the peak amplitude is reduced to a maximum of 3 dB above the rms value; see Figure 6.19.

As an example of the peak cancellation technique, Figure 6.20 shows simulated power spectral densities for an OFDM system with 32 carriers. Without clipping or peak cancellation, the worst case PAP ratio of this system is 15 dB, and the undistorted spectrum is depicted by curve (a). If the signal is clipped such that the PAP ratio reduces to 4 dB, a significant spectral distortion is visible; see curve (c). When peak cancellation is applied (b), a negligible distortion is present for the same PAP ratio of 4 dB.



**Figure 6.18** (a) OFDM symbol envelope, (b) cancellation signal envelope.



**Figure 6.19** (a) OFDM symbol envelope, (b) signal envelope after peak cancellation.

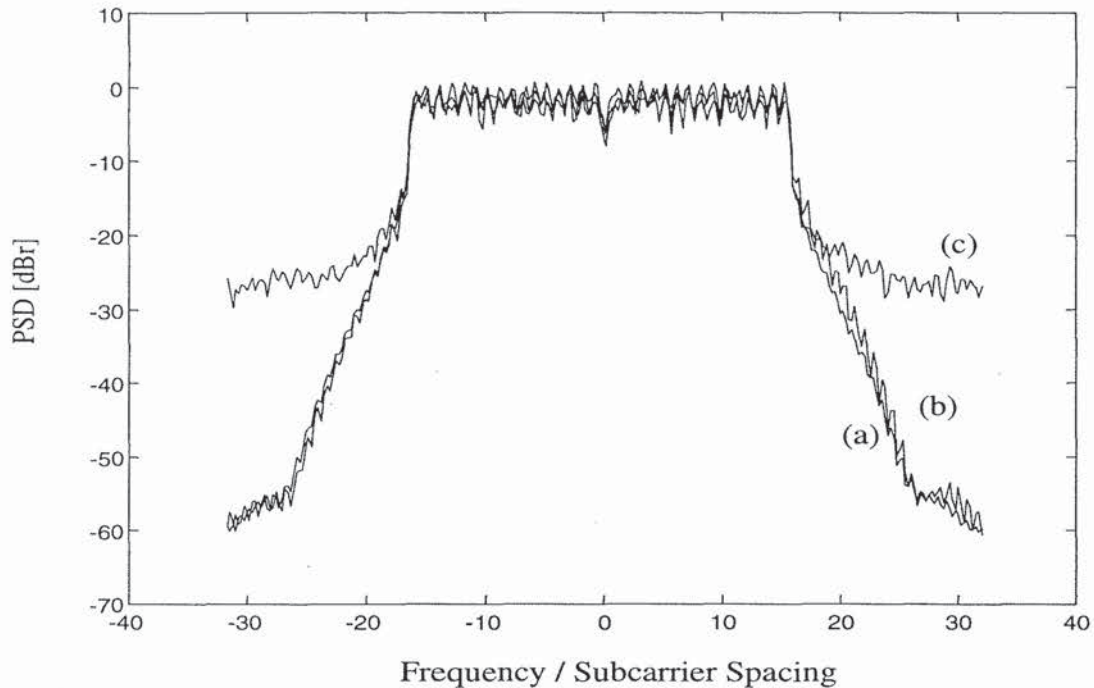


**Figure 6.20** Power spectral density for (a) undistorted spectrum with 32 subcarriers, PAP = 15dB, (b) spectrum after peak cancellation to PAP = 4 dB, and (c) clipping to PAP = 4 dB. Reference cancellation function has a length equal to  $\frac{1}{4}$  of the length of an OFDM symbol.

The effect of the peak cancellation on the PER is depicted in Figure 6.21. A rate  $\frac{1}{2}$ , constraint length 7 convolutional code is used to encode the input bits. The coded bits are then modulated onto 48 OFDM subcarriers using 16-QAM. The curves show an SNR degradation of about 0.6 dB in AWGN when peak cancellation is used to reduce the PAP ratio to 6 dB.

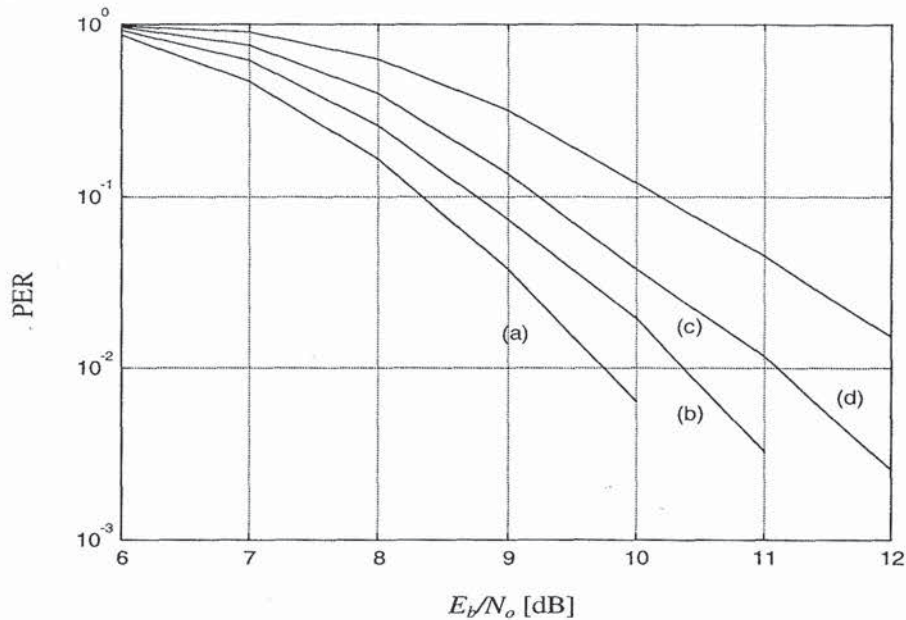


**Figure 6.21** PER versus  $E_b/N_0$  for 64-byte packets in AWGN. Peak cancellation is applied to reduce the PAP ratio to (a) 16 (= no distortion), (b) 6, (c) 5, and (d) 4 dB.

At first sight, peak cancellation seems to be a fundamentally different approach than clipping or peak windowing. It can be shown, however, that peak cancellation is in fact almost identical to clipping followed by filtering. If a sampled OFDM signal  $x(n)$  is clipped to reduce the PAP ratio, the output signal  $r(n)$  can be written as

$$r(n) = x(n) - \sum_i a_i e^{j\varphi_i} \delta(n - \tau_i) \quad (6.6)$$

Here,  $a_i$ ,  $\varphi_i$ , and  $\tau_i$  are the amplitude, phase, and delay of the correction that is applied to the  $i$ th sample in order to reach the desired clipping level. Hence, it is possible to describe clipping as a linear process, even though this is not the way clipping is performed in practice. Now suppose the clipped signal is filtered by an ideal lowpass filter with an impulse response of  $\text{sinc}(\pi nT)$ , where  $T$  is chosen such that the filter bandwidth is equal or larger than the bandwidth of the OFDM signal. The filtered output is given by

$$r'(n) = x'(n) - \sum_i a_i e^{j\varphi_i} \text{sinc}(\pi T(n - \tau_i)) \quad (6.7)$$

This expression is identical to a peak cancellation operation, with the only exception that with peak cancellation, a sum of sinc functions is subtracted from the unfiltered OFDM signal  $x(n)$ , while in (6.7) we see a filtered signal  $x'(n)$ . In practice, however, also for peak cancellation, the OFDM signal needs to be filtered anyway to

remove aliasing after the digital-to-analog conversion. Hence, for practical purposes, it may be concluded that peak cancellation has the same effect as clipping followed by filtering, which was proposed as a PAP reduction technique in [5].

As a final comparison of the three described signal distortion techniques, Figure 6.22 shows the PERs for an OFDM system with 48 subcarriers for which the PAP ratio is reduced to 5 dB. In addition to the three PAP reduction techniques, the nonlinear amplifier model described in section 6.3.1 was applied such that the output backoff of the transmitted OFDM signal was 6 dB. We can see from the figure that clipping (without filtering) performs slightly better than peak cancellation, and that peak windowing is slightly worse than peak cancellation.

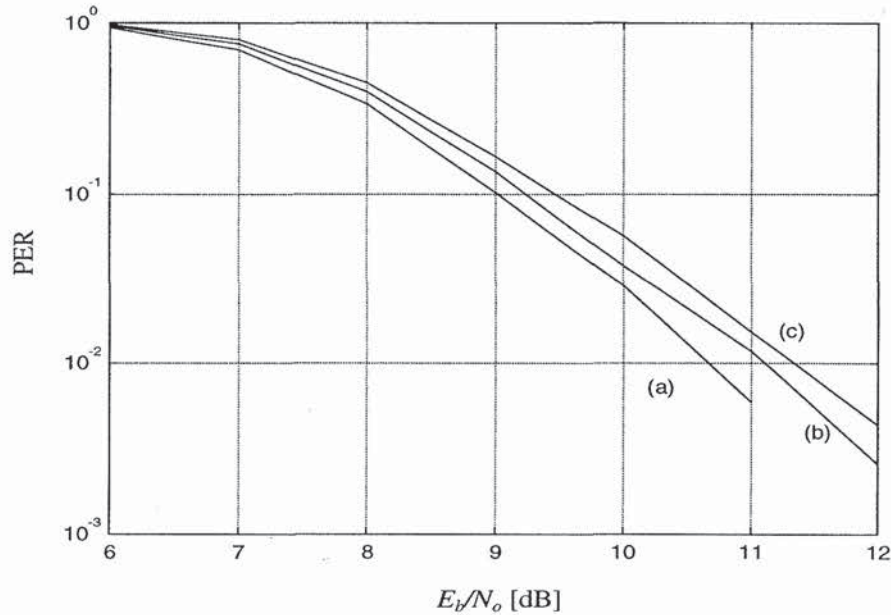


**Figure 6.22** Packet error ratio versus  $E_b/N_o$  for 64-byte packets in AWGN. PAP ratio is reduced to 5 dB by (a) clipping, (b) peak cancellation, and (c) peak windowing.

## 6.5 PAP REDUCTION CODES

As Section 6.2 shows, only a small fraction of all possible OFDM symbols has a bad peak-to-average power ratio. This suggests another solution to the PAP problem, based on coding. The PAP ratio can be reduced by using a code which only produces OFDM symbols for which the PAP ratio is below some desirable level. Of course, the smaller the desired PAP level, the smaller the achievable code rate is. Section 6.2, however, already demonstrated that for a large number of subcarriers, a reasonable coding rate larger than 3/4 can be achieved for a PAP level of 4 dB. In [6], it was found that for eight channels, a rate 3/4 code exists that provides a maximum PAP ratio of 3 dB. The results in [6] are based on an exhaustive search through all possible (QPSK)



codewords. Unfortunately, these results only tell us that there exists a large number of code words; it does not say if there exists a structured way of encoding and decoding to generate a large part of these code words, nor what the minimum distance properties of the code are. However, [6] did mention the interesting fact that a large part of the codes found are *Golay complementary sequences*, which opened the way to a structured way of generating PAP-reduction codes. Golay complementary sequences are sequence pairs for which the sum of autocorrelation functions is zero for all delay shifts unequal to zero [7–9]. It was already mentioned in [10] that the correlation properties of complementary sequences translate into a relatively small PAP-ratio of 3 dB when the codes are used to modulate an OFDM signal. Based on all these hints towards Golay sequences, [11] presented a specific subset of Golay codes together with decoding techniques that combined peak-to-average power reduction with good forward-error correction capabilities. Based on this work, Golay codes were actually implemented in a prototype 20-Mbps OFDM modem for the European Magic WAND project [12]. Fundamental studies on the coding properties of Golay sequences appeared in [13–16], proving code set sizes, distance properties, the relation to Reed-Muller codes, and many more interesting details.

A sequence  $x$  of length  $N$  is said to be complementary to another sequence  $y$  if the following condition holds on the sum of both autocorrelation functions:

$$\begin{aligned} \sum_{k=0}^{N-1} (x_k x_{k+i} + y_k y_{k+i}) &= 2N, \quad i = 0 \\ &= 0, \quad i \neq 0 \end{aligned} \quad (6.8)$$

By taking the Fourier transforms of both sides of (6.8), the above condition is translated into

$$|X(f)|^2 + |Y(f)|^2 = 2N \quad (6.9)$$

Here,  $|X(f)|^2$  is the power spectrum of  $x$ , which is the Fourier transform of its autocorrelation function. The discrete Fourier transform  $X(f)$  is defined as

$$X(f) = \sum_{k=0}^{N-1} x_k e^{-j2\pi k f T_s} \quad (6.10)$$

Here,  $T_s$  is the sampling interval of the sequence  $x$ . From the spectral condition (6.9), it follows that the maximum value of the power spectrum is bounded by  $2N$ :

$$|X(f)|^2 \leq 2N \quad (6.11)$$

Because the average power of  $X(f)$  (6.10) is equal to  $N$ , assuming that the power of the sequence  $x$  is equal to 1, the PAP ratio of  $X(f)$  is bounded as

$$\text{PAP ratio} \leq \frac{2N}{N} = 2 \quad (6.12)$$

In an OFDM transmission, normally the IFFT is applied to the input sequence  $x$ . However, because the IFFT is equal to the conjugated FFT scaled by  $1/N$ , the conclusion that the PAP ratio is upper bounded by 2 is also valid when  $X(f)$  is replaced by the inverse Fourier transform of the sequence  $x$ . Hence, by using a complementary code as input to generate an OFDM signal, it is guaranteed that the PAP ratio does not exceed 3 dB. Figure 6.23 shows a typical example of an OFDM signal envelope when using a complementary sequence. For this case of 16 channels, the PAP ratio is reduced by approximately 9 dB in comparison with the uncoded case of Figure 6.1.

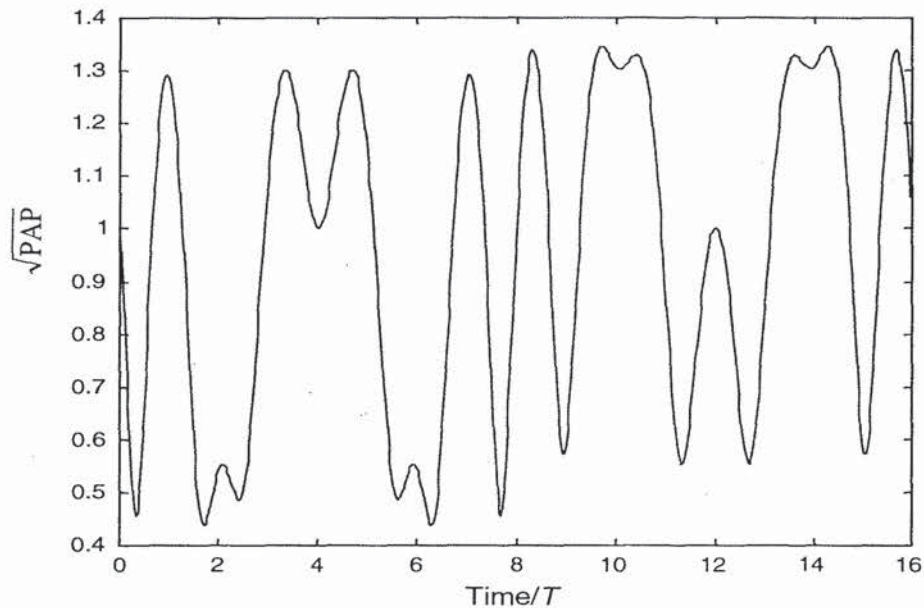


**Figure 6.23** Square root of peak-to-average power ratio for a 16-channel OFDM signal, modulated with a complementary code.

### 6.5.1 Generating Complementary Codes

In [7–9], several coding rules are given for generating a set of complementary sequences, based upon some starting complementary pair, the *kernel*. For complementary sequences of length 2, for instance, a possible kernel is the pair 1, 1 and 1, -1. The basic coding rules for generating complementary codes from this kernel are [7, 9]:

1. Interchanging both codes,
2. Reversing and conjugating second code,
3. Phase-rotating second code,
4. Phase-rotating elements of even order in both codes,
5. Phase-rotating first code, and
6. Reversing and conjugating first code.

When rules 1 to 4 are applied, the following 16 different length 4 codes can be obtained for the case of 4 phase modulation (see Table 6.1):

**Table 6.1**  
Length 4 complementary codes

1	1	1	-1
1	1	-1	1
1	-1	1	1
1	-1	-1	-1
1	j	1	-j
1	j	-1	j
1	-j	1	j
1	-j	-1	-j
1	1	j	-j
1	1	-j	j
1	-1	j	j
1	-1	-j	-j
1	j	j	1
1	j	-j	-1
1	-j	-j	1
1	-j	j	-1

The number of codes can be extended to 64 by applying the fifth and sixth rules, which gives the same result as applying 4 different phase shifts to the 16 codes. Hence, these 4-symbol codes can easily be generated by using a 16-word-long lookup table to encode 4 bits, followed by a phase rotation to map a total of 6 bits onto all possible complementary codes.

Unfortunately, as the previous example already indicated, the six coding rules do not unambiguously produce all complementary sequences. This makes it difficult to find the size of the code set and to find a systematic way to produce complementary sequences. Thus, some other algorithm has to be found to generate complementary codes.

[9] showed that from one set of complementary sequences, others can be generated by multiplying the original sequences with columns of the discrete Fourier transform matrix. Although [9] only mentions this method to generate sets with longer

code length by using the *Kronecker product*, it can also be used to generate different sequences with the same length, by multiplying an original sequence elementwise with columns of the DFT matrix. It is easy to show that such multiplications do not change the correlation properties. Each DFT column is a delta function in the frequency domain. Because multiplication in the time domain is equivalent to a convolution in the frequency domain, the power spectrum of a complementary sequence multiplied by a DFT column remains the same. Hence, also its correlation function, which is the Fourier transform of the power spectrum, remains the same, so that the outcome again is a complementary sequence.

Another interesting remark in [9] is that complementary sequences can be multiplied by columns of the binary *Walsh-Hadamard matrix*, without losing their complementary characteristics. Further, it is stated in [9] that "if the code is an expansion of shorter lengths, an arbitrary phase angle can be added to all elements in any orthogonal subset." These operations turn out to be very useful in generating distinct codes.

The coding algorithm for generating complementary sequences is now given by the following steps:

1. **Make a kernel;** that is, one complementary pair from which all other complementary sequences can be derived. For lengths equal to a power of two, kernels can easily be formed by using Golay's rule for length expansion. Starting with the length 2 sequence  $A_1 B_1$ , where  $A_1 = 1$  and  $B_1 = 1$ , longer length codes can be formed by making  $A_n B_n$  with  $A_n = A_{n-1} B_{n-1}$  and  $B_n = A_{n-1} - B_{n-1}$ . In this way, codes of length  $2^{n+1}$  are formed from the codes of length  $2^n$ . For example, the following codes up to length 16 can be obtained:

$$\begin{aligned}
 \text{length 2} & : A_1 B_1 = 1 \ 1 \\
 \text{length 4} & : A_2 B_2 = 1 \ 1 \ 1 \ -1 \\
 \text{length 8} & : A_3 B_3 = 1 \ 1 \ 1 \ -1 \ 1 \ 1 \ -1 \ 1 \\
 \text{length 16} & : A_4 B_4 = 1 \ 1 \ 1 \ -1 \ 1 \ 1 \ -1 \ 1 \ 1 \ 1 \ -1 \ -1 \ -1 \ 1 \ -1
 \end{aligned} \tag{6.13}$$

2. **Determine the number of orthogonal subsets.** For length  $N$  codes, formed by the length expansion method described above, there are  $\log_2 N$  orthogonal subsets, all of which can be given an arbitrary phase offset. The orthogonal subsets within a code are formed by all single elements, pairs, quads, and so forth, which are of even order. Thus, a length 16 code has 4 orthogonal subsets, being all even elements, pairs, quads, and one octet. All of these can be given a different phase without changing the complementary characteristics of the code. Further, it is also possible to apply an arbitrary phase shift to the entire code. Hence, a complementary code set based upon the kernel of (6.13) can be written as:

$$c = \{ e^{j(\varphi_1+\varphi_2+\varphi_3+\varphi_4)}, e^{j(\varphi_1+\varphi_3+\varphi_4)}, e^{j(\varphi_1+\varphi_2+\varphi_4)}, -e^{j(\varphi_1+\varphi_4)}, \\ e^{j(\varphi_1+\varphi_2+\varphi_3)}, e^{j(\varphi_1+\varphi_3)}, -e^{j(\varphi_1+\varphi_2)}, e^{j\varphi_1} \} \quad (6.14)$$

Notice that this code is actually implemented in a 20-Mbps OFDM modem for the Magic WAND project [12]. It is also used in the 11-Mbps IEEE 802.11 wireless LAN standard [17]. The latter is not an OFDM system, but here the benefit from using complementary sequences is in its good aperiodic autocorrelation properties, which makes it easier to build a receiver with sufficient robustness to multipath.

An alternative code description is to write the code phases as

$$\begin{bmatrix} \theta_1 \\ \theta_2 \\ \theta_3 \\ \theta_4 \\ \theta_5 \\ \theta_6 \\ \theta_7 \\ \theta_8 \end{bmatrix} = \begin{bmatrix} 1 & 1 & 1 & 1 & 0 \\ 1 & 0 & 1 & 1 & 0 \\ 1 & 1 & 0 & 1 & 0 \\ 1 & 0 & 0 & 1 & 1 \\ 1 & 1 & 1 & 0 & 0 \\ 1 & 0 & 1 & 0 & 0 \\ 1 & 1 & 0 & 0 & 1 \\ 1 & 0 & 0 & 0 & 0 \end{bmatrix} \begin{bmatrix} \varphi_1 \\ \varphi_2 \\ \varphi_3 \\ \varphi_4 \\ \pi \end{bmatrix} \quad (6.15)$$

The output code is given by  $\exp(j \cdot 2\pi\theta_i/M)$ , where  $\theta_i$  is the coded phase and  $M$  is the size of the phase constellation. For BPSK ( $M=2$ ), the code set is equal to the Walsh-Hadamard codes, which is offset by the kernel—defined by the fourth column in (6.15).

3. **Finally, a transformation can be applied** that unfortunately cannot be described by simple multiplications or phase rotations. Instead, it can be described as an interleaving operation on the underlying shorter length codes that are used to make a longer length code [14]. For a length 8 sequence, for instance, two new length 8 codes can be generated by interleaving the first and second half of the original code. Interleaving the code three times reproduces the original code. In general, a code with a length of  $2^n$  can be interleaved  $n-1$  times before reproducing itself. The following example shows three different codes out of a length 8 code produced by interleaving:

$$\begin{array}{l} 0: 1 1 1 -1 \quad 1 1 -1 1 \\ 1: 1 1 1 1 \quad 1 -1 -1 1 \\ 2: 1 1 1 -1 \quad 1 -1 1 1 \end{array} \quad (6.16)$$

For a length 16 code, it turns out that except for four different codes that can be produced by interleaving the first and second half of the code, more codes can be made by simultaneously interleaving the quarters of the code, giving a total of  $3 \cdot 4 = 12$  different codes. The described coding rules can now be used to determine the size of

complementary code sets. For an  $N$ -length code with  $M$  possible phases, the kernel can be multiplied by  $1 + \log_2 N$  modified Walsh-Hadamard rows with  $M$  different phases. This gives a code set size of  $M^{1+\log_2 N}$ . The amount of bits per codeword can be expressed as  $(1 + \log_2 N)\log_2 M$ . For instance, a length 8 code with four possible phases gives 8 bits per code word. The above numbers did not yet take into account the interleaving rule, which adds another  $\log_2((\log_2 N)!/2)$  bits to the total number of bits per symbol (for  $N > 4$  and  $N$  being a power of 2). Notice that the interleaving rule does not necessarily produce an integer number of bits per encoded symbol.

### 6.5.2 Minimum Distance of Complementary Codes

In OFDM systems, the effects of multipath are mitigated by error correction coding over the various subchannels. Thus, when using a PAP-reduction code, it would be very desirable if you could use this code also for forward-error correction. Otherwise, a separate code would be required, with the disadvantage of additional complexity and a reduction in the overall coding rate and spectral efficiency.

Therefore, the question arises as to what minimum distance the above mentioned complementary sequences have. Looking at (6.15), we can state that if this is the only generating rule used, then  $N/2 + 1$  correctly received symbols are always sufficient to calculate the  $1 + \log_2 N$  phases used to generate the complementary sequence. This is because with  $1 + N/2$  phase observations, it is always possible to form  $1 + \log_2 N$  independent equations which can be used to solve for the  $1 + \log_2 N$  unknown phases. In fact, there are a certain number of combinations of  $1 + \log_2 N$  independent equations. The equations are independent only if each phase—except  $\varphi_1$ —is present in at least one and at most  $\log_2 N$  Equations. Since each phase—except  $\varphi_1$ —is present in exactly  $N/2$  observations,  $1 + N/2$  observations are sufficient to obtain at least one set of  $1 + \log_2 N$  independent phase equations. Therefore, we can conclude that the minimum distance between 2 different complementary codes of length  $N$  is  $N/2$  symbols, so it is possible to correct  $N/4 - 1$  symbol errors or  $N/2 - 1$  erasures.

The *minimum Euclidean distance*, which determines the performance in flat fading with additive noise, can be found by observing that a minimum distance between two code words is obtained if  $N/2$  symbols have a minimum phase rotation of  $2\pi/M$ , where  $M$  is the number of phases. Thus, the minimum Euclidean distance  $d_{min}$  is

$$d_{min} = \sqrt{\frac{N}{2}} \left\| 1 - \exp(j \frac{2\pi}{M}) \right\| \quad (6.17)$$

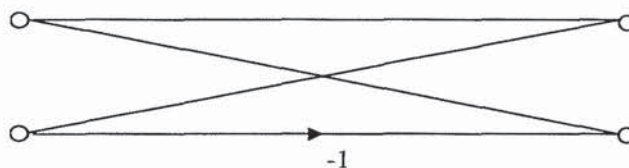
For instance, for 8-PSK and 8 channels, the minimum distance becomes 1.53, which is 6 dB larger than the distance of uncoded 8-PSK ( $= 0.765$ ). Because the rate of the length-8 complementary codes is  $1/2$ , a maximum coding gain of 3 dB can be achieved compared with uncoded 8-PSK.

The above distance calculations are only valid for complementary codes generated without using the interleaving rule. Two codes formed by interleaving generally have a distance that is less than  $N/2$  symbols. For  $N=8$ , for instance, the interleaved codes (6.16) have a distance of only two symbols instead of four.

### 6.5.3 Maximum Likelihood Decoding of Complementary Codes

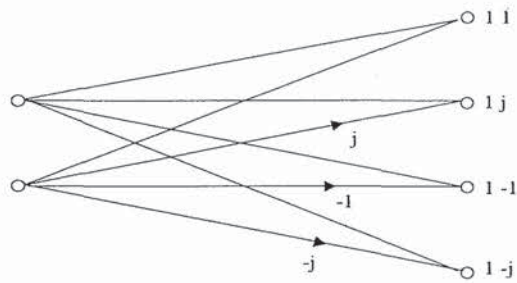
This section describes an optimal decoding technique for specific subsets of complementary codes, based on generalized Walsh-Hadamard encoding. With generalized Walsh-Hadamard coding, we mean that for a length  $N = 2^n$  code,  $n + 1$  phases are encoded into  $2^n$  output phases by adding the first phase to all code phases, the second to all odd code phases, the third to all odd pairs of code phases, and so on. For a length 8 code, for instance, the phase encoding is given by (6.15). For BPSK ( $M = 2$ ), the coding reduces to normal Walsh-Hadamard coding. For this case, the efficient fast Walsh transform can be used to realize maximum likelihood decoding. For larger constellation sizes, maximum likelihood decoding seems less trivial. In the worst case, it would require  $M^{n+1}$  Euclidean distance calculations or correlations, giving a total number of operations of  $NM^{n+1}$  (complex multiplications and additions). There is, however, quite some redundancy in the calculation of all possible correlations, just as for the binary case. This means it is possible to reduce the complexity of the maximum likelihood decoder by generalizing the fast Walsh transform to general phase constellations, as was first described in [18].

Figure 6.24 shows a butterfly that is used to calculate a 2-point binary fast Walsh transform. Using these butterflies, an  $N$ -point fast Walsh transform can be calculated with  $N \log_2 N$  additions and subtractions.



**Figure 6.24** Butterfly of binary fast Walsh transform.

Now consider a 4-PSK generalized Walsh-Hadamard code. For length 2, the transform can be depicted as a butterfly with two inputs and four outputs (see Figure 6.25).



**Figure 6.25** Butterfly of 4-PSK fast Walsh transform.

The right side of the butterfly shows the sequences used to correlate with the input sequence.

Using this butterfly, a transform of double length  $N$  can be constructed by doing two transforms on half of the code length, plus an additional stage of  $4^{n-1}$  butterflies. A length 4 transform, for instance, can be constructed as depicted in the Figure 6.26. The four input points at the left are transformed into 16 output points by correlations with the complex sequences listed on the right.

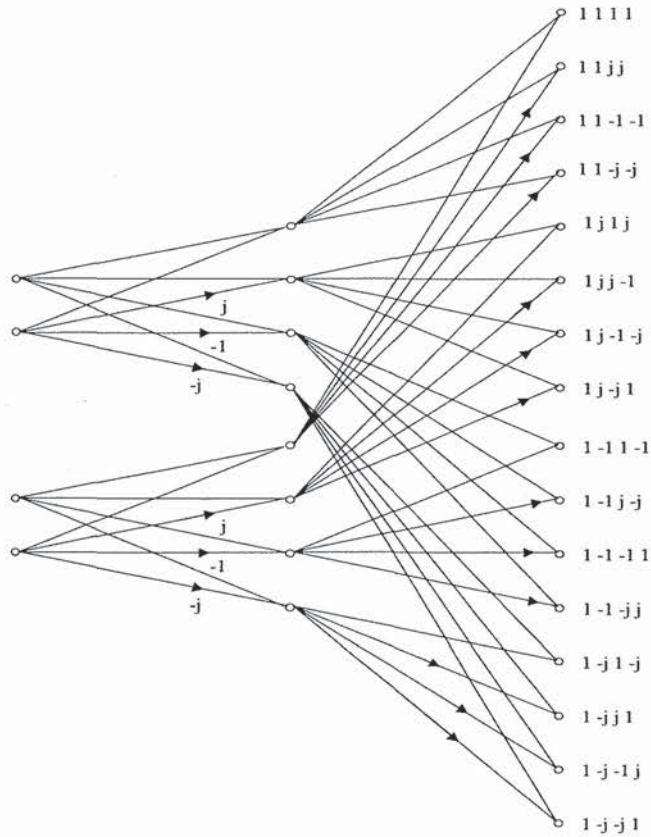


**Figure 6.26** Length 4 4-PSK fast Walsh transform.



The 4-point transform can be extended to an 8-point transform by performing two length 4 transforms on two groups of 4 samples, and adding an additional stage of 16 butterflies to produce the length 8 results. Figure 6.27 shows this 8-point transform, where the first two 4-point transforms are drawn as a line to simplify the picture. In reality, each 4-point transform has 16 outputs, which are combined with the 16 outputs of the other 4-point transform in 4 different ways. Hence, the total number of outputs is 64.

There are 28 butterflies needed for a length 8 transform. Each butterfly requires four additions (the phase rotations are trivial for 4-PSK), so the total number of operations is 112 complex additions. The direct calculation method with 64 separate correlators requires 512 complex additions, so the fast transform reduces the complexity by almost a factor of 5.

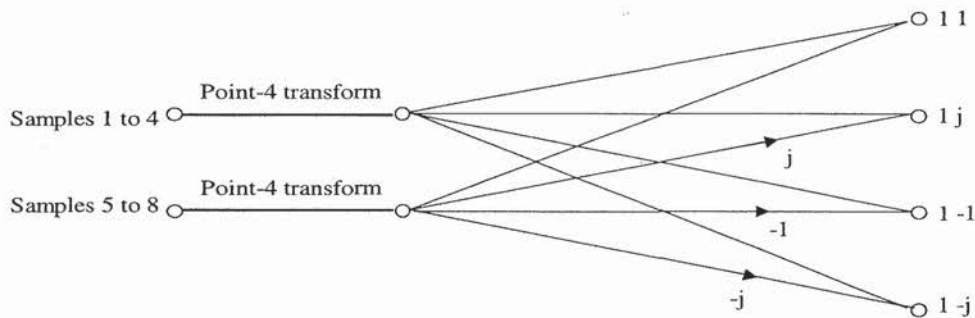


**Figure 6.27** Length-8 4-PSK fast Walsh transform using length-4 transforms.

#### 6.5.4 Suboptimal Decoding of Complementary Codes

For any coding technique to be successful, there have to be decoding techniques that are not too complex and with a performance not too far from that of optimal maximum likelihood decoding. For a complementary code for which the number of phases  $M$  is larger than 2 and the code length is larger than about 8, maximum likelihood decoding quickly becomes too complex for practical implementation. Hence, we want to find *suboptimal* decoding techniques that are less complex to implement. One way to decode the phase that is applied to all alternating elements of a complementary code is to multiply the complex odd samples with the complex conjugate of the even samples. By summing the results, we obtain a vector that has the desired phase value. The same procedure can be followed for even and odd pairs, quads, and so on. The phase that is applied to the entire code has to be found by correcting the complex samples for all other phases. For the length 8 code with complex samples  $x_i$ , the phase equations are given by

$$\begin{aligned}
\varphi_2 &= \arg\{x_1 x_2^* + x_3 x_4^* + x_5 x_6^* + x_7 x_8^*\} \\
\varphi_3 &= \arg\{x_1 x_3^* + x_2 x_4^* + x_5 x_7^* + x_6 x_8^*\} \\
\varphi_4 &= \arg\{x_1 x_5^* + x_2 x_6^* + x_3 x_7^* + x_4 x_8^*\} \\
\varphi_1 &= \arg\{x_1 e^{-j(\varphi_2+\varphi_3+\varphi_4)} + x_2 e^{-j(\varphi_3+\varphi_4)} + x_3 e^{-j(\varphi_2+\varphi_4)} + \\
&\quad x_4 e^{-j(\varphi_4)} + x_5 e^{-j(\varphi_2+\varphi_3)} + x_6 e^{-j(\varphi_3)} + x_7 e^{-j(\varphi_2)} + x_8\}
\end{aligned} \tag{6.18}$$

Here,  $\arg\{\}$  means the calculation of the phase of a complex vector, and  $*$  denotes the complex conjugate. To convert the phases to bits, we have to make decisions for those constellation points that are closest to the phases found, just as we do in normal phase shift keying.

There are some alternative ways to estimate the phase of the entire code word. In (6.18), the estimated phases were used to eliminate the phase rotations caused by all phases except for  $\varphi_1$ . The same effect can be achieved by multiplying the received code samples with complex conjugates of  $y_i$ , where  $y_i$  is the term within the  $\arg\{\}$  expression of  $\varphi_i$  in (6.18):

$$\begin{aligned}
\varphi_1 &= \arg\{x_1 y_2^* y_3^* y_4^* + x_2 y_3^* y_4^* + x_3 y_2^* y_4^* + x_4 y_4^* \\
&\quad + x_5 y_2^* y_3^* + x_6 y_3^* + x_7 y_2^* + x_8\}
\end{aligned} \tag{6.19}$$

The disadvantage of this method is that there is a certain noise enhancement because of the double and triple products of noisy phasors. A better estimate can be found by using only those terms that have no more than one phasor multiplication:

$$\varphi_1 = \arg\{x_4 y_4^* + x_6 y_3^* + x_7 y_2^* + x_8\} \tag{6.20}$$

Following the same argument, it is also possible to simplify (6.19) by using only terms with one or zero phase rotations:

$$\varphi_1 = \arg\{x_4 e^{-j\varphi_4} + x_6 e^{-j\varphi_3} + x_7 e^{-j\varphi_2} + x_8\} \tag{6.21}$$

The advantage of the above-described decoding technique is that it provides automatic weighting of the subchannels; erroneous channels with low amplitudes will only give a minor contribution to the phase estimates. In additive white Gaussian noise (AWGN), the described technique performs 3 dB worse than optimal maximum likelihood decoding, which can be argued as follows: the performance of maximum likelihood decoding is determined by the minimum Euclidean distance, which is four times the distance of uncoded 8-PSK for the length 8 complementary code with 8-PSK.

Looking at the decoding structure of (6.18), we can see that for each phase estimate, four or more vectors are added, which gives a 6-dB SNR improvement. Each of the added vectors, however, consists of a multiplication of two separate vectors with independent noise contributions. Hence, the detection SNR is improved by 3 dB only, as compared with 6 dB for a maximum likelihood decoding technique. Note that the difference with maximum likelihood decoding decreases in the case of frequency-selective channels. In the extreme case that four out of eight subchannels are completely lost, both will have the same symbol error probability.

Except for the soft-decision technique described above, it is also possible to do hard-decision erasure decoding. In this case, four out of eight subchannels are erased, based upon amplitude measurements obtained during training. Three subchannels can be erased arbitrarily; the fourth must be chosen such that all phase estimates in (6.18) have at least one element. Erasure decoding will fail if one of the unerased subchannels is in error. Thus, in AWGN, the bit-error probability is equal to that of uncoded 8-PSK, so there is a 6-dB loss compared with that of maximum likelihood decoding. Again, this loss is less in the case of frequency-selective channels.

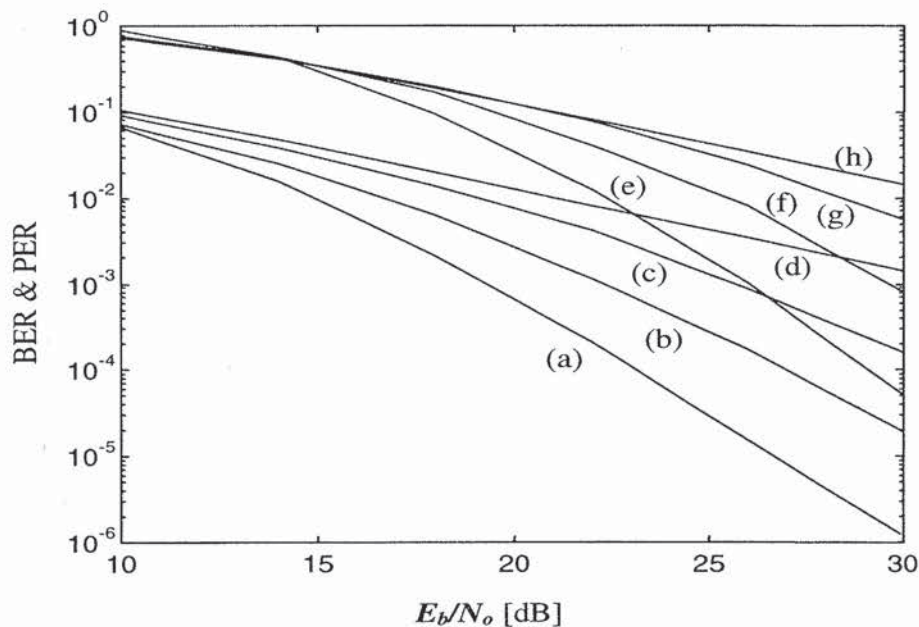


**Figure 6.28** BER (a-d) and PER (e-h) versus mean  $E_b/N_o$  for delay spreads of (a) and (e) 50 ns, (b) and (f) 20 ns, (c) and (g) 10 ns, (d) and (h) 0.

Figure 6.28 shows BER and PER for single ATM cell packet versus mean  $E_b/N_o$ , averaged over a large ( $10^4$ ) number of Rayleigh fading channels with an exponentially decaying power-delay profile. The results clearly show that the combination of OFDM and complementary coding can efficiently exploit the frequency diversity of the channel for delay spreads of 10 ns or more. In this simulation, the use

of 8-PSK length 8 complementary codes is assumed. Two independent codes together encode 24 bits into 16 OFDM channels. For a symbol duration of 1.2  $\mu$ s, including a guard time of 400 ns, this gives a data rate of 20 Mbps. These parameters are used in the OFDM modem of Magic WAND.

### 6.5.5 Large Code Lengths

For OFDM systems with a large number of subcarriers, it may not be feasible to generate a sufficient number of complementary codes with a length equal to the number of channels. To avoid this problem, the total number of channels can be split into groups of channels; applying a complementary code to each group of subchannels increases the coding rate, at the cost of reduced error correction capability and PAP ratio. For 32 channels, for instance, 18 bits per symbol could be encoded using 8-PSK complementary codes. These codes would have a PAP ratio of 3 dB and a distance of 16 channel symbols, so 7 erroneous channels or 15 erased channels could be corrected. Instead of 32-channel codes, it is also possible to use four 8-channel codes or some other combination of shorter length codes. The sum of four 8-channel codes give a total of 48 bits per symbol and a PAP ratio of 9 dB (6-dB reduction), while it is possible to correct one error or three erasures per group of eight channels.

## 6.6 SYMBOL SCRAMBLING

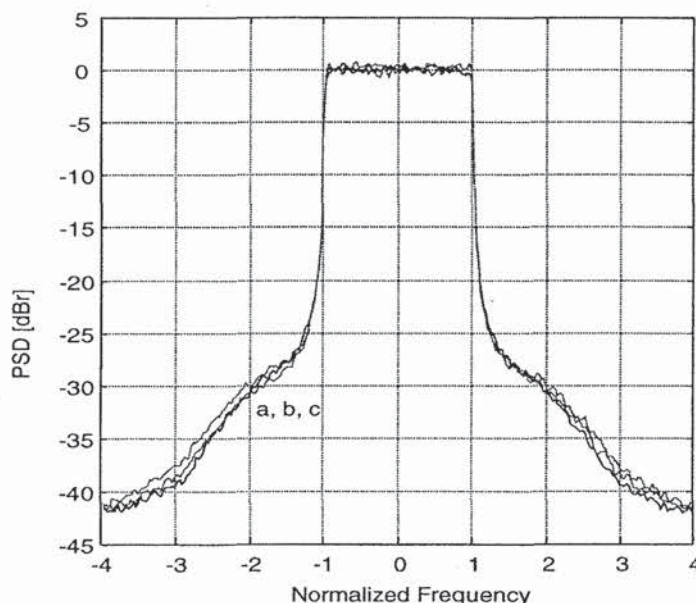
Symbol scrambling techniques to reduce the PAP ratio of a transmitted OFDM signal can be seen as a special case of PAP reduction codes. The difference is that symbol scrambling does not try to combine forward-error correction and PAP reduction such as is done by the complementary codes. The basic idea of symbol scrambling is that for each OFDM symbol, the input sequence is scrambled by a certain number of scrambling sequences. The output signal with the smallest PAP ratio is transmitted. For uncorrelated scrambling sequences, the resulting OFDM signals and corresponding PAP ratios will be uncorrelated, so if the PAP ratio for one OFDM symbol has a probability  $p$  of exceeding a certain level without scrambling, the probability is decreased to  $p^k$  by using  $k$  scrambling codes. Hence, symbol scrambling does not guarantee a PAP ratio below some low level; rather, it decreases the probability that high PAP ratios occur. Scrambling techniques were first proposed in [19, 20] under the names *selected mapping* and *partial transmit sequences*. The difference between the two is that the first applies independent scrambling rotations to all subcarriers, while the latter only applies scrambling rotations to groups of subcarriers.

Figure 6.29 shows OFDM spectra for 64 subcarriers where the backoff is adjusted to maintain a  $-30$  dB bandwidth that is twice the  $-3$ -dB bandwidth. A perfect linear power amplifier model is used, which clips the signal when the output power exceeds the saturation power level. The effect of scrambling has been simulated by scrambling the IFFT input data for each OFDM symbol with a certain number of

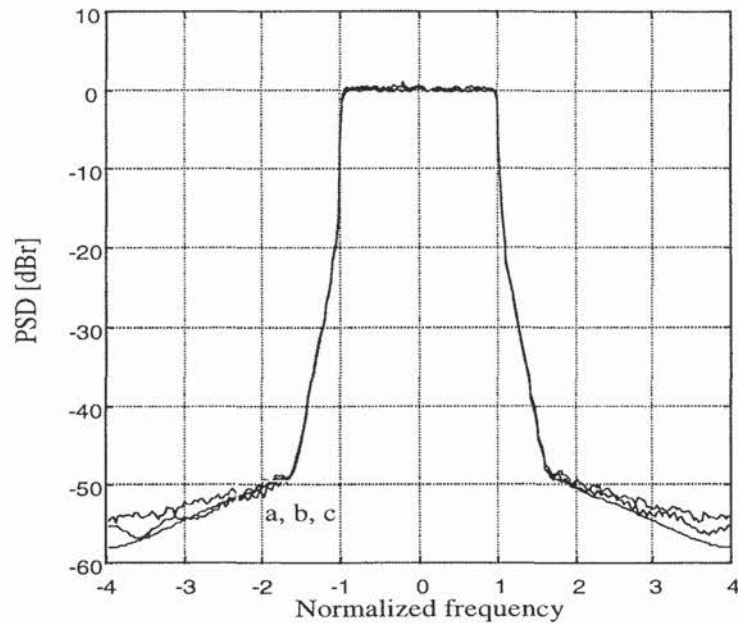
independent complementary sequences and selecting the output symbol that gives the smallest PAP ratio. We can see from Figure 6.29 that scrambling with 1 and 10 codes gives rather small improvements of 0.25 and 0.75 dB in the required backoff, respectively, compared with the no scrambling case.

Figure 6.30 shows similar spectra as in Figure 6.29, but now for a more strict requirement of a  $-50$ -dB bandwidth that is twice the  $-3$ -dB bandwidth. In this case, scrambling gives more gain in the required backoff, up to 2 dB for 10 scrambling codes. This is caused by the fact that with scrambling, the probability of exceeding a PAP ratio of 7 dB is much less than the probability of exceeding 4 dB (whose probability is close to 1). As a result of this, for a backoff value of 4 or 5 dB, the amount of clipping interference is not much different from that without scrambling.

Figures 6.29 and 6.30 assume a perfectly linear power amplifier. In reality, however, the amplifier has a certain nonlinear transfer function. Figure 6.31 shows simulated spectra using Rapp's power amplifier model with nonlinearity parameter  $p = 2$ , which closely resembles practical RF power amplifiers. We can see that the amplifier model changes the shape of the spectrum, but the relative gain of scrambling does not change significantly. Because for wireless systems the  $-30$ -dB bandwidth requirement of Figure 6.29 and 6.31 is more realistic than the  $-50$ -dB requirement of Figure 6.30, we can conclude that the benefits of scrambling are rather limited.



**Figure 6.29** OFDM spectra for 64 subcarriers and  $p=100$  using (a) no scrambling with 5.0-dB backoff, (b) 1 scrambling code with 4.7-dB backoff, and (c) 10 scrambling codes with 4.25-dB backoff.



**Figure 6.30** OFDM spectra for (a) no scrambling with a 8.5-dB backoff, (b) 1 scrambling code with a 7.2 dB backoff and (c) 10 scrambling codes with a 6.5-dB backoff.

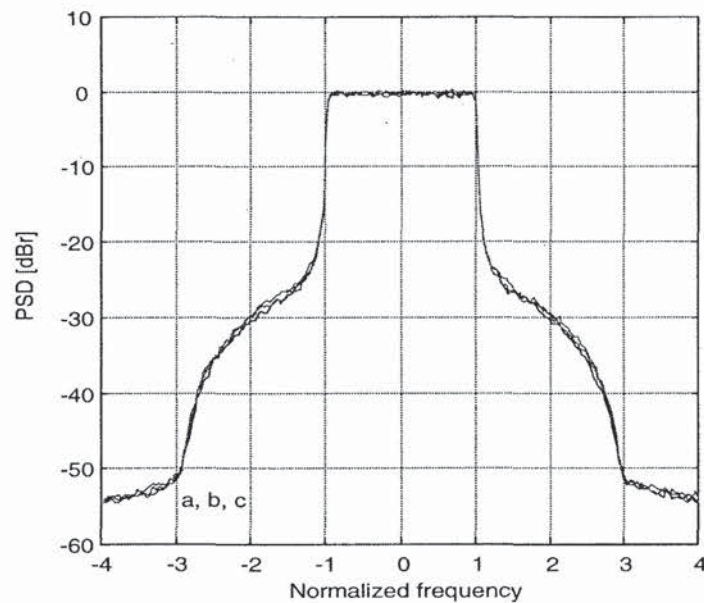


**Figure 6.31** OFDM spectra for 64 subcarriers and Rapp's amplifier model with  $p = 2$  using (a) no scrambling with 5.8-dB backoff, (b) 1 scrambling code with 5.3-dB backoff, and (c) 10 scrambling codes with 5.2-dB backoff.

**REFERENCES**

- [1] Pauli, M., and H. P. Kuchenbecker, "Minimization of the Intermodulation Distortion of a Nonlinearly Amplified OFDM Signal," *Wireless Personal Communications*, Vol. 4, No. 1, pp. 93–101, Jan. 1997.
- [2] Rapp, C., "Effects of HPA-Nonlinearity on a 4-DPSK/OFDM Signal for a Digital Sound Broadcasting System," *Proceedings of the Second European Conference on Satellite Communications*, Liège, Belgium, pp.179–184, Oct. 22–24, 1991.
- [3] De Wild, A., "The Peak-to-Average Power Ratio of OFDM," M.Sc. thesis, Delft University of Technology, Delft, The Netherlands, Sept. 1997.
- [4] May, T., and H. Rohling, "Reducing the Peak-to-Average Power Ratio in OFDM Radio Transmission Systems," *Proceedings of IEEE VTC '98*, Ottawa, Canada, pp. 2774–2778, May 18–21, 1998.
- [5] Li, X., and L.J. Cimini, "Effects of Clipping and Filtering on the Performance of OFDM," *Proceedings of IEEE VTC'97*, pp.1634–1638, 1997.
- [6] Wilkinson, T. A., and A. E. Jones, "Minimisation of the Peak-to-Mean Envelope Power Ratio of Multicarrier Transmission Schemes by Block Coding," *Proceedings of IEEE Vehicular Technology Conference*, Chicago, pp. 825–829, July 1995.
- [7] Golay, M. J. E., "Complementary Series," *IRE Transactions on Information Theory*, Vol. IT-7, pp. 82–87, April 1961.
- [8] Sivaswamy, R., "Multiphase Complementary Codes," *IEEE Transactions on Information Theory*, Vol. IT-24, No. 5, Sept. 1978.
- [9] Frank, R. L., "Polyphase Complementary Codes," *IEEE Transactions on Information Theory*, Vol. IT-26, No. 6, Nov. 1980.
- [10] Popovic, B. M., "Synthesis of Power Efficient Multitone Signals with Flat Amplitude Spectrum," *IEEE Transactions on Communications*, Vol. 39, No. 7, July 1991.
- [11] Van Nee, R. D. J., "OFDM Codes for Peak-to-Average Power Reduction and Error Correction," *IEEE Global Telecommunications Conference*, London, pp. 740–744, Nov. 18–22, 1996.
- [12] Van Nee, R. D. J., "An OFDM Modem for Wireless ATM," *IEEE Symposium on Communications and Vehicular Technology*, Gent, Belgium, October 7-8, 1996.
- [13] Davis, J. A., and J. Jedwab, "Peak-to-Mean Power Control and Error Correction for OFDM Transmission Using Golay Sequences and Reed-Muller Codes," *Electronics Letters*, Vol. 33, pp. 267–268, 1997.
- [14] Urbanke, R., and A. S. Krishnakumar, "Compact Description of Golay Sequences and their Extensions," *Proceedings of the Thirty-Fourth Annual Allerton*

- Conference on Communication, Control and Computing Pagnation*, Urbana, IL, pp. 693–702, Oct. 2–4, 1996.
- [15] Urbanke, R., and A. S. Krishnakumar, “Compact Description of Golay Sequences and their Extensions,” Lucent Technologies Technical Memorandum, Doc. No. BL011217-961204-28TM, Dec. 20, 1996.
- [16] Davis, J. A., and J. Jedwab, “Peak-to-Mean Power Control in OFDM, Golay Complementary Sequences and Reed-Muller Codes,” HP Laboratories Technical Report, HPL-97-158, Dec. 1997.
- [17] IEEE, ‘Draft Supplement to Standard Part 11: Wireless LAN MAC and PHY Specifications: Higher Speed PHY Extension in the 2.4 GHz Band’, P802.11B/D6.0, May 1999.
- [18] Grant, A., and R. van Nee, “Efficient Maximum Likelihood Decoding of Q-ary Modulated Reed-Muller Codes,” *IEEE Communications Letters*, Vol. 2, No. 5, pp. 134–136, May 1998.
- [19] Müller, S. H., R. W. Bäuml, R. F. H. Fischer, and J. B. Huber, “OFDM with Reduced Peak-to-Average Power Ratio by Multiple Signal Representation,” *Annals of Telecommunications*, Vol. 52, No. 1–2, pp. 58–67, Feb. 1997.
- [20] Müller, S. H., and J. B. Huber, “OFDM with Reduced Peak-to-Average Power Ratio by Optimum Combination of Partial Transmit Sequences,” *Electronics Letters*, Vol. 33, No. 5, pp. 368–369, Feb. 1997.



## Chapter 7

# BASICS OF CDMA

### 7.1 INTRODUCTION

This chapter illustrates the basic principles of CDMA to obtain a better understanding of combinations of CDMA with OFDM, as discussed in Chapters 8 and 9. The scope of the chapter is to give generic understanding of CDMA without overwhelming mathematical details. Readers should refer to Chapters 5 and 6 of [1] for a more extensive discussion on direct-sequence CDMA air interface design aspects and wideband CDMA air interface proposals, respectively. Furthermore, [1–15] provide details of spread-spectrum (SS) and CDMA technologies.

This chapter is divided into three sections. Section 7.2 presents a brief state-of-the-art of CDMA. Section 7.3 introduces the CDMA concept in general. It explains those criteria the transmitted signal has to fulfill to constitute a spread-spectrum modulation. Processing gain is defined. The fundamental properties of CDMA signals, namely multiple access capability, protection against multipath interference, privacy, interference rejection, antijamming capability, and low probability of interception are introduced. Different modulation methods for CDMA are treated in detail. These are direct-sequence spread-spectrum, frequency-hopping spread-spectrum, time-hopping spread-spectrum, and hybrid modulation. Each modulation scheme is described with the help of block diagrams for the transmitter and the receiver. In addition, how each spread-spectrum modulation scheme achieves the above-listed six properties of CDMA signals is discussed.

In Section 7.4, we review the fundamental elements of direct-sequence CDMA and its application into third-generation systems, namely RAKE receiver, power control, soft handover, interfrequency handover, and multiuser detection.

## 7.2 CDMA: PAST, PRESENT, AND FUTURE

The origins of spread-spectrum are in the military field and navigation systems. Techniques developed to counteract intentional jamming have also proved suitable for communication through dispersive channels in cellular applications. In this section we highlight the milestones for CDMA development starting from the 1950s after the formulation of the Shannon theorem [16]. An extensive overview of spread-spectrum history is given in [17].

In 1949, John Pierce wrote a technical memorandum in which he described a multiplexing system in which a common medium carries coded signals that need not be synchronized. This system can be classified as a time-hopping spread-spectrum multiple access system [17]. Claude Shannon and Robert Pierce introduced the basic ideas of CDMA in 1949 by describing the interference averaging effect and the graceful degradation of CDMA [18]. In 1950, De Rosa-Rogoff proposed a direct-sequence spread-spectrum system and introduced the processing gain equation and noise multiplexing idea [17]. In 1956, Price and Green filed for the antimultipath “RAKE” patent [17]. Signals arriving over different propagation paths can be resolved by a wideband spread-spectrum signal and combined by the RAKE receiver. The near-far problem (i.e., a high interference overwhelming a weaker spread-spectrum signal) was first mentioned in 1961 by Magnuski [17].

The cellular application of spread-spectrum was suggested by Cooper and Nettleton in 1978 [19]. During the 1980s, Qualcomm investigated DS-SS-CDMA techniques, which finally led to the commercialization of cellular spread-spectrum communications in the form of the narrowband CDMA IS-95 standard in July 1993. Commercial operation of IS-95 systems started in 1996. In 1984, direct-sequence CDMA and hybrid CDMA/Frequency-Division Multiple Access (FDMA) were proposed among several proposals for the Group Special Mobile (the origin of the term GSM, which now stands for the Global System for Mobile Communications) multiple access schemes. They were investigated during 1984–86. Multiuser detection (MUD) has been subject to extensive research since 1986 when Verdu formulated an optimal multiuser detection for the AWGN channel, maximum likelihood sequence estimator (MLSE) [20].

During the 1990s, wideband CDMA techniques with a bandwidth of 5 MHz or more have been studied intensively throughout the world, and several trial systems have been built and tested [21]. These include FRAMES FMA2 (FRAMES Multiple Access) in Europe, Core-A in Japan, the European/Japanese harmonized WCDMA scheme, cdma2000 in the United States, and the TTA I and TTA II (Telecommunication Technology Association) schemes in Korea. Introduction of third-generation wireless communications systems using wideband CDMA is expected around the year 2000.

Wideband CDMA has a bandwidth of 5 MHz or more. The nominal bandwidth for all third-generation proposals is 5-MHz. There are several reasons for choosing this bandwidth. First, data rates of 144 and 384 Kbps, the main target of third-generation systems, are achievable within the 5-MHz bandwidth with a reasonable capacity. Even

a 2-Mbps peak rate can be provided under limited conditions. Second, lack of spectrum calls for reasonably small minimum spectrum allocation, especially if the system has to be deployed within the existing frequency bands occupied already by second-generation systems. Third, the 5-MHz bandwidth can resolve (separate) more multipaths than narrower bandwidths, increasing diversity and thus improving performance. Larger bandwidths of 10, 15, and 20-MHz have been proposed to support higher data rates more effectively.

Based on the above description, the CDMA era is divided in to three periods: (1) pioneer CDMA era, (2) narrowband CDMA era, and (3) wideband CDMA era, as shown in Table 7.1.

**Table 7.1**  
CDMA Era

Pioneer Era	
1949	John Pierce: time-hopping spread-spectrum
1949	Claude Shannon and Robert Pierce: basic ideas of CDMA
1950	De Rosa-Rogoff: direct-sequence spread-spectrum
1956	Price and Green: antimultipath RAKE patent
1961	Magnuski: near-far problem
1970s	Several developments for military field and navigation systems
Narrowband CDMA Era	
1978	Cooper and Nettleton: cellular application of spread-spectrum
1980s	Investigation of narrowband CDMA techniques for cellular applications
1984	DS-CDMA and Hybrid CDMA/FDMA proposal for the Group Special Mobile in Europe
1986	Formulation of optimal multiuser detection by Verdu
1993	IS-95 standard
Wideband CDMA Era	
1995	Europe: FRAMES FMA2 Japan : Core-A USA : cdma2000 Korea : TTA I, TTA II
	} WCDMA
2000	Commercialization of wideband CDMA systems

### 7.3 CDMA CONCEPTS

In CDMA, each user is assigned a unique code sequence (spreading code) it uses to encode its information-bearing signal. The receiver, knowing the code sequences of the user, decodes a received signal after reception and recovers the original data. This is possible because the cross-correlations between the code of the desired user and the codes of the other users are small. Because the bandwidth of the code signal is chosen to be much larger than the bandwidth of the information-bearing signal, the encoding process enlarges (spreads) the spectrum of the signal and is therefore also known as

spread-spectrum modulation. The resulting signal is also called a spread-spectrum signal, and CDMA is often denoted as spread-spectrum multiple access (SSMA).

The spectral spreading of the transmitted signal gives to CDMA its multiple access capability. It is therefore important to know the techniques necessary to generate spread-spectrum signals and the properties of these signals. A spread-spectrum modulation technique must fulfill two criteria:

1. The transmission bandwidth must be much larger than the information bandwidth.
2. The resulting radio-frequency bandwidth is determined by a function other than the information being sent (so the bandwidth is statistically independent of the information signal). This excludes modulation techniques like frequency modulation (FM) and phase modulation (PM).

The ratio of transmitted bandwidth to information bandwidth is called the *processing gain*  $G_p$  of the spread-spectrum system:

$$G_p = \frac{B_t}{B_i} \quad (7.1)$$

where  $B_t$  is the transmission bandwidth and  $B_i$  is the bandwidth of the information-bearing signal.

The receiver correlates the received signal with a synchronously generated replica of the spreading code to recover the original information-bearing signal. This implies that the receiver must know the code used to modulate the data.

Because of the coding and the resulting enlarged bandwidth, spread-spectrum (SS) signals have a number of properties that differ from the properties of narrowband signals. The most interesting from the communications systems point of view are discussed below. To have a clear understanding, each property has been briefly explained with the help of illustrations, if necessary, by applying direct-sequence spread-spectrum techniques.

*Multiple access capability.* If multiple users transmit a spread-spectrum signal at the same time, the receiver will still be able to distinguish among the users provided each user has a unique code that has a sufficiently low cross-correlation with the other codes. Correlating the received signal with a code signal from a certain user will then only despread the signal of this user, while the other spread-spectrum signals will remain spread over a large bandwidth. Thus, within the information bandwidth the power of the desired user will be larger than the interfering power provided there are not too many interferers, and the desired signal can be extracted. The multiple access capability is illustrated in Figure 7.1. In Figure 7.1(a), two users generate a spread-spectrum signal from their narrowband data signals. In Figure 7.1(b) both users transmit their spread-spectrum signals at the same time. At receiver 1, only the signal of user 1 is coherently summed by user 1, despreader and the user 1 data recovered.

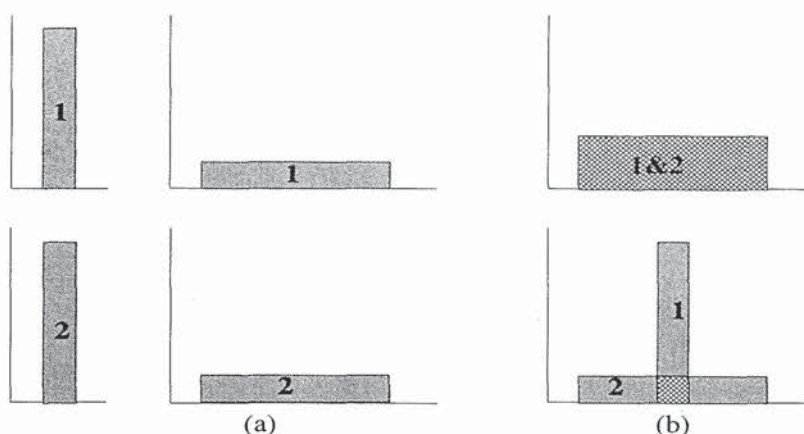


**Figure 7.1** Principle of spread-spectrum multiple access.

*Protection against multipath interference.* In a radio channel there is not just one path between a transmitter and receiver. Because of reflections (and refractions), a signal is received from a number of different paths. The signals of the different paths are all copies of the same transmitted signal but with different amplitudes, phases, delays, and arrival angles. Adding these signals at the receiver will be constructive at some of the frequencies and destructive at others. In the time domain, this results in a dispersed signal. Spread-spectrum modulation can combat this multipath interference; however, the way in which this is achieved depends very much on the type of modulation used. In the next section, where CDMA schemes based on different modulation methods are discussed, we show for each scheme how multipath interference rejection is obtained.

*Privacy.* The transmitted signal can only be despread and the data recovered if the code is known to the receiver.

*Interference rejection.* Cross-correlating the code signal with a narrowband signal spreads the power of the narrowband signal thereby reducing the interfering power in the information bandwidth. Figure 7.2 illustrates this. The receiver observes spread-spectrum signal  $s$  summed with a narrowband interference  $i$ . At the receiver, the spread-spectrum signal is despread while the interference signal is spread, making it appear as background noise compared with the despread signal. Demodulation will be successful if the resulting background is of sufficiently weak energy in the despread information bandwidth.

*Antijamming capability, especially narrowband jamming.* This is more or less the same as interference rejection except the interference is now willfully inflicted on the system. It is this property, together with the next one, that makes spread-spectrum modulation attractive for military applications.

*Low probability of interception (LPI).* Because of its low power density, the spread-spectrum signal is difficult to detect and intercept by a hostile listener.

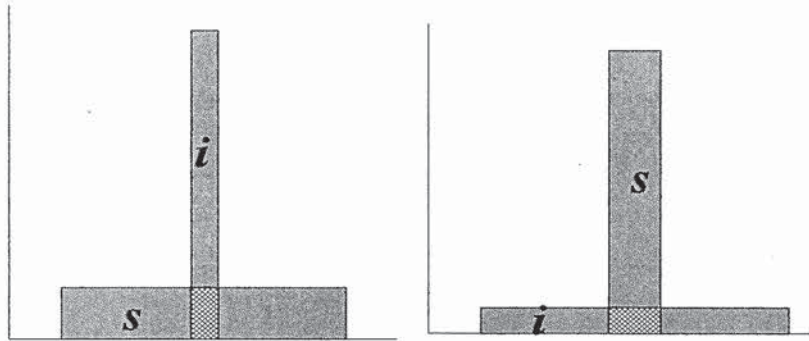


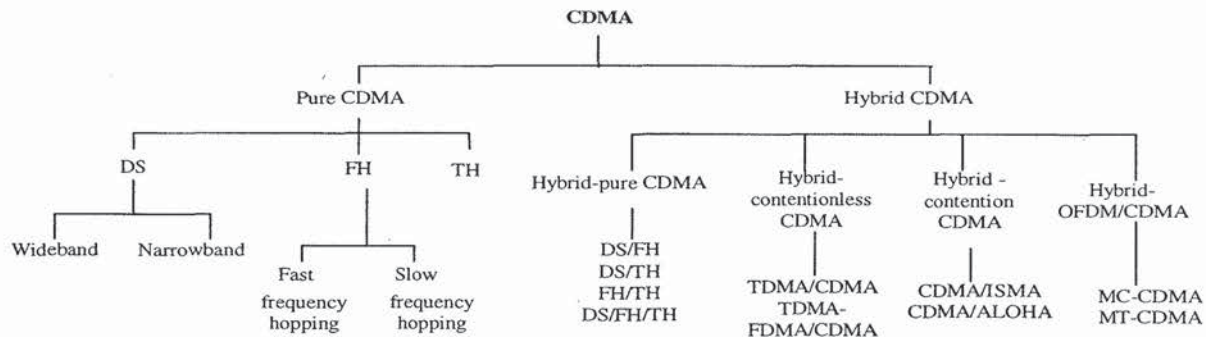
Figure 7.2 Interference rejection.

Figure 7.3 gives general classification of CDMA showing pure and hybrid CDMA.

*Pure CDMA.* There are three modulation techniques that generate spread-spectrum signals, known as Pure CDMA. These three techniques are as follows:

- *Direct-sequence (DS) CDMA.* The information-bearing signal is multiplied directly by a high-chip-rate spreading code.
- *Frequency-hopping (FH) CDMA.* The carrier frequency at which the information-bearing signal is transmitted is rapidly changed according to the spreading code.
- *Time-hopping (TH) CDMA.* The information-bearing signal is not transmitted continuously. Instead the signal is transmitted in short bursts where the times of the bursts are decided by the spreading code.

*Hybrid CDMA.* Two or more of the pure CDMA techniques can be used together to combine (known as *hybrid pure CDMA*) the advantages and, it is hoped, to combat their disadvantages. Further, it is possible to combine CDMA with other multiple access methods: contentionless (scheduling) access schemes (FDMA, TDMA), known as hybrid contentionless CDMA (e.g., TDMA/CDMA) [2], contention (random) access scheme (ISMA), known as hybrid contention CDMA (e.g., CDMA/ISMA) [2, 3], and orthogonal frequency division multiplexing (OFDM), known as hybrid OFDM/CDMA (e.g., MC-CDMA) [2]. Multicarrier (MC)-CDMA and multitone (MT)-CDMA are introduced in Chapter 8.



**Figure 7.3** Classification of CDMA.

In the next section, the above-mentioned pure CDMA modulation techniques are used to show the multiple access capability of CDMA. The remainder of the chapters, however, mainly concentrate on direct-sequence (DS)-CDMA and its related subjects.

### 7.3.1 Pure CDMA

We can classify CDMA protocols in two different ways: by *concept* or by *modulation* method. The first classification gives us two protocol groups: *averaging systems* and *avoidance systems*. The averaging systems reduce the interference by averaging the interference over a wide time interval. The avoidance systems reduce the interference by avoiding it for a large part of the time.

Classifying by modulation gives us five protocols: direct-sequence (or pseudo-noise), frequency- and time-hopping protocols based on chirp modulation and hybrid methods. Of these, the first (DS) is an averaging CDMA protocol while the hybrid protocols can be averaging protocols depending on whether DS is used as part of the hybrid method. All the other protocols are of the avoidance type. Table 7.2 summarizes both ways of classification.

**Table 7.2**  
Classifying CDMA protocols.

	DS	TH	FH	Chirp	Hybrid
Averaging	x				x
Avoidance		x	x	x	x

*Direct-sequence.* In DS-CDMA, the modulated information-bearing signal (the data signal) is directly modulated by a digital, discrete-time, discrete-valued code signal. The data signal can be either an analog signal or a digital one. In most cases it is a digital signal. In the case of a digital signal, the data modulation is often omitted and the data signal is directly multiplied by the code signal and the resulting signal modulates the wideband carrier. It is from this direct multiplication that the DS-CDMA gets its name.

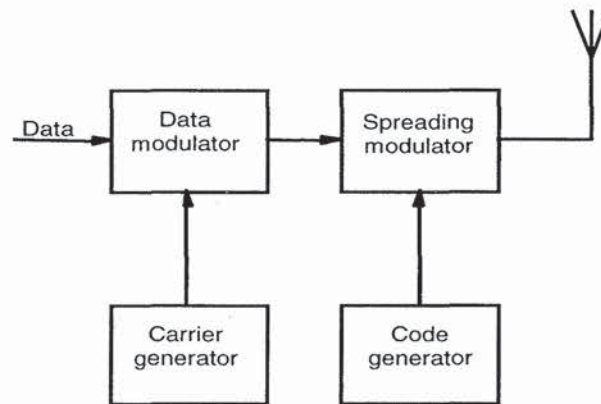


**Figure 7.4** Block diagram of a DS-SS transmitter.

Figure 7.4 gives a block diagram of a DS-CDMA transmitter. The binary data signal modulates an RF carrier. The modulated carrier is then modulated by the code signal. This code signal consists of a number of code bits called “chips” that can be either +1 or  $-1$ . To obtain the desired spreading of the signal, the chip rate of the code signal must be much higher than the chip rate of the information signal. For the spreading modulation, various modulation techniques can be used, but usually some form of phase-shift keying (PSK) like binary phase-shift keying (BPSK), differential binary phase-shift keying (D-BPSK), quadrature phase-shift keying (QPSK), or minimum-shift keying (MSK) is employed.

If we omit the data modulation and use BPSK for the code modulation, we attain the block diagram given in Figure 7.5. The DS-SS signal resulting from this transmitter is shown in Figure 7.6. The rate of the code signal is called the *chip rate*; one chip denotes one symbol when referring to spreading code signals. In this figure, 10 code chips per information symbol are transmitted (i.e., the code chip rate is 10 times the data rate), so the processing gain is equal to 10.



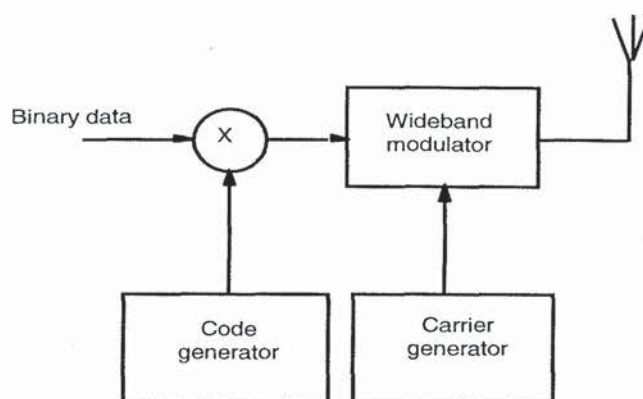


**Figure 7.5** Modified block diagram of a DS-SS transmitter.

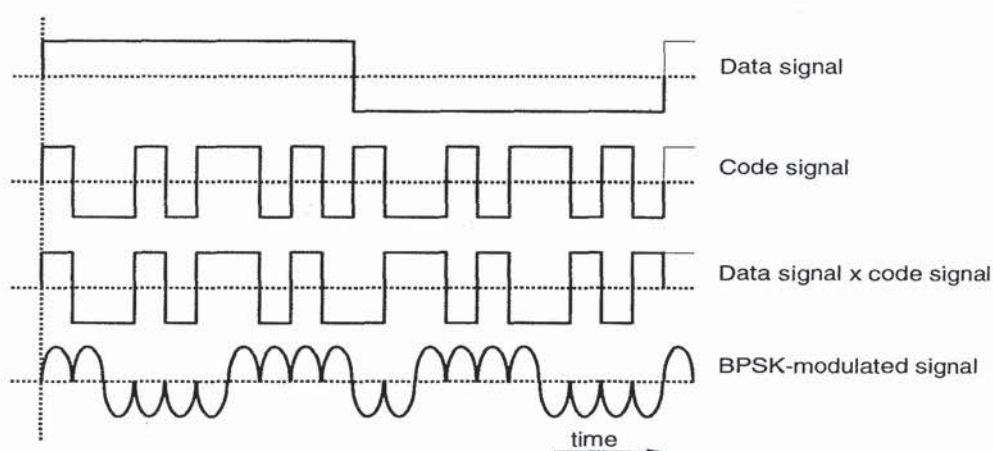


**Figure 7.6** Generation of a BPSK-modulated spread-spectrum signal.

After transmission of the signal, the receiver (shown in Figure 7.7) despreads the spread-spectrum signal using a locally generated code sequence. To be able to perform the despreading operation, the receiver must not only know the code sequence used to spread the signal, but the codes of the received signal and the locally generated code must also be synchronized. This synchronization must be accomplished at the beginning of the reception and maintained until the whole signal has been received. The code synchronization/tracking block performs this operation. After despreading, a data-modulated signal results, and after demodulation, the original data can be recovered.

The previous section mentioned a number of advantages of spread-spectrum signals. The most important of those properties from the viewpoint of CDMA is the multiple access capability, the multipath interference rejection, the narrowband interference rejection, and with respect to secure/private communication, the LPI. We explain these four properties for the case of DS-CDMA.

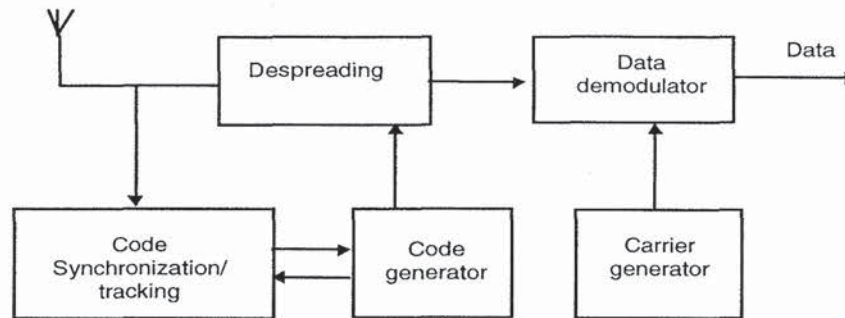


Figure 7.7 Receiver of a DS-SS signal.

*Multiple access.* If multiple users use the channel at the same time, multiple DS signal will overlap in time and frequency. At the receiver, despreading is used to remove the spreading code. This operation concentrates the power of the desired user in the information bandwidth. If the cross-correlations between the code of the desired user and the codes of the interfering users are small, coherent detection will only put a small part of the power of the interfering signals into the information bandwidth.

*Multipath interference.* If the code sequence has an ideal autocorrelation function, then the autocorrelation function is zero outside the interval  $[-T_c, T_c]$ , where  $T_c$  is the chip duration. This means that if the desired signal and a version that is delayed for more than  $2T_c$  are received, despreading will treat the delayed version as an interfering signal, putting only a small part of the power in the information bandwidth.

*Narrowband interference.* The coherent detection at the receiver involves a multiplication of the received signal by a locally generated code sequence. As we saw at the transmitter, however, multiplying a narrowband signal with a wideband code sequence spreads the spectrum of the narrowband signal so that its power in the information bandwidth decreases by a factor equal to the processing gain.

*LPI.* Because the DS signal uses the whole signal spectrum all the time, it will have a very low transmitted power per hertz. This makes it very difficult to detect a DS signal.

Apart from the above-mentioned properties, DS-CDMA has a number of other specific properties that we can divide into advantageous (+) and disadvantageous (–) behavior:

- + The generation of the coded signal is easy to implement. It can be performed by a simple multiplication.
- + Because only one carrier frequency has to be generated, the frequency synthesizer (carrier generator) is simple.
- + No synchronization among the users is necessary.
- It is difficult to acquire and maintain the synchronization of the locally generated code signal and the received signal. Synchronization has to be kept within a fraction of the chip time.

- For correct reception, the synchronization error of locally generated code sequence and the received code sequence must be very small, a fraction of the chip time. This, combined with the nonavailability of large contiguous frequency bands, practically limits the bandwidth to 10 to 20 MHz.
- The power received from users close to the base station is much higher than that received from users further away. Because a user continuously transmits over the whole bandwidth, a user close to the base constantly creates a lot of interference for users far from the base station, making their reception impossible. This near-far effect can be solved by applying a power control algorithm so that all users are received by the base station with the same average power. This control, however, proves to be quite difficult because of feedback delays, imperfect power estimates, errors in the feedback channel, and traffic conditions.

*Frequency-hopping.* In frequency-hopping CDMA, the carrier frequency of the modulated information signal is not constant but changes periodically. During time intervals  $T$ , the carrier frequency remains the same, but after each time interval, the carrier hops to another (or possibly the same) frequency. The hopping pattern is decided by the spreading code. The set of available frequencies the carrier can attain is called the *hop-set*.

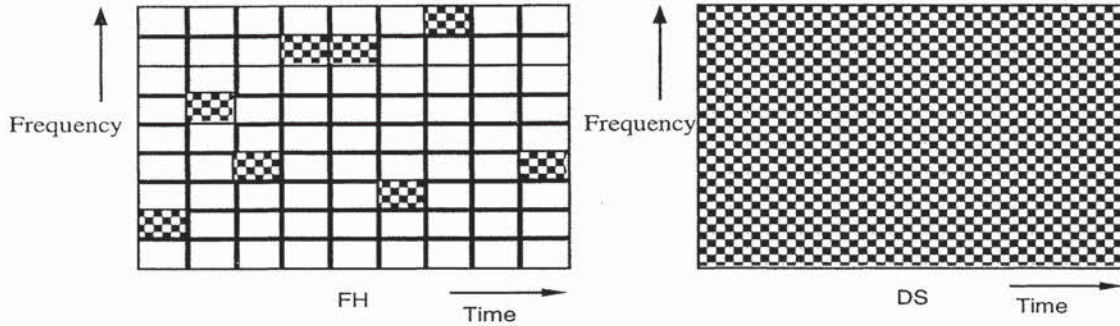
The frequency occupation of an FH-SS system differs considerably from a DS-SS system. A DS system occupies the whole frequency band when it transmits, whereas an FH system uses only a small part of the bandwidth when it transmits, but the location of this part differs in time.

Figure 7.8 illustrates the difference between the FH-SS and the DS-SS frequency usage. Suppose an FH system is transmitting in frequency band 2 during the first time period. A DS system transmitting in the same time period spreads its signal power over the whole frequency band so the power transmitted in frequency band 2 will be much less than that of the FH system. The DS system transmits in frequency band 2 during all time periods, however, while the FH system only uses this band part of the time. On average, both systems transmit the same power in the frequency band.

Figure 7.9 gives the block diagram for an FH-CDMA system. The data signal is baseband modulated. Using a fast frequency synthesizer that is controlled by the code signal, the carrier frequency is converted up to the transmission frequency.

The inverse process takes place at the receiver. Using a locally generated code sequence, the received signal is converted down to the baseband. The data are recovered after (baseband) demodulation. The synchronization/tracking circuit ensures that the hopping of the locally generated carrier synchronizes to the hopping pattern of the received carrier so that correct despreading of the signal is possible.

Within frequency-hopping CDMA, a distinction is made based on the hopping rate of the carrier. If the hopping rate is (much) greater than the symbol rate, the modulation is considered to be *fast frequency-hopping (F-FH)*. In this case, the carrier frequency changes a number of times during the transmission of one symbol, so that



**Figure 7.8** Time/frequency occupancy of FH and DS signals.

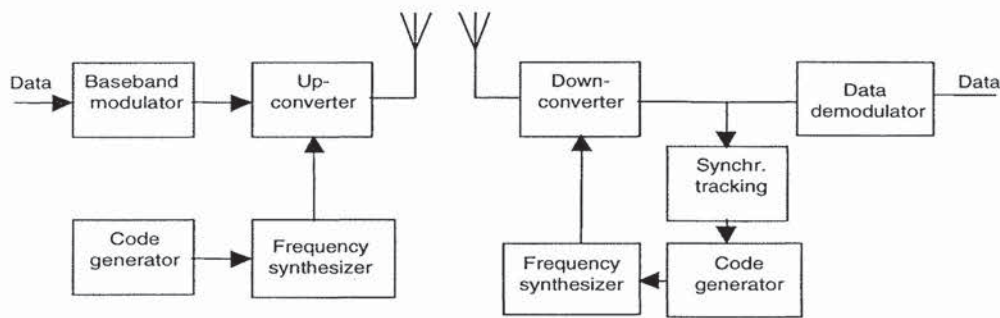


**Figure 7.9** Block diagram of an FH-CDMA transmitter and receiver.

one bit is transmitted at different frequencies. If the hopping rate is (much) smaller than the symbol rate, it is *slow frequency-hopping (S-FH)*. In this case, multiple symbols are transmitted at the same frequency.

The occupied bandwidth of the signal on one of the hopping frequencies depends not only on the bandwidth of the information signal, but also on the shape of the hopping signal and the hopping frequency. If the hopping frequency is much smaller than the information bandwidth (which is the case in slow frequency-hopping), then the information bandwidth is the main factor that decides the occupied bandwidth. If, however, the hopping frequency is much greater than the information bandwidth, the pulse shape of the hopping signal decides the occupied bandwidth at one hopping frequency. If this pulse shape is very abrupt (resulting in very abrupt frequency changes), the frequency band is very broad, limiting the number of hop frequencies. If we make sure that the frequency changes are smooth, the frequency band at each hopping frequency is about  $1/T_h$  times the frequency bandwidth, where  $T_h$  is equal to the hopping frequency. We can make the frequency changes smooth by decreasing the transmitted power before a frequency hop and increasing it again when the hopping frequency has changed.

As has been done for DS-CDMA, we discuss the properties of FH-CDMA with respect to multiple access capability, multipath interference rejection, narrowband interference rejection, and probability of interception.

*Multiple access.* It is easy to visualize how the F-FH and S-FH CDMA obtain their multiple access capability. In the F-FH, one symbol is transmitted in different frequency bands. If the desired user is the only one to transmit in most of the frequency bands, the received power of the desired signal is much higher than the interfering power and the signal will be received correctly.

In the S-FH, multiple symbols are transmitted at one frequency. If the probability of other users transmitting in the same frequency band is low enough, the desired user is received correctly most of the time. For those times that interfering users transmit in the same frequency band, error-correcting codes are used to recover the data transmitted during that period.

*Multipath interference.* In the F-FH CDMA the carrier frequency changes a number of times during the transmission of one symbol. Thus, a particular signal frequency is modulated and transmitted on a number of carrier frequencies. The multipath effect is different at the different carrier frequencies. As a result, signal frequencies that are amplified at one carrier frequency are attenuated at another carrier frequency and vice versa. At the receiver, the responses at the different hopping frequencies are averaged, thus reducing the multipath interference. Because usually noncoherent combining is used, this is not as effective as the multipath interference rejection in a DS-CDMA system, but it still gives quite an improvement.

*Narrowband interference.* Suppose a narrowband signal is interfering on one of the hopping frequencies. If there are  $G_p$  hopping frequencies (where  $G_p$  is the processing gain), the desired user (on average) uses the hopping frequency where the interferer is located  $1/G_p$  percent of the time. The interference is therefore reduced by a factor  $G_p$ .

*LPI.* The difficulty in intercepting an FH signal lies not in its low transmission power. During a transmission, it uses as much power per hertz as a continuous transmission. But the frequency at which the signal is going to be transmitted is unknown, and the duration of the transmission at a particular frequency is quite small. Therefore, although the signal is more readily intercepted than a DS signal, it is still a difficult task to perform.

Apart from the above-mentioned properties, the FH-CDMA has a number of other specific properties that we can divide into advantageous (+) and disadvantageous (−) behavior:

- + Time synchronization is much easier with FH-CDMA than with DS-CDMA. FH-CDMA synchronization has to be within a fraction of the hop time. Because spectral spreading is not obtained by using a very high hopping frequency but by using a large hop-set, the hop time will be much longer than the chip time of a DS-CDMA system. Thus, an FH-CDMA system allows a larger synchronization error.

- + The different frequency bands that an FH signal can occupy do not have to be contiguous because we can make the frequency synthesizer easily skip over certain parts of the spectrum. Combined with the easier synchronization, this allows much higher spread-spectrum bandwidths.
- + The probability of multiple users transmitting in the same frequency band at the same time is small. A user transmitting far from the base station is received by it even if users close to the base station are transmitting, as those users are probably transmitting at different frequencies. Thus, the near-far performance is much better than that of DS.
- + Because of the larger possible bandwidth a FH system can employ, it offers a higher possible reduction of narrowband interference than a DS system.
- A sophisticated frequency synthesizer is necessary.
- An abrupt change of the signal when changing frequency bands leads to an increase in the occupied spectrum. To avoid this, the signal has to be ramped up and down when changing frequency.
- Coherent demodulation is difficult because of the problems in maintaining a coherent reference phase between hops.

*Time-hopping.* In time-hopping CDMA, the data signal is transmitted in rapid bursts at time intervals determined by the code assigned to the user. The time axis is divided into frames, and each frame is divided into  $M$  timeslots. During each frame, the user transmits in one of the  $M$  timeslots. Which of the  $M$  timeslots is transmitted depends on the code signal assigned to the user. Because a user transmits all of its data in one, instead of  $M$  timeslots, the frequency it needs for its transmission has increased by a factor  $M$ . A block diagram of a TH-CDMA system is given in Figure 7.10.

Figure 7.11 shows the time-frequency plot of the TH-CDMA systems. Comparing Figure 7.11 with Figure 7.10, we see that the TH-CDMA uses the whole wideband spectrum for short periods instead of parts of the spectrum all of the time.

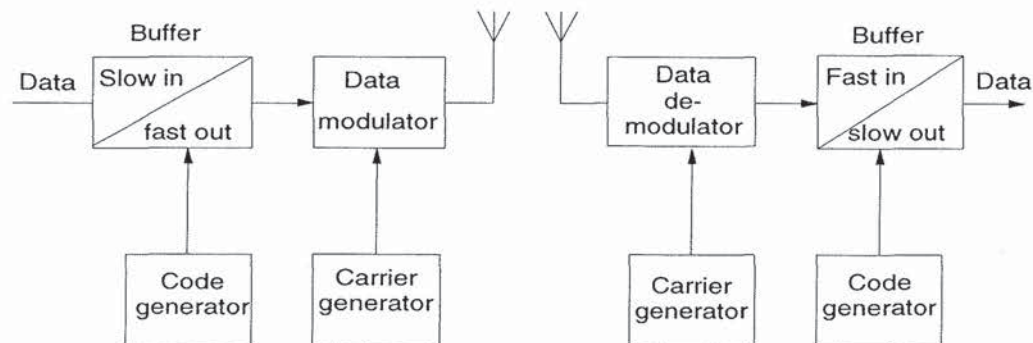


**Figure 7.10** Block diagram of a TH-CDMA transmitter and receiver.

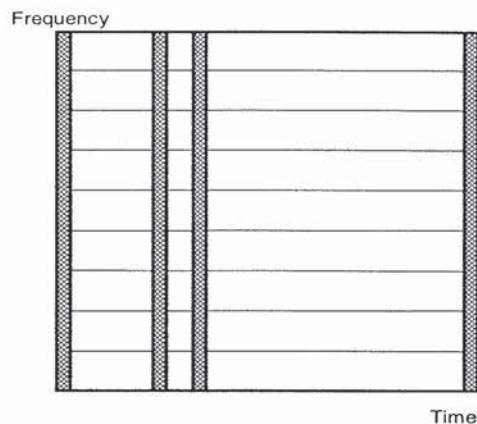


**Figure 7.11** Time-frequency plot of TH-CDMA.

Following the same procedure as for the previous CDMA schemes, we discuss the properties of TH-CDMA with respect to multiple access capability, multipath interference rejection, narrowband interference rejection, and probability of interception.

*Multiple access.* The multiple access capability of TH-SS signals is acquired in the same manner as that of the FH-SS signals; namely, by making the probability of users' transmissions in the same frequency band at the same time small. In the case of time-hopping, all transmissions are in the same frequency band, so the probability of more than one transmission at the same time must be small. This is again achieved by assigning different codes to different users. If multiple transmissions do occur, error-correcting codes ensure that the desired signal can still be recovered.

If there is synchronization among the users, and the assigned codes are such that no more than one user transmits at a particular slot, then the TH-CDMA reduces to a TDMA scheme where the slot in which a user transmits is not fixed but changes from frame to frame.

*Multipath interference.* In the TH-CDMA, a signal is transmitted in reduced time. The signaling rate, therefore, increases, and dispersion of the signal now leads to overlap of adjacent bits. Therefore, no advantage is gained with respect to multipath interference rejection.

*Narrowband interference.* A TH-CDMA signal is transmitted in reduced time. This reduction is equal to  $1/G_p$ , where  $G_p$  is the processing gain. At the receiver we receive only an interfering signal during the reception of the desired signal. Thus, we receive only the interfering signal  $1/G_p$  percent of the time, reducing the interfering power by a factor  $G_p$ .

*LPI.* With TH-CDMA, the frequency at which a user transmits is constant but the times at which a user transmits are unknown, and the durations of the transmissions are very short. Particularly when multiple users are transmitting, this makes it difficult for an

intercepting receiver to distinguish the beginning and end of a transmission and to decide which transmissions belong to which user.

Apart from the above-mentioned properties, the TH-CDMA has a number of other specific properties that we can divide into advantageous (+) and disadvantageous (−) behavior:

- + Implementation is simpler than that of FH-CDMA, as no relatively complex hopping frequency synthesizer is required.
- + TH-CDMA is a very useful method when the transmitter is average-power limited but not peak-power limited because the data are transmitted in short bursts at high power.
- + As with the FH-CDMA, the near-far problem is much less of a problem as most of the time a terminal far from the base station transmits alone and is not hindered by transmissions from stations close by.
- − It takes a long time before the code is synchronized, and the time in which the receiver has to perform the synchronization is short.
- − If multiple transmissions occur, a large number of data bits are lost, so a good error-correcting code and data interleaving are necessary.

*Hybrid-pure-CDMA.* The hybrid-pure-CDMA systems include all CDMA systems that employ a combination of two or more of the above-mentioned spread-spectrum modulation techniques or a combination of CDMA with some other multiple access technique. By combining the basic spread-spectrum modulation techniques, we have four possible hybrid systems: DS/FH, DS/TH, FH/TH, and DS/FH/TH; and by combining CDMA with TDMA or multicarrier modulation we have two more: CDMA/TDMA and MC-CDMA.

The idea of the hybrid system is to combine the specific advantages of each of the modulation techniques. If we take, for example, the combined DS/FH system, we have the advantage of the anti-multipath property of the DS system combined with the favorable near-far operation of the FH system. Of course, the disadvantage lies in the increased complexity of the transmitter and receiver. For illustration purposes, we give a block diagram of a combined DS/FH CDMA transmitter in Figure 7.12.

The data signal is first spread using a DS code signal. The spread signal is then modulated on a carrier whose frequency hops according to another code sequence. A code clock ensures a fixed relation between the two codes.



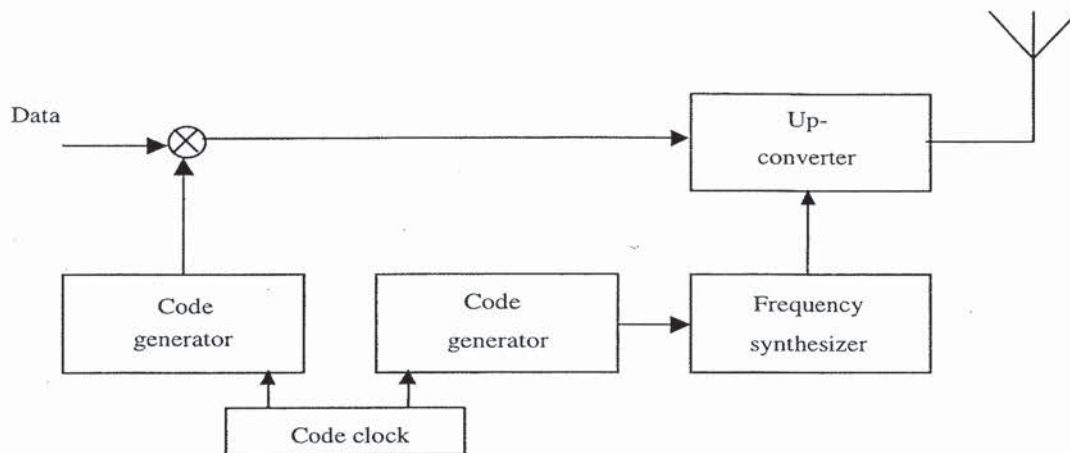


Figure 7.12 Hybrid DS-FH transmitter.

## 7.4 BASIC DS-CDMA ELEMENTS

In this section, we review the fundamental elements for understanding DS-CDMA and its application into third-generation systems; namely, RAKE receiver, power control, soft handover, interfrequency handover, and multiuser detection.

### 7.4.1 RAKE Receiver

A DS spread-spectrum signal waveform is well matched to the multipath channel. In a multipath channel, the original transmitted signal reflects from obstacles such as buildings and mountains, and the receiver receives several copies of the signal with different delays. If the signals arrive more than one chip apart from each other, the receiver can resolve them. Actually, from each multipath signal's point of view, other multipath signals can be regarded as interference and are suppressed by the processing gain. A further benefit is obtained, however, if the resolved multipath signals are combined using a *RAKE receiver*. Thus, the signal waveform of CDMA signals facilitates use of multipath diversity. Expressing the same phenomenon in the frequency domain means that the bandwidth of the transmitted signal is larger than the coherence bandwidth of the channel and the channel is frequency selective (i.e., only part of the signal is affected by the fading).

A RAKE receiver consists of correlators, each receiving a multipath signal. After despreading by correlators, the signals are combined using, for example, maximal ratio combining. Because the received multipath signals are fading independently, diversity order and thus performance are improved. Figure 7.13 illustrates the principle

of a RAKE receiver. After spreading and modulation, the signal is transmitted and it passes through a multipath channel, which can be modeled by a tapped delay line (i.e., the reflected signals are delayed and attenuated in the channel). In Figure 7.13 we have three multipath components with different delays ( $\tau_1$ ,  $\tau_2$ , and  $\tau_3$ ) and attenuation factors ( $a_1$ ,  $a_2$ , and  $a_3$ ), each corresponding to a different propagation path. The RAKE receiver has a receiver finger for each multipath component. In each finger, the received signal is correlated by the spreading code, which is time-aligned with the delay of the multipath signal. After despreading, the signals are weighted and combined. In Figure 7.13, maximal ratio combining is used; that is, each signal is weighted by the (conjugated) path gain (or path attenuation factor). Because of transmitter or receiver movements, the scattering environment will change, and thus, the delays and attenuation factors change as well. Therefore, it is necessary to measure the tapped-delay-line profile and to reallocate RAKE fingers whenever the delays have changed by a significant amount. Small-scale changes, less than one chip, are taken care of by a code tracking loop, which tracks the time delay of each multipath signal.

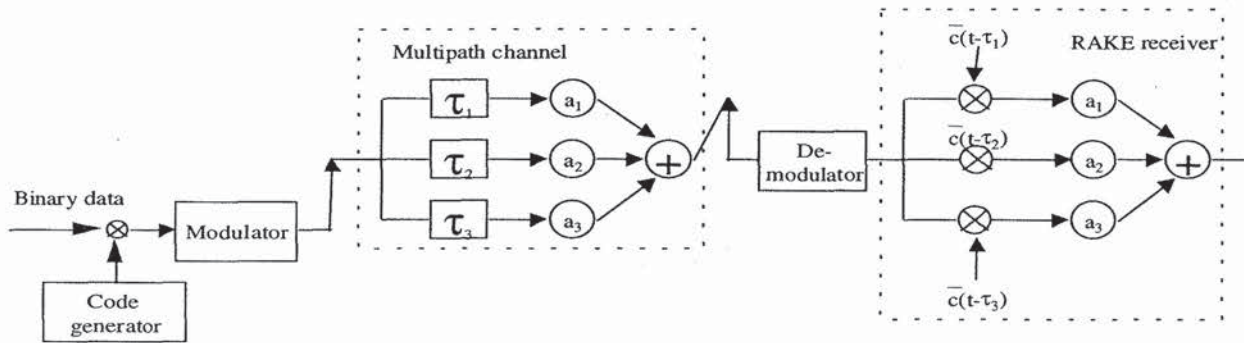


Figure 7.13 Principle of RAKE receiver.

#### 7.4.2 Power Control

In the uplink of a DS-CDMA system, the requirement for power control is the most serious negative point. The power control problem arises because of the multiple access interference. All users in a DS-CDMA system transmit the messages by using the same bandwidth at the same time, and therefore users interfere with one another. Because of the propagation mechanism, the signal received by the base station from a user terminal close to the base station is stronger than the signal received from another terminal located at the cell boundary. Hence, the distant users are dominated by the close user. This is called the *near-far effect*. To achieve a considerable capacity, all signals, irrespective of distance, should arrive at the base station with the same mean power. A solution to this problem is power control, which attempts to achieve a constant received mean power for each user. Therefore, the performance of the transmitter power control (TPC) is one of the several dependent factors when deciding on the capacity of a DS-CDMA system.

In contrast to the uplink, in the downlink all signals propagate through the same channel and thus are received by a mobile station with equal power. Therefore, no power control is required to eliminate the near-far problem. Power control is still desirable, however, to minimize the interference to other cells. Ideally, you want to transmit just enough power to each user so that all users experience the same signal-to-interference ratio at the minimum required level. Unfortunately, power control in the DS-CDMA downlink actually creates a near-far problem. Therefore, the power for all users cannot be much smaller than that for the most remote user, resulting in more interference to other cells than in the case of ideal power control.

In addition to being useful against interfering users, power control improves the performance of DS-CDMA against fading channel by compensating the fading dips. If it followed the channel fading perfectly, power control would turn a fading channel into an AWGN channel by eliminating the fading dips completely.

Two types of power control principles exist: *open loop* and *closed loop*. In open-loop power control, the transmitter measures the interference conditions from the channel and adjusts the transmission power accordingly to meet the desired frame error rate (FER) target. Because the fast fading does not correlate between uplink and downlink, however, open loop power control will achieve the right power target only on average. Therefore, closed-loop power control is required. In closed-loop power control, the receiver measures the signal-to-interference ratio (SIR) and sends commands to the transmitter on the other end to adjust the transmission power.

### 7.4.3 Soft Handover

In soft handover, a mobile station is connected to more than one base station simultaneously. Soft handover is used in CDMA to reduce the interference into other cells and to improve performance through macrodiversity. Softer handover is a soft handover between two sectors of a cell.

Neighboring cells of a cellular system using either FDMA or TDMA do not use the same frequencies. The spatial separation between cells using the same frequencies is determined by the *frequency reuse factor*, which is the ratio of the total number of cells and the number of cells that use one particular frequency. Because of the processing gain, such spatial separation is not needed in CDMA, and a frequency reuse factor of one can be used. Usually, a mobile station performs a handover when the signal strength of a neighboring cell exceeds the signal strength of the current cell with a given threshold. This is called *hard handover*. To avoid excessive interference, an instantaneous handover from the current cell to the new cell is required when the signal strength of the new cell exceeds the signal strength of the current cell. This is not, however, feasible in practice because of rapid fluctuations of the signal strength. The handover mechanism should always allow the mobile station to connect into a cell, which it receives with the highest power (i.e., with the lowest path loss). Because in soft handover the mobile station is connected to either two or more base stations, its

transmission power can be controlled according to the cell, which the mobile station receives with the highest signal strength. A mobile station enters the soft handover state when the signal strength of a neighboring cell exceeds a certain threshold but is still below the current base station's signal strength.

Fortunately, the signal structure of CDMA is well suited for the implementation of soft handover. This is because in the uplink, two or more base stations can receive the same signal because of the reuse factor of one; and in the downlink, the mobile station can coherently combine the signals from different base stations since it sees them as just additional multipath components—provided that the base stations are time-synchronized to within a few chip intervals. This provides an additional benefit called macro diversity (i.e., the diversity gain provided by the reception of one or more additional signals). A separate pilot channel is usually used for the signal strength measurements for handover purposes.

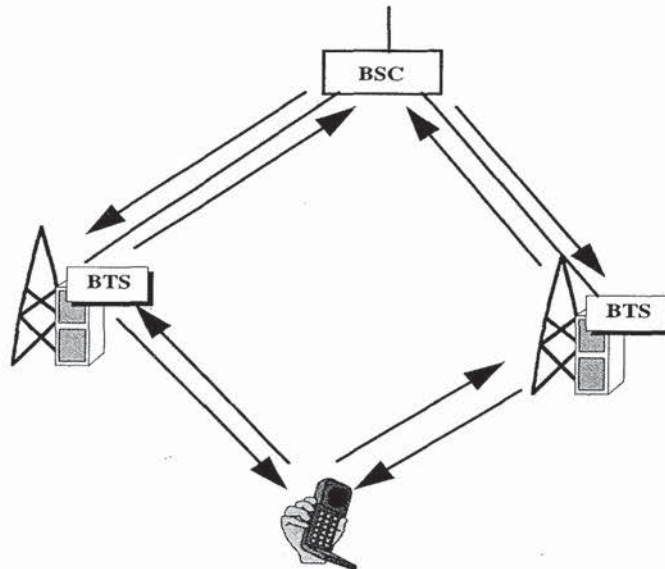


**Figure 7.14** Principle of soft handover with two base station transceivers (BTS).

In the downlink, however, soft handover creates more interference to the system because the new base station now transmits an additional signal for the mobile station. It is possible that the mobile station cannot collect all of the energy that the base station transmits because of a limited number of RAKE fingers. Thus, the gain of soft handover in the downlink depends on the gain of macrodiversity and the loss of performance due to increased interference.

Figure 7.14 illustrates the soft handover principle with two base stations involved. In the uplink the mobile station signal is received by the two base stations, which, after demodulation and combining, pass the signal forward to the combining

point, typically to the base station controller (BSC). In the downlink, the same information is transmitted through both base stations, and the mobile station receives the information from two base stations as separate multipath signals and can therefore combine them.

#### 7.4.4 Interfrequency Handover

The third-generation CDMA networks will have multiple frequency carriers in each cell, and a hot-spot cell could have a larger number of frequencies than neighboring cells. Further, in hierarchical cell structures, microcells will have a different frequency than the macrocell overlaying the microcells. Therefore, an efficient procedure is needed for a handover between different frequencies. A blind handover used by second generation CDMA does not result in an adequate call quality. Instead, the mobile station has to be able to measure the signal strength and quality of another carrier frequency, while still maintaining the connection in the current carrier frequency. Because a CDMA transmission is continuous, there are no idle slots for the interfrequency measurements as in the TDMA-based systems. Therefore, compressed mode and dual receiver have been proposed as a solution to interfrequency handover [22]. In the compressed mode, measurement slots are created by transmitting the data of a frame, for example, with a lower spreading ratio during a shorter period, and the rest of the frame is used for the measurements on other carriers. The dual receiver can measure other frequencies without affecting the reception of the current frequency.

#### 7.4.5 Multiuser Detection

The current CDMA receivers are based on the RAKE receiver principle, which considers other users' signals as interference. In an optimal receiver, however, all signals would be detected jointly or interference from other signals would be removed by subtracting them from the desired signal. This is possible because the interference is deterministic and not random.

The capacity of a DS-CDMA system using RAKE receiver is interference limited. In practice this means that when a new user, or interferer, enters the network, other users' service quality degrades. The more the network can resist interference the more users can be served. Multiple access interference that disturbs a base or mobile station is a sum of both intra- and intercell interference.

*Multiuser detection* (MUD), also called joint detection and interference cancellation (IC), can reduce the effect of multiple access interference, and hence increases the system capacity. In the first place, MUD is considered to cancel only the intracell interference, meaning that in a practical system the capacity will be limited by the efficiency of the algorithm and the intercell interference.

In addition to capacity improvement, MUD alleviates the near-far problem typical to DS-CDMA systems. A mobile station close to a base station may block the whole cell traffic by using too high a transmission power. If this user is detected first and subtracted from the input signal, the other users do not see the interference.

Because optimal multiuser detection is very complex and difficult to implement in practice for any reasonable number of users, a number of suboptimal multiuser and interference cancellation receivers have been developed. The suboptimal receivers can be divided into two main categories: *linear detectors* and *interference cancellation*. Linear detectors apply a linear transform to the outputs of the matched filters that are trying to remove the multiple access interference (i.e., the interference due to correlations among user codes). Examples of linear detectors are decorrelator and linear minimum mean square error (LMMSE) detectors. In interference cancellation, multiple access interference is first estimated and then subtracted from the received signal. Parallel interference cancellation (PIC) and successive (serial) interference cancellation (SIC) are examples of interference cancellation.

## REFERENCES

- [1] Ojanperä, T., and R. Prasad, "*Wideband CDMA for Third Generation Mobile Communications*," Norwood, MA: Artech House, 1998.
- [2] Prasad, R., "*Universal Wireless Personal Communications*," Norwood, MA: Artech House, 1998.
- [3] Prasad, R., "*CDMA for Wireless Personal Communications*," Norwood, MA: Artech House, 1996.
- [4] "Special Issue on Spread-Spectrum Communication," *IEEE Transactions on Communications*, Vol. COM-30, May 1982.
- [5] Simon, M. K., J. K. Omura, R. A. Scholtz, and B. K. Levitt, *Spread-Spectrum Communications*, Vol. I, II, III, *Comp. Sci.*, 1985.
- [6] Scholtz, R. A., "The Spread-Spectrum Concept," *IEEE Transactions on Communications*, Vol. COM-25, pp. 74 – 55, Aug. 1977.
- [7] Torrieri, D. J., "*Principles of Secure Communication Systems*," Artech House, Norwood, Mass., 1985.
- [8] Cooper, G. R., and C. D. McGillem, "*Modern Communication and Spread-Spectrum*," McGraw-Hill Book Company, New York 1986.
- [9] Glisic, S. G., and P. A. Leppanen (eds.), "*Code Division Multiple Access Communications*," Kluwer Academic Publishers, Boston, MA, 1995.
- [10] Viterbi, A. J., "*CDMA Principles of Spread-Spectrum Communications*," Addison-Wesley Publishing Company, Reading, Mass., 1995.
- [11] Dixon, R. C., "*Spread-Spectrum Systems*," John Wiley & Sons, New York, 1984.

- 
- [12] Glisic, S., and B. Vucetic, "Spread-spectrum CDMA Systems for Wireless Communications," Norwood, MA: Artech House, 1997.
- [13] Glisic, S., and P. Leppänen, "Wireless Communications: TDMA versus CDMA," Boston, MA: Kluwer Academic Publishers, 1997.
- [14] Ojanperä, T., and R. Prasad, "Overview of Air Interface Multiple Access for IMT-2000/UMTS," *IEEE Communications Magazine*, Vol. 36, pp. 82 - 95, Sep. 1998.
- [15] Ojanperä, T., and R. Prasad, "An Overview of Third Generation Wireless Personal Communications: A European Perspective," *IEEE Personal Communications*, Vol. 5, pp. 59 - 65, Dec. 1998.
- [16] Shannon, C. E., "A Mathematical Theory of Communication," *Bell System Technical Journal*, Vol. 27, pp. 379 - 423 and 623 - 656, 1948.
- [17] Scholtz, R. A., "The Evolution of Spread-Spectrum Multiple-Access Communications," in *Code Division Multiple Access Communications* (eds.), Kluwer Academic Publishers, Boston, MA, 1995.
- [18] Glisic, S. G., and P. A. Leppänen, "A conversation with Claude Shannon," *IEEE Communications Magazine*, Vol. 22, No. 5, pp. 123 - 126, May 1984.
- [19] Cooper, G. R., and R. W. Nettleton, "A spread-spectrum technique for high-capacity mobile communications," *IEEE Trans. Veh. Tech.*, Vol. 27, No. 4, pp. 264 - 275, Nov. 1978.
- [20] Verdu, S., "Minimum Probability of Error for Asynchronous Gaussian Multiple Access," *IEEE Trans. on IT.*, Vol. IT-32, No. 1, pp. 85 - 96, Jan. 1986.
- [21] Ojanperä, T., "Overview of Research Activities for Third Generation Mobile Communication," *Wireless Communications TDMA vs. CDMA* (eds.), Kluwer Academic Publishers, Dordrecht, Netherlands, pp. 415 - 446, 1997.
- [22] Gustafsson, M., K. Jamal, and E. Dahlman, "Compressed Mode Techniques for Interfrequency Measurements in a Wide-band DS-SS-CDMA System," *Proceedings of PIMRC'97*, Helsinki, Finland, pp. 23 - 35, Sep. 1997.





## CHAPTER 8

### MULTI - CARRIER CDMA

#### 8.1 INTRODUCTION

Chapter 7 presented an overview of code division multiple access (CDMA). CDMA has been considered a candidate to support multimedia services in mobile communications because it has its own capabilities to cope with the asynchronous nature of multimedia data traffic, to provide higher capacity over conventional access schemes such as TDMA and FDMA, and to combat hostile channel frequency selectivity. Direct sequence (DS-) and Frequency hopping (FH-) CDMA systems have been subject to extensive research [1]. The development of a third generation mobile communications system has already been taking place using the wideband CDMA systems [2, 3].

Recently, a new CDMA system based on a combination of CDMA and orthogonal frequency division multiplexing (OFDM) signaling, which is called *Multi-Carrier (MC-) CDMA system*, has been reported in [4–6]. It has gained much attention, because the signal can be easily transmitted and received using the fast fourier transform (FFT) device without increasing the transmitter and receiver complexities and is potentially robust to channel frequency selectivity with a good frequency use efficiency.

So far, many reports have been dedicated for the bit-error ratio (BER) analysis of MC-CDMA system and the BER comparison between MC-CDMA and DS-CDMA systems in frequency selective Rayleigh fading channels [7–14]. In these works, “independent fading characteristic at each received path” has been often assumed for the BER analysis of DS-CDMA system, whereas “independent fading characteristic at each received subcarrier” is likewise for the BER analysis of MC-CDMA system. In general, however, fading characteristics among subcarriers are highly correlated, and the subcarrier correlation is uniquely determined by the multipath delay profile of the channel. Therefore, when we discuss BER performance of MC-CDMA systems and compare it with that of other multiple access systems such as DS-CDMA, it is essential

to make a fair assumption for all the systems compared, such as the same channel frequency selectivity and channel time selectivity as well as the same modulation/demodulation format, transmission rate, and processing gain. Further, when we design a MC-CDMA system and discuss the BER performance, it is essential to carefully determine two transmission parameters: the length of guard interval and the number of subcarriers. These significantly affect BER performance.

In Chapter 8, we discuss the advantages and disadvantages of the MC-CDMA system. To focus more attention on the MC-CDMA concept, we introduce a conventional DS-CDMA system for a comparison. The MC-CDMA system inevitably requires linear amplification because it is very sensitive to nonlinear amplification. This requirement could be realizable for base stations, so in this sense, we can say that the MC-CDMA system is well suited for a downlink channel. Therefore, in the BER investigation, we further discuss the downlink performance, although the uplink performance is shown as well. We show the BER performance with four different combining strategies such as orthogonality restoring combining (ORC), equal gain combining (EGC), maximum ratio combining (MRC), and minimum mean square error combining (MMSEC). They are all categorized into *single-user detection scheme* applicable for downlink and uplink channels, however, as shown later, the MC-CDMA uplink performance is still poor even with quasisynchronous scenario.

The chapter is organized as follows. Section 8.2 explains a frequency-selective fast Rayleigh fading channel to carry out the MC-CDMA system design and the BER evaluation. Section 8.3 shows the DS-CDMA and MC-CDMA systems and outlines the four different combining strategies for the MC-CDMA system. Section 8.4 discusses a MC-CDMA design method, namely, how to determine the number of subcarriers and the length of guard interval to minimize the BER for a given channel condition. Section 8.5 shows the theoretical BER lower bounds for both systems and proves their equivalence. Section 8.6 demonstrates the BER performance of MC-CDMA and DS-CDMA schemes in (synchronous) downlink and quasisynchronous uplink channels and discusses the advantages and disadvantages in terms of “bandwidth of transmitted signal spectrum” and “attainable BER performance.” And finally, Section 8.7 draws our conclusions.

## 8.2 CHANNEL MODEL

As a frequency selective fast Rayleigh fading channel, we assume a wide sense stationary uncorrelated scattering (WSSUS) channel [15] with  $L$  received paths in the complex equivalent low-pass time-variant impulse response:

$$h^j(\tau; t) = \sum_{l=1}^L g_l^j(t) \delta(\tau - \tau_l) \quad (8.1)$$

where  $j$  is the user index,  $t$  and  $\tau$  are the time and the delay, respectively,  $\delta(\cdot)$  is the Dirac delta function,  $g_l^j(t)$  is the  $l^{\text{th}}$  path gain for user  $j$  which is a mutually independent complex Gaussian random process with zero mean and variance  $\sigma_l^2$  for different  $l$ , and  $\tau_l$  is the propagation delay for the  $l$ -th path. Figure 8.1 shows the corresponding multipath power delay profile given by (we assume that there is no signal whose propagation delay exceeds the symbol duration)

$$\phi_c^j(\tau) = \frac{1}{2} E[h^{j*}(\tau; t) \cdot h^j(\tau; t)] = \sum_{l=1}^L \sigma_l^2 \delta(\tau - \tau_l) \quad (8.2)$$

where  $E(\cdot)$  is the expectation and  $*$  is the complex conjugate. With (8.2), the RMS (root mean square) delay spread ( $\tau_{RMS}$ ) can be calculated [16].

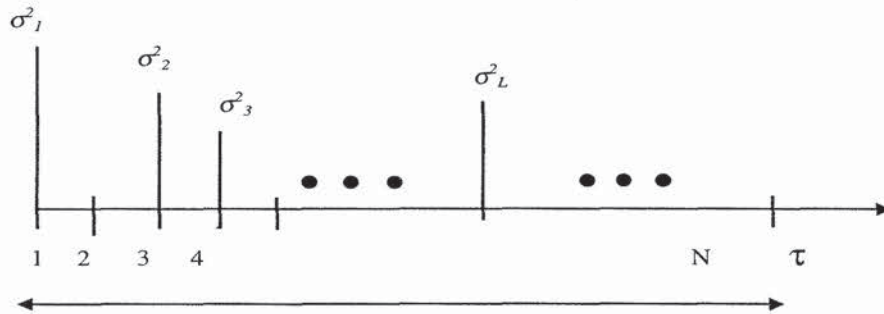


Figure 8.1 Multipath power delay profile.

On the other hand, the channel time selectivity is characterized by the normalized time autocorrelation function [15]:

$$\rho_l^j(\Delta t) = \frac{1}{2\sigma_l^2} E[g_l^j(t + \Delta t) \cdot g_l^{j*}(t)] \quad (8.3)$$

Assuming that an omnidirectional antenna is used at the receiver and the angular distribution of wave arrivals on each path is uniform, the autocorrelation is given by [17]

$$\rho_l^j(\Delta t) = J_0(2\pi f_D \Delta t) \approx 1 - (\pi f_D \Delta t)^2 \quad (f_D \Delta t) \ll 1, \quad (8.4)$$

where  $J_0(\cdot)$  and  $f_D$  are the zero-order Bessel function of the first kind and the maximum Doppler frequency, respectively. Note that, for different  $j$ , the path gains  $\{g_l^j(t)\}$  are independent, identically distributed (i.i.d.) in an uplink channel and identically distributed in a downlink channel.

### 8.3 DS-CDMA AND MC-CDMA SYSTEMS

The OFDM scheme is robust to frequency-selective fading; however, it has some disadvantages such as difficulty in subcarrier synchronization and sensitivity to frequency offset and nonlinear amplification, which result from the fact that it is composed of many subcarriers with their overlapping power spectra and exhibits a non-constant nature in its envelope, see Chapters 4 and 6, respectively. In contrast to this, DS-CDMA is quite robust to frequency offsets and nonlinear distortion. The combination of OFDM signaling and CDMA scheme has one major advantage, however, in that it can lower the symbol rate in each subcarrier so that a longer symbol duration makes it easier to quasisynchronize the transmissions [18]. For instance, in [19], a multicarrier-based DS-CDMA scheme is proposed for a quasisynchronous system. In this chapter, we assume a quasisynchronous uplink channel, in addition to a (synchronous) downlink channel. We discuss the BER performance of MC-CDMA and DS-CDMA systems in multipath fading channels. To focus attention on the BER variations by different combining strategies, we assume a perfect subcarrier synchronization with no frequency offset and no nonlinear distortion and perfect subcarrier amplitude/phase estimation for MC-CDMA system. On the other hand, for the DS-CDMA system, we assume a perfect carrier synchronization and perfect path gain estimation.

#### 8.3.1 DS-CDMA System

Figure 8.2(a) shows the DS-CDMA transmitter for the  $j^{\text{th}}$  user with binary PSK modulation/coherent (CBPSK) format. The complex equivalent lowpass transmitted signal is written as

$$s_{DS}^j(t) = \sum_{i=-\infty}^{+\infty} \sum_{k=0}^{K_{DS}-1} b_j(i) c_j(k) p_c(t - kT_c - iT_s) \quad (8.5)$$

where,  $b_j(i)$  and  $c_j(k)$  are the  $i^{\text{th}}$  information bit and the  $k^{\text{th}}$  chip of the spreading code with length  $K_{DS}$  and chip duration  $T_c$ , respectively,  $T_s (= 1/R)$  is the symbol duration ( $R$  is the symbol rate), and  $p_c(t)$  is the chip pulse waveform. For instance, when a rectangular pulse is used,  $p_c(t)$  is given by

$$p_c(t) = \begin{cases} 1 & (0 \leq t \leq T_c) \\ 0 & (\text{otherwise}) \end{cases} \quad (8.6)$$

The mainlobe bandwidth of the transmitted signal spectrum for a rectangular pulse waveform is given by

$$B_{DS} = 2K_{DS}/T_s \quad (8.7)$$

and for the Nyquist pulse waveform with rolloff factor of  $\alpha$  (see Figure 8.2(b)),

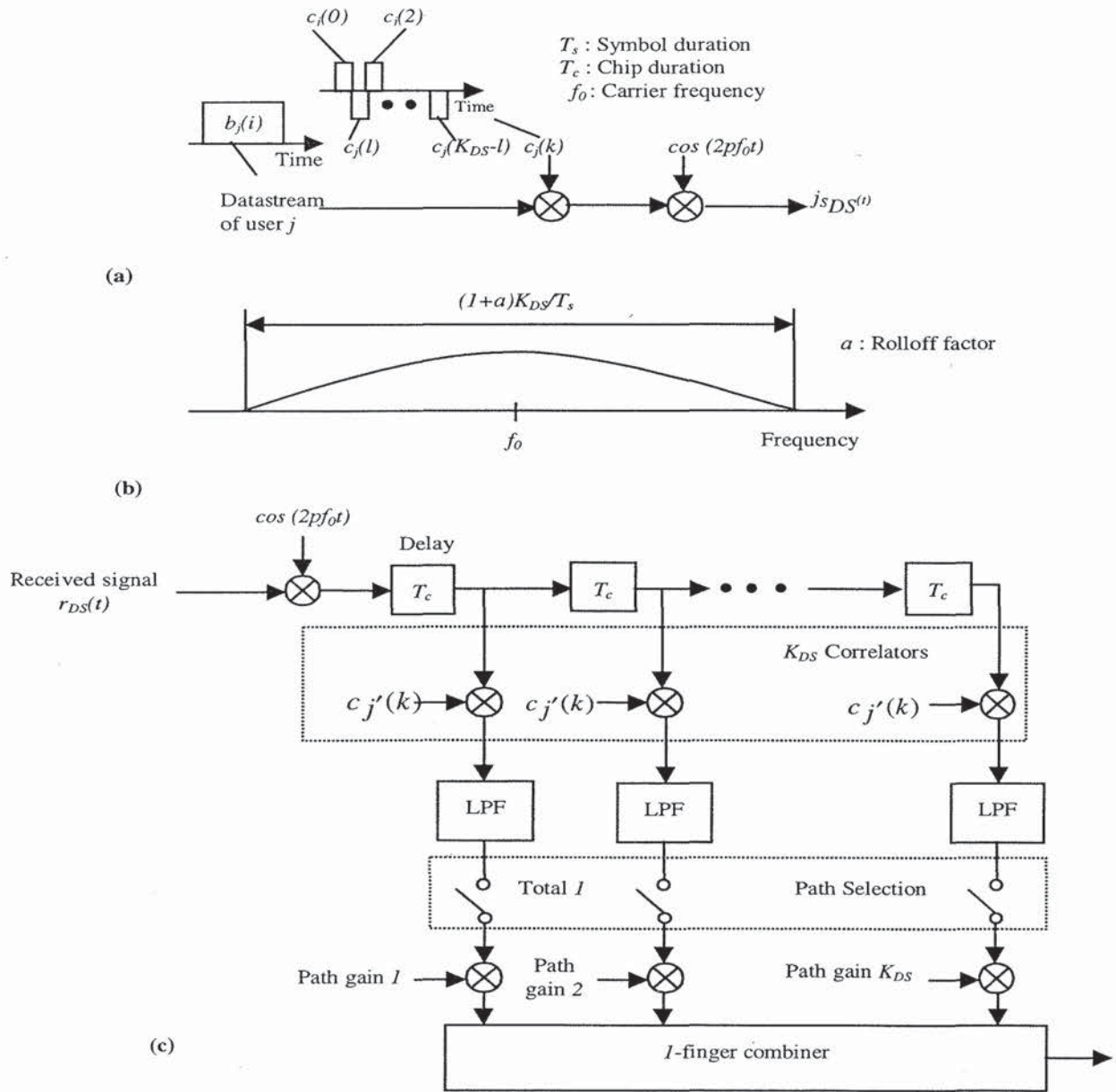
$$B_{DS} = (1+\alpha)K_{DS}/T_s \quad (0 \leq \alpha \leq 1.0). \quad (8.8)$$

Figure 8.2(c) shows the  $I$ -finger DS-CDMA RAKE receiver for the  $j^{\text{th}}$  user. The received signal through the channel given by (8.1) is written as

$$\begin{aligned} r_{DS}(t) &= \sum_{j=1}^J \int_{-\infty}^{+\infty} s_{DS}^j(t-\tau) \otimes h^j(\tau;t) d\tau + n(t) \\ &= \sum_{l=1}^L \sum_{j=1}^J s_{DS}^j(t-\tau_l) g_l^j(t) + n(t) \end{aligned} \quad (8.9)$$

where  $J$  is the number of total active users,  $\otimes$  is the convolution operation, and  $n(t)$  is the complex additive Gaussian noise (AWGN) with zero mean and variance  $\sigma_n^2$ . The decision variable at  $t = iT_s$  is written as

$$D_{DS}^j = \sum_{v=1}^I g_v^* (iT_s) \cdot \frac{1}{T_s} \int_{iT_s+\tau_v}^{iT_s+\tau_v+T_s} \sum_{k=0}^{K_{DS}-1} c_j'(k) p_c(t-kT_c-iT_s-\tau_v) r_{DS}(t) dt \quad (8.10)$$



**Figure 8.2** DS-SS-SSA system: (a) transmitter, (b) power spectrum of its transmitted signal, and (c) RAKE receiver.

### 8.3.2 MC-CDMA System

The MC-CDMA transmitter spreads the original signal using a given spreading code in the frequency domain. In other words, a fraction of the symbol corresponding to a chip of the spreading code is transmitted through a different subcarrier. For Multi-Carrier transmission, it is essential to have frequency nonselective fading over each subcarrier. Therefore, if the original symbol rate is high enough to become subject to frequency-selective fading, the signal needs to be serial-to-parallel converted first before being spread over the frequency domain. The basic transmitter structure of MC-CDMA scheme is similar to that of a normal OFDM scheme as described in Chapter 2. The main difference is that the MC-CDMA scheme transmits the same symbol in parallel through many subcarriers, whereas the OFDM scheme transmits different symbols.

Figure 8.3(a) shows the MC-CDMA transmitter for the  $j^{\text{th}}$  user with CBPSK format. The input information sequence is first converted into  $P$  parallel data sequences ( $a_{j,0}(i), a_{j,1}(i), \dots, a_{j,P-1}(i)$ ) and then each serial/parallel converter output is multiplied with the spreading code with length  $K_{MC}$ . All the data in total  $N = P \times K_{MC}$  (corresponding to the total number of subcarriers) are modulated in baseband by the inverse discrete fourier transform (IDFT) and converted back into serial data. The guard interval  $\Delta$  is inserted between symbols to avoid intersymbol interference caused by multipath fading, and finally the signal is transmitted after RF up-conversion. The complex equivalent lowpass transmitted signal is written as

$$s_{MC}^j(t) = \sum_{i=-\infty}^{+\infty} \sum_{p=0}^{P-1} \sum_{m=0}^{K_{MC}-1} a_{j,p}(i) d_j(m) p_s(t - iT'_s) e^{j2\pi(Pm+p)\Delta f'(t-iT'_s)} \quad (8.11)$$

$$T'_s = PT_s, \quad (8.12)$$

$$\Delta f' = 1/(T'_s - \Delta) \quad (8.13)$$

where  $\{d_j(0), d_j(1), \dots, d_j(K_{MC}-1)\}$  is the spreading code with length  $K_{MC}$ ,  $T'_s$  is the symbol duration at subcarrier,  $\Delta f'$  is the minimum subcarrier separation, and  $p_s(t)$  is the rectangular symbol pulse waveform defined as

$$p_s(t) = \begin{cases} 1 & (-\Delta \leq t \leq T'_s - \Delta) \\ 0 & \text{(otherwise)} \end{cases} \quad (8.14)$$

The bandwidth of the transmitted signal spectrum is written as (see Figure 8.3(b))

$$\begin{aligned} B_{MC} &= (P \cdot K_{MC} - 1)/(T'_s - \Delta) + 2/T'_s \\ &\approx K_{MC}/T_s / (1 - \Delta/P) \\ &= (1 + \beta)K_{MC}/T_s, \end{aligned} \quad (8.15)$$

$$\beta = \Delta / P \quad (0 \leq \beta \leq 1.0), \quad (8.16)$$

where  $\beta$  is the bandwidth expansion factor associated with the guard interval insertion.

Note that, in (8.11), no spreading operation is done in the time domain. (8.12) shows that the symbol duration at subcarrier level is  $P$  times as long as the original symbol duration because of serial/parallel conversion. Although the minimum subcarrier separation is given by (8.13), the subcarrier separation for  $a_{j,p}(i)$  is  $\Delta f = P/(T'_s - \Delta)$  (see the hatched subcarrier power spectra in Figure 8.3(b)). Therefore, when setting  $K_{MC}$  to 1, the transmitted waveform given by (8.11) becomes all the same as an OFDM waveform with  $P$  subcarriers.

On the other hand, the received signal is written as

$$\begin{aligned} r_{MC}(t) &= \sum_{j=1}^J \int_{-\infty}^{+\infty} s_{MC}^j(t-\tau) \otimes h^j(\tau;t) d\tau + n(t) \\ &= \sum_{i=-\infty}^{+\infty} \sum_{p=0}^{P-1} \sum_{m=0}^{K_{MC}-1} \sum_{j=1}^J z_{m,p}^j(t) a_{j,p}(i) d_m^j p_s(t - iT'_s) e^{j2\pi(Pm+p)\Delta f i} + n(t) \end{aligned} \quad (8.17)$$

where  $z_{m,p}^j(t)$  is the received complex envelope at the  $(mP+p)^{\text{th}}$  subcarrier of the  $j^{\text{th}}$  user.

The MC-CDMA receiver requires coherent detection for successful despreading operation. Figure 8.3(c) shows the MC-CDMA receiver for the  $j^{\text{th}}$  user. After down-conversion, the  $m$ -subcarrier components ( $m = 0, 1, \dots, K_{MC} - 1$ ) corresponding to the received data  $a_{j,p}(i)$  is first coherently detected with DFT and then multiplied with the gain  $G_j(m)$  to combine the energy of the received signal scattered in the frequency domain. The decision variable is the sum of the weighted baseband components given by (we can omit the subscription  $p$  without loss of generality)

$$D_{MC}^j(t = iT_s) = \sum_{m=0}^{K_{MC}-1} G_j(m) y(m) \quad (8.18)$$

$$y(m) = \sum_{j=1}^J z_m^j(iT_s) a_j d_m^j + n_m(iT_s) \quad (8.19)$$

where  $y(m)$  and  $n_m(iT_s)$  are the complex baseband component of the received signal after down-conversion and the complex additive Gaussian noise at the  $m^{\text{th}}$  subcarrier at  $t = iT_s$ , respectively. Now, we discuss the following four combining strategies.

### Orthogonality Restoring Combining

Choosing the gain in the down-link channel ( $z_m^1 = z_m^2 = \dots = z_m^J = z_m^1$ ) as

$$G_j(m) = d_j(m) z_m^* / |z_m|^2 \quad (8.20)$$



the receiver can eliminate the multiple access interference (MAI) perfectly [6]:

$$\hat{a}^{j'} = a^{j'} + \sum_{m=1}^{K_{MC}} d_{j'}(m) z_m^* / |z_m|^2 n_m \quad (8.21)$$

In (8.21), however, low-level subcarriers tend to be multiplied by the high gains, and the noise components are amplified at weaker subcarriers. This noise amplification effect degrades BER performance. Note that ORC is applicable only for the downlink channel.

### ***Equal Gain Combining***

The gain for EGC is given by [4]

$$G_{j'}(m) = d_{j'}(m) z_m^{j'*} / |z_m^{j'}| \quad (8.22)$$

### ***Maximal Ratio Combining***

The gain for MRC is given by [4]

$$G_{j'}(m) = d_{j'}(m) z_m^{j'*} \quad (8.23)$$

In the case of a single user, the MRC method minimizes the BER.

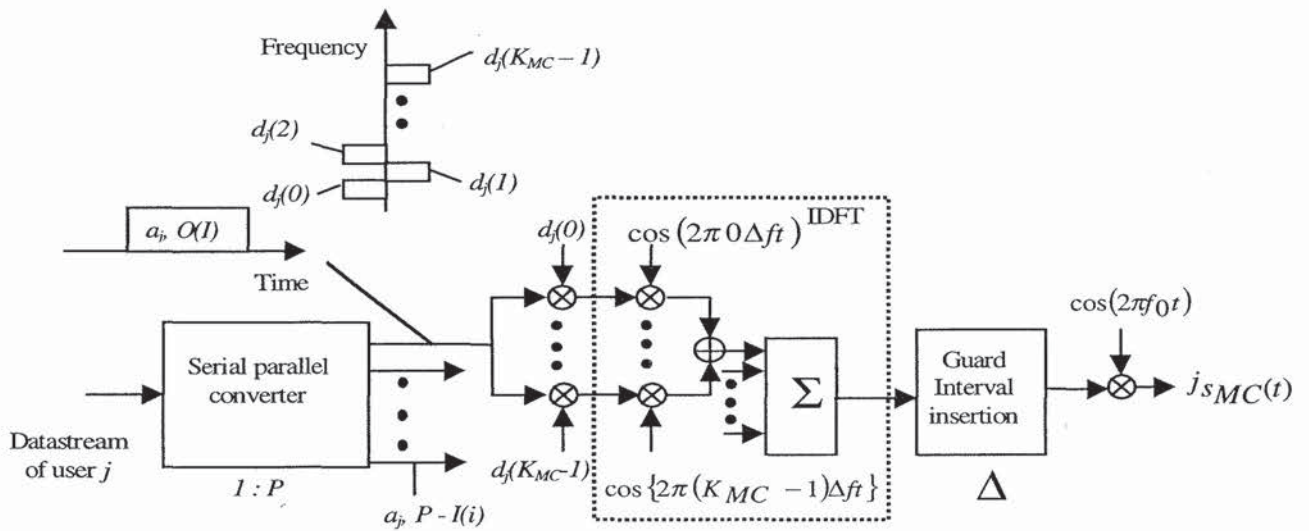
### ***Minimum Mean Square Error Combining***

The MMSEC criterion states that the error in the estimated data symbols must be orthogonal to the baseband components of the received subcarriers:

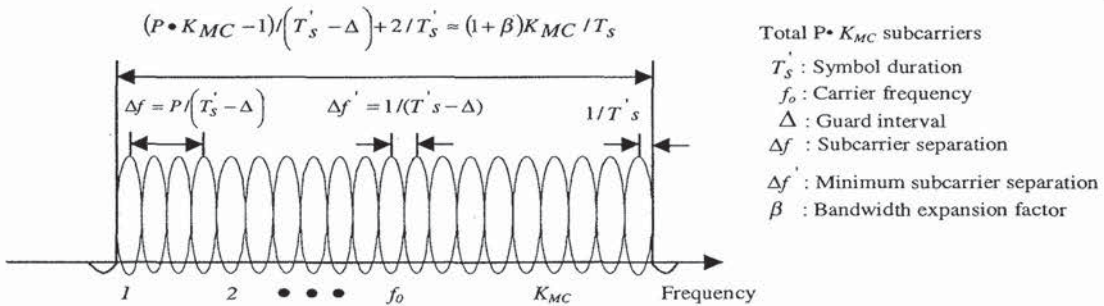
$$E\left[(a^{j'} - \hat{a}^{j'}) y(m')^*\right] = 0 \quad \left(m' = 1, 2, \dots, K_{MC}\right) \quad (8.24)$$

$G_{j'}(m)$  is given by [6]

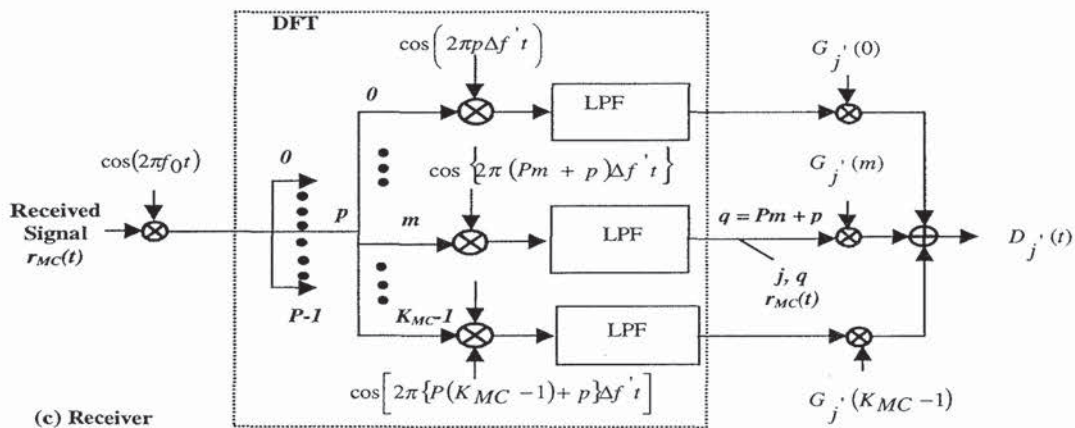
$$G_{j'}(m) = d_{j'}(m) z_m^{j'*} / \left( \sum_{j=1}^J |z_m^j|^2 + \sigma_n^2 \right) \quad (8.25)$$



(a) Transmitter



(b) Power spectrum of transmitted signal



(c) Receiver

Figure 8.3 MC-CDMA system.

Note that, in the downlink application, for small  $|z_m|$ , the gain becomes small to avoid excessive noise amplification, while for large  $|z_m|$ , it becomes proportional to the inverse of the subcarrier envelope  $z_m^*/|z_m|^2$  to recover orthogonality among users [6].

#### 8.4 MC-CDMA SYSTEM DESIGN

To determine the number of subcarriers and the length of guard interval, we derive the autocorrelation function of the received signal. The received signal for the  $j^{\text{th}}$  user is given by

$$r_{MC}^j(t) = \int_{-\infty}^{+\infty} s_{MC}^j(t-\tau) \otimes h(\tau;t) d\tau + n(t) \quad (8.26)$$

where  $h^j(\tau;t)$  is given by (8.1) and  $\{\tau_l\}$  is classified as follows:

$$\begin{aligned} 0 \leq \tau_l \leq \Delta & \quad (l = 1, \dots, L_1) \\ \Delta < \tau_l < T_s & \quad (l = L_1 + 1, \dots, L_1 + L_2 (= L)) \end{aligned} \quad (8.27)$$

The Fourier coefficient of the  $q^{\text{th}}$  ( $q = mP + p$ ) subcarrier at  $t = iT'_s$  is given by (see Figure 8.3(c))

$$r_{MC}^{j,q}(iT'_s) = \frac{1}{T'_s - \Delta} \int_{iT'_s}^{iT'_s + T'_s - \Delta} r_{MC}^j(t) e^{-j2\pi q \Delta f'(t - iT'_s)} dt \quad (8.28)$$

The normalized autocorrelation function of the  $q^{\text{th}}$  subcarrier between  $t = iT'_s$  and  $t = (i-1)T'_s$  for the  $j^{\text{th}}$  user is written as (see Appendix 8A)

$$\begin{aligned} R_{MC}^{j,q}(\Delta, N, R', f_D, \tau_{\text{RMS}}) &= \frac{E[r_{MC}^{j,q}(iT'_s) \cdot r_{MC}^{j,q*}((i-1)T'_s)]}{E[r_{MC}^{j,q}(iT'_s) r_{MC}^{j,q*}(iT'_s)]} \\ &= \frac{\sigma_{S1}^2}{\sigma_{S2}^2 + \sigma_I^2 + \sigma_n^2} \end{aligned} \quad (8.29)$$

$$\begin{aligned} \sigma_{S1}^2 &= \sum_{l=1}^{L_1} \sigma_l^2 \left\{ 1 - \left( \frac{\pi f_D}{R'} \right)^2 \left( \frac{(N - \Delta R')^2}{6} + N^2 \right) \right\} \\ &+ \sum_{l=L_1+1}^{L_1+L_2} \sigma_l^2 \frac{(N - \tau_l R')^2}{(N - \Delta R')^2} \left\{ 1 - \left( \frac{\pi f_D}{R'} \right)^2 \left( \frac{(N - \tau_l R')^2}{6} + N^2 \right) \right\} \end{aligned} \quad (8.30)$$

$$\begin{aligned}
\sigma_{S2}^2 = & \sum_{l=1}^{L_1} \sigma_l^2 \left\{ 1 - \left( \frac{\pi f_D}{R'} \right)^2 \frac{(N - \Delta R')^2}{6} \right\} \\
& + \sum_{l=L_1+1}^{L_1+L_2} \sigma_l^2 \frac{(N - \tau_l R')^2}{(N - \Delta R')^2} \left\{ 1 - \left( \frac{\pi f_D}{R'} \right)^2 \frac{(N - \tau_l R')^2}{6} \right\} \\
& + \sum_{l=L_1+1}^{L_1+L_2} \sigma_l^2 \frac{(-\Delta R' + \tau_l R')^2}{(N - \Delta R')^2} \left\{ 1 - \left( \frac{\pi f_D}{R'} \right)^2 \frac{(-\Delta R' + \tau_l R')^2}{6} \right\} \quad (8.31)
\end{aligned}$$

$$\begin{aligned}
\sigma_l^2 = & \sum_{l=1}^{L_1} \sum_{k=0, k \neq q}^{N-1} \sigma_l^2 \frac{\left( \frac{\pi f_D}{R'} \right)^2 (N - \Delta R')^2}{2\pi^2 (k - q)^2} \\
& + \sum_{l=L_1+1}^{L_1+L_2} \sum_{k=0, k \neq q}^{N-1} \sigma_l^2 \left\{ \frac{\left( \frac{\pi f_D}{R'} \right)^2 (N - \tau_l R')^2}{2\pi^2 (k - q)^2} \cos \left( \frac{2\pi(k - q)(N - \tau_l R')}{N - \Delta R'} \right) \right\} \\
& + \frac{\left( \frac{\pi f_D}{R'} \right)^2 (N - \Delta R')(N - \tau_l R')}{\pi^3 (k - q)^3} \sin \left( \frac{2\pi(k - q)(N - \tau_l R')}{N - \Delta R'} \right) \\
& + \left( \frac{1}{2\pi^2 (k - q)^2} + \frac{3 \left( \frac{\pi f_D}{R'} \right)^2 (N - \Delta R')^2}{4\pi^4 (k - q)^4} \right) \cdot \left( 1 - \cos \left( \frac{2\pi(k - q)(N - \tau_l R')}{N - \Delta R'} \right) \right)
\end{aligned}$$

$$\begin{aligned}
& + \frac{\left(\frac{\pi f_D}{R'}\right)^2 (-\Delta R' + \tau_l R')^2}{2\pi^2 (k-q)^2} \cos\left(\frac{2\pi(k-q)(-\Delta R' + \tau_l R')}{N - \Delta R'}\right) \\
& + \frac{\left(\frac{\pi f_D}{R'}\right)^2 (N - \Delta R')(-\Delta R' + \tau_l R')}{\pi^3 (k-q)^3} \sin\left(\frac{2\pi(k-q)(-\Delta R' + \tau_l R')}{N - \Delta R'}\right) \\
& + \left[ \frac{1}{2\pi^2 (k-q)^2} + \frac{3\left(\frac{\pi f_D}{R'}\right)^2 (N - \Delta R')^2}{4\pi^4 (k-q)^4} \right] \cdot \left(1 - \cos\left(\frac{2\pi(k-q)(-\Delta R' + \tau_l R')}{N - \Delta R'}\right)\right)
\end{aligned} \tag{8.32}$$

where  $R' (= K_{MC}R)$  is the chip rate.

In an OFDM scheme, generally, when the transmission rate,  $R'$ , in the case of MC-CDMA scheme) is given, the transmission performance becomes more sensitive to time selective fading as the number of subcarriers  $N$  increases, because the longer symbol duration means an increase in the amplitude and phase variation during a symbol, causing an increased level of ICI. As  $N$  decreases, the modulation becomes more robust to fading in time, but it becomes more vulnerable to delay spread, as the ratio of delay spread and symbol time increases, see Figure 8.4. The latter is not necessarily true if the guard time is kept at a fixed value, but as the symbol duration decreases, a fixed guard interval ( $\Delta$ ) means an increased loss of power, see Figure 8.5. Therefore, for given  $R$  ( $R'$ ),  $f_D$  and  $\tau_{RMS}$ , there exists an optimum that minimizes the BER in both  $N$  and  $\Delta$  [21].

In the MC-CDMA scheme,  $N_{opt}$  and  $\Delta_{opt}$  maximizes the ACF given by (8.29) to (8.32), because it means a measure to show how much the received signal is distorted in the time frequency, selective fading channel (i.e., how we can place the signal on the time-frequency plane, so that it suffers from minimum distortion):

$$\left[ N_{opt}, \Delta_{opt} \right] = \arg\left\{ \max R_j(N, \Delta | R', f_D, \tau_{RMS}) \right\} \tag{8.33}$$

Therefore, with (8.33), we determine two parameters,  $N_{opt}$  and  $\Delta_{opt}$ .

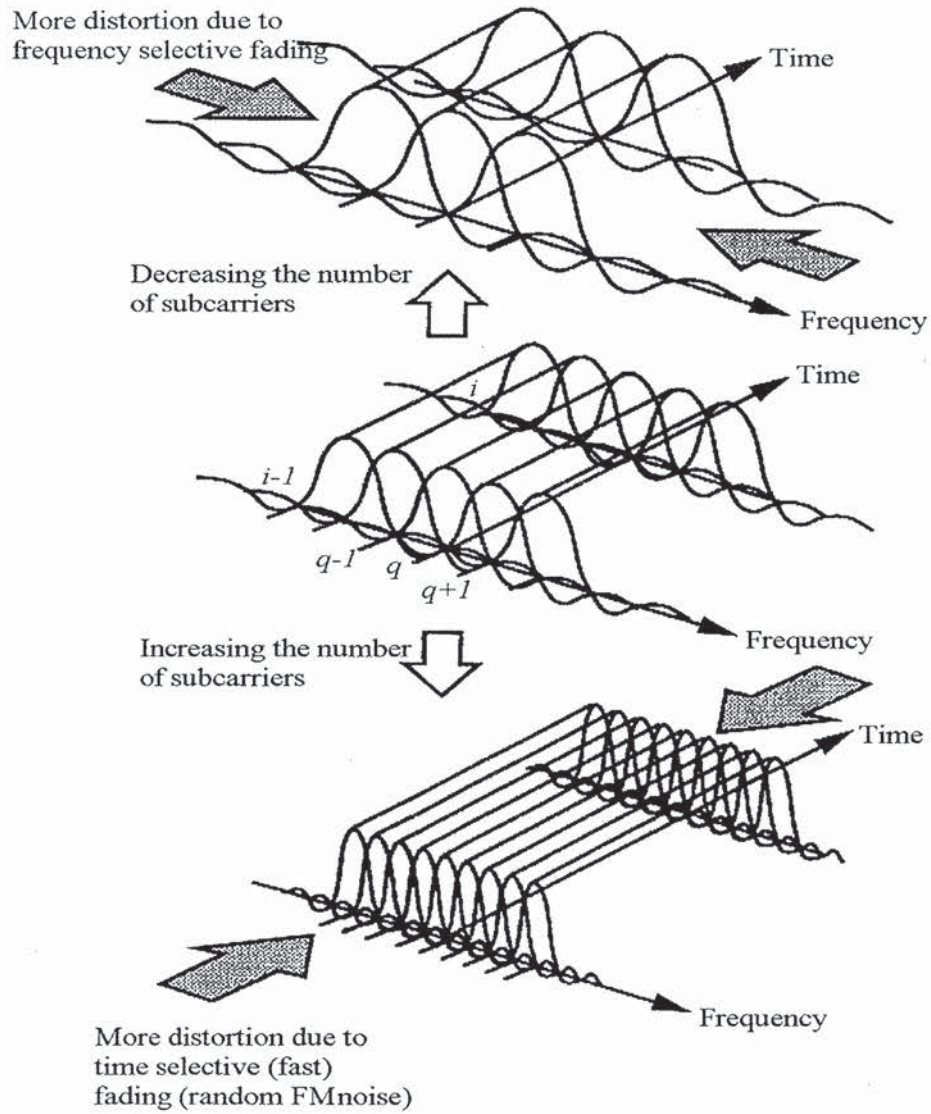


**Figure 8.4** Optimum in the number of subcarriers.

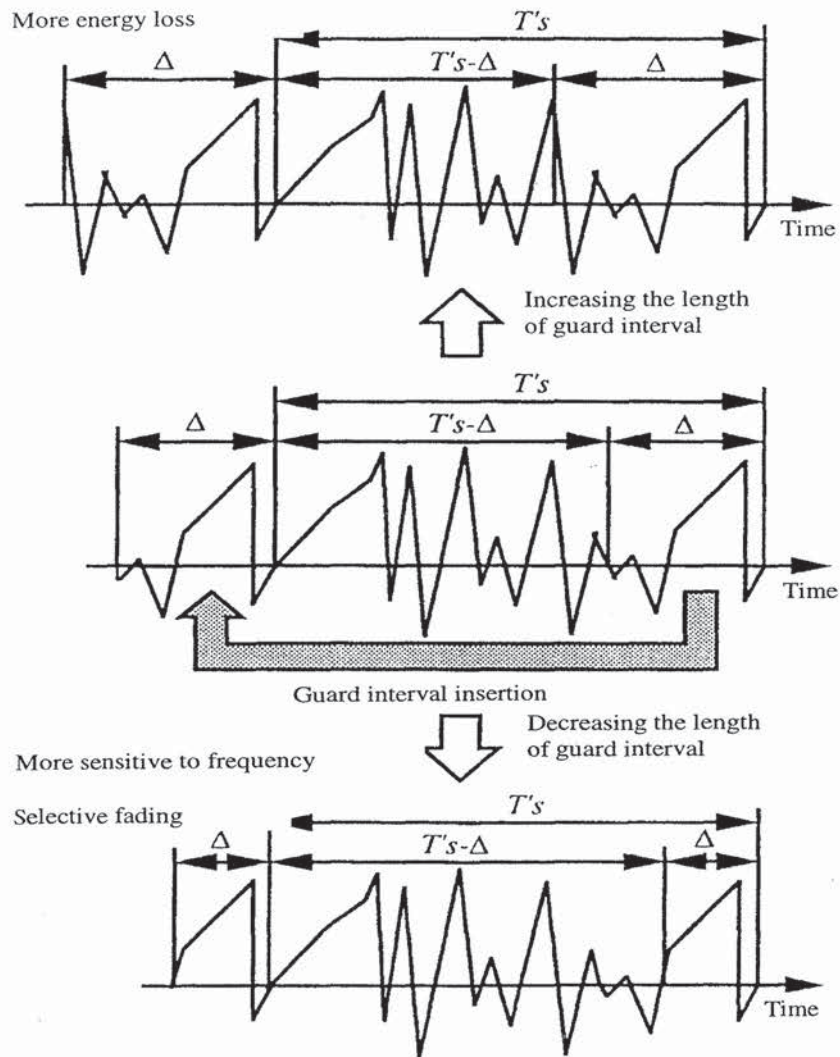


Figure 8.5 Optimum in the length of guard interval.

## 8.5 BER LOWER BOUND

### 8.5.1 DS-CDMA System

Defining  $\mathbf{r}_t$  as the received signal vector, the time domain covariance matrix  $\mathbf{M}_t$  is given by

$$\mathbf{r}_t = [r_1, r_2, \dots, r_L]^T, \quad (8.34)$$

$$\begin{aligned} \mathbf{M}_t &= \frac{1}{2} E[\mathbf{r}_t \cdot \mathbf{r}_t^T] \\ &= \begin{bmatrix} \sigma_1^2 & 0 & \cdot & \cdot & \cdot & 0 \\ 0 & \sigma_2^2 & & & & \cdot \\ \cdot & & \cdot & & & \cdot \\ \cdot & & & \cdot & & \cdot \\ \cdot & & & & \cdot & 0 \\ 0 & \cdot & \cdot & \cdot & 0 & \sigma_L^2 \end{bmatrix}, \end{aligned} \quad (8.35)$$

In the above equation, we assume a perfect auto-correlation characteristic for the spreading codes.

The BER of time domain  $L$ -finger DS-CDMA RAKE receiver in the case of a single user is uniquely determined by the eigenvalues of  $\mathbf{M}_t$  (in this case, the eigenvalues are  $\sigma_1^2, \sigma_2^2, \dots, \sigma_L^2$ ) [22]. For example, when  $\sigma_l^2 (l=1, \dots, L)$  are different from each other, BER is given by

$$\text{BER}_{\text{DS}} = \sum_{l=1}^L w_l \frac{1}{2} \left\{ 1 - \sqrt{\frac{\sigma_l^2 / \sigma_n^2}{1 + \sigma_l^2 / \sigma_n^2}} \right\} \quad (8.36)$$

$$w_l = \frac{1}{\prod_{v=1, v \neq l}^L \left( 1 - \frac{\sigma_v^2}{\sigma_l^2} \right)} \quad (8.37)$$

$$\sigma_t^2 = \sum_{l=1}^L \sigma_l^2 \quad (8.38)$$

where  $\sigma_t^2$  is the total power of the received signal. If all multipath signals have equal power, so  $\sigma_l^2 (l=1, \dots, L)$  are all the same ( $=\sigma_s^2$ ) [15], then the BER is given as



$$\text{BER}_{\text{DS}} = \left( \frac{1 - \mu_{\text{DS}}}{2} \right)^I \sum_{l=0}^{I-1} \binom{I-1+l}{l} \left( \frac{1 + \mu_{\text{DS}}}{2} \right)^l, \quad (8.39)$$

$$\mu_{\text{DS}} = \sqrt{\frac{\sigma_s^2 / \sigma_n^2}{1 + \sigma_s^2 / \sigma_n^2}}, \quad (8.40)$$

Note that the  $L$ -finger RAKE receiver achieves the minimum BER (the BER lower bound) [15].

### 8.5.2 MC-CDMA System

For the case of a single user, the frequency domain MC-CDMA RAKE receiver based on the MRC method achieves the minimum BER (the BER lower bound) [15].

Defining  $\mathbf{r}_f$  as the received signal vector, the frequency domain covariance matrix  $\mathbf{M}_f$  is given by

$$\mathbf{r}_f = [z_1, z_2, \dots, z_{K_{\text{MC}}}]^T, \quad (8.41)$$

$$\begin{aligned} \mathbf{M}_f &= \frac{1}{2} E[\mathbf{r}_f \cdot \mathbf{r}_f^T] = \{m_f^{a,b}\}, \\ m_f^{a,b} &= \Phi_c((a-b)\Delta f), \end{aligned} \quad (8.42)$$

where  $\{m_f^{a,b}\}$  is the  $a$ - $b$  element of  $\mathbf{M}_f$ , and  $\Phi_c(\Delta f)$  is the spaced frequency correlation function defined as the Fourier transform of the multipath delay profile:

$$\Phi_c(\Delta f) = \int_{-\infty}^{+\infty} \phi_c(\tau) e^{-j2\pi\Delta f\tau} d\tau. \quad (8.43)$$

Defining  $\lambda_1, \lambda_2, \dots, \lambda_{K_{\text{MC}}}$  as the nonzero eigenvalues of  $\mathbf{M}_f$ , BER is given by a form similar to (8.36) or (8.40) [22]. For example, when  $\lambda_m (m=1, \dots, K_{\text{MC}})$  are different from each other,

$$\text{BER}_{\text{MC}} = \sum_{m=1}^{K_{\text{MC}}} v_m \frac{1}{2} \left\{ 1 - \sqrt{\frac{\lambda_m / N_0}{1 + \lambda_m / N_0}} \right\} \quad (8.44)$$

$$v_m = \frac{1}{\prod_{u=1, u \neq m}^{K_{\text{MC}}} \left( 1 - \frac{\lambda_u}{\lambda_m} \right)} \quad (8.45)$$

Also, when  $\lambda_m (m=1, \dots, K_{\text{MC}})$  are all the same ( $= \lambda$ ):

$$\text{BER}_{\text{MC}} = \left( \frac{1 - \mu_{\text{MC}}}{2} \right)^{K_{\text{MC}}} \sum_{m=0}^{K_{\text{MC}}-1} \binom{M-1+m}{m} \left( \frac{1 + \mu_{\text{MC}}}{2} \right)^m$$

$$\mu_{\text{MC}} = \sqrt{\frac{\lambda / N_0}{1 + \lambda / N_0}} \quad (8.46)$$

### 8.5.3 BER Lower Bound Equivalence

When there are  $L$  paths in the symbol duration at subcarrier  $T_s'$  in the multipath delay profile shown in Figure 8.1, we obtain the following  $N \times N$  time-domain covariance matrix with time resolution of  $T_s'/N$ :

$$\mathbf{M}'_t = \begin{bmatrix} \sigma_1^2 & 0 & \dots & \dots & \dots & 0 \\ 0 & 0 & & & & \dots \\ \dots & & \sigma_1^2 & & & \dots \\ \dots & & & \sigma_3^2 & & \dots \\ \dots & & & & \dots & 0 \\ 0 & \dots & \dots & \dots & 0 & \dots \end{bmatrix}, \quad (8.47)$$

where the nonzero eigenvalues of  $\mathbf{M}'_t$  are  $\sigma_1^2, \sigma_2^2, \sigma_3^2, \dots, \sigma_L^2$ .

The corresponding  $N \times N$  frequency domain covariance matrix with frequency resolution of  $1/T_s$  is given by

$$\mathbf{M}'_f = \mathbf{W} \mathbf{M}'_t \mathbf{W}^*, \quad (8.48)$$

where  $\mathbf{W}$  is the  $N \times N$  DFT matrix given by

$$\mathbf{W} = \{w^{i,j}\}$$

$$w^{i,j} = e^{j2\pi \frac{ij}{N}} \quad (8.49)$$

We define  $\mathbf{r}_l$  as the eigenvector corresponding to the eigenvalue  $\sigma_l^2$ :

$$\mathbf{M}'_t \mathbf{r}_l = \sigma_l^2 \mathbf{r}_l \quad (l = 1, 2, \dots, L) \quad (8.50)$$

Also, we define  $\mathbf{z}_l$  as

$$\mathbf{z}_l = \mathbf{W} \mathbf{r}_l \quad (l = 1, 2, \dots, L) \quad (8.51)$$

Now we can theoretically prove that the frequency domain covariance matrix has all the same eigenvalues as the time domain covariance matrix as follows:

$$\begin{aligned}
 \mathbf{M}'_f \mathbf{z}_1 &= \mathbf{W} \mathbf{M}'_t \mathbf{W}^* \cdot \mathbf{W} \mathbf{r}_1 \\
 &= \mathbf{W} \mathbf{M}'_t \mathbf{r}_1 \\
 &= \mathbf{W} \sigma_l^2 \mathbf{r}_1 \\
 &= \sigma_l^2 \mathbf{W} \mathbf{r}_1 \\
 &= \sigma_l^2 \mathbf{z}_1
 \end{aligned} \tag{8.52}$$

The above equation shows that the nonzero eigenvalues of  $\mathbf{M}'_f$  are  $\sigma_1^2, \sigma_2^2, \sigma_3^2, \dots, \sigma_L^2$ . Therefore, as long as we use the same frequency-selective fading channel, the BER lower bound of the MC-CDMA system is the same as that of the DS-CDMA system. Also, the assumption of independent fading characteristic at each subcarrier implies a frequency selective fading at each subcarrier, because it requires independent  $N$  paths uniformly scattered in the symbol duration at subcarrier.

## 8.6 NUMERICAL RESULTS

To demonstrate the numerical results, we assume

- RMS delay spread  $\tau_{RMS} = 20$  ns,
- Doppler power spectrum with maximum Doppler frequency  $f_D = 10$  Hz,
- Transmission rate  $R = 3$  Msymbols/s (BPSK format),
- Walsh Hadamard codes with  $K_{MC} = 32$  for the MC-CDMA system,
- Gold codes with  $K_{DS} = 31$  for the DS-CDMA system ( $K_{MC} \approx K_{DS}$ ).

First, to design the MC-CDMA system and to select one best suited combining strategy in the MC-CDMA system, we assume a simple 2-path multipath delay profile often encountered in urban and hilly areas [23, 24], where the first and second paths have the same power (2-path i.i.d. delay profile) [25].

### 8.6.1 MC-CDMA System Design

Figure 8.6 shows the optimal values in the number of subcarriers  $N$  and the length of guard interval  $\Delta$  versus the normalized RMS delay spread  $\sigma_{RMS}$  as a function of the Doppler frequency  $f_D$ , where  $\Delta$ ,  $\sigma_{RMS}$  and  $f_D$  are normalized by  $R'$ . This figure is obtained from the maximization of (8.33). For given  $f_D$  and  $R'$ , both  $N_{opt}$  and  $\Delta_{opt}$  increases as  $\sigma_{RMS}$  increases. For the above parameters, we obtain  $f_D / R' \approx 10^{-7}$  and  $\tau_{RMS} R' = 1.92$ , so we choose  $[N_{opt}, \Delta_{opt} / T_s] = [256, 0.015]$  as an optimal set. It means

that the original data sequence is first converted into eight parallel sequences ( $P = 8$ ), and then each sequence is mapped onto 32 subcarriers, and the length of the guard interval is negligibly short, as compared with the symbol duration at subcarrier.

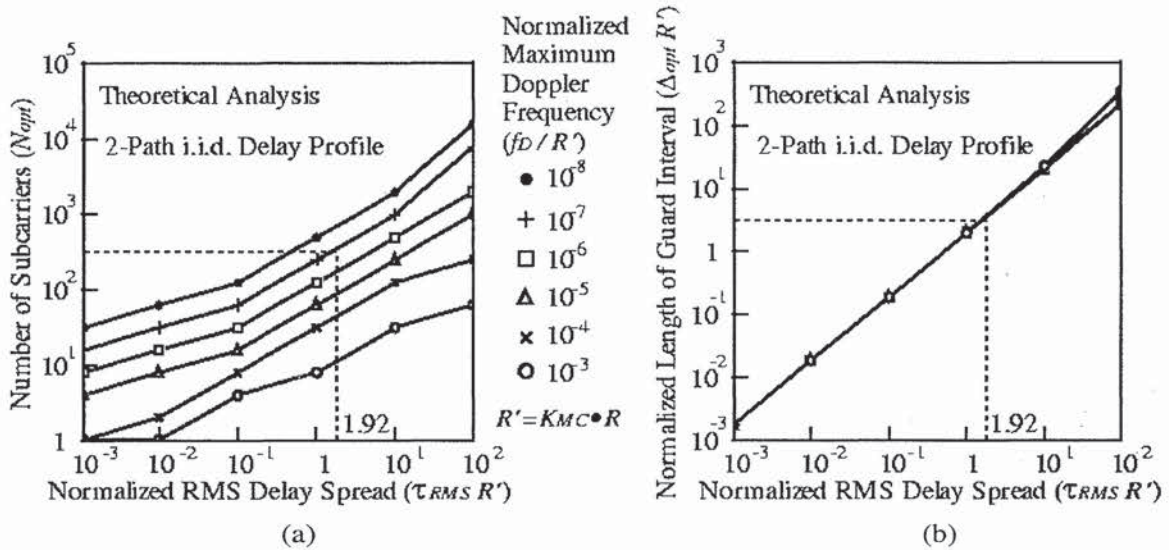


Figure 8.6 (a) Optimum number of subcarriers, and (b) optimum length of guard interval.

From (8.7) and (8.16),  $B_{MC}$  and  $B_{DS}$  are calculated as 97.8 MHz and 186 MHz, respectively, so the bandwidth of the DS-CDMA signal is 1.9 times as wide as that of the MC-CDMA signal as long as the same rectangular pulse format is employed. From (8.8), however, if a Nyquist pulse is employed in the DS-CDMA system, the difference in the signal bandwidth diminishes as the roll-off factor becomes small (there is no difference when  $\alpha = 0.05$ ). Therefore, we can conclude that MC-CDMA system has no major advantage in terms of signal bandwidth, as compared with the DS-CDMA system. Note, however, that when Nyquist filters are introduced in the transmitter and receiver for base bandpulse shaping in a DS-CDMA system, the RAKE receiver may wrongly combine paths. This is because noise-causing distortion in the autocorrelation characteristic often results in a wrong correlation [26].

How many users the system can accommodate depends on the attainable BER performance; in other words, the combining strategy employed in the MC-CDMA system and the number of fingers in the DS-CDMA system. We discuss BER performance in the following two subsections.

### 8.6.2 Down-Link BER Performance

Figures 8.7, 8.8, and 8.9 show the downlink BER performance of MC-CDMA scheme with EGC, MRC and MMSEC for the 2-path i.i.d. delay profile, respectively. Here, the theoretical BER lower bound is given by (8.39) with  $I = 2$ . In these figures, the BER for the ORC is shown, and further, the BER of MC-FDMA scheme is also shown, which supports 32 users at most, assigning a different set of eight subcarriers to each user. This scheme obtains no frequency diversity effect, so the theoretical BER is given by [15].

$$BER_{MC-FDMA} = \frac{1}{2} \left( 1 - \sqrt{\frac{E_b / N_0}{1 + E_b / N_0}} \right) \quad (8.53)$$

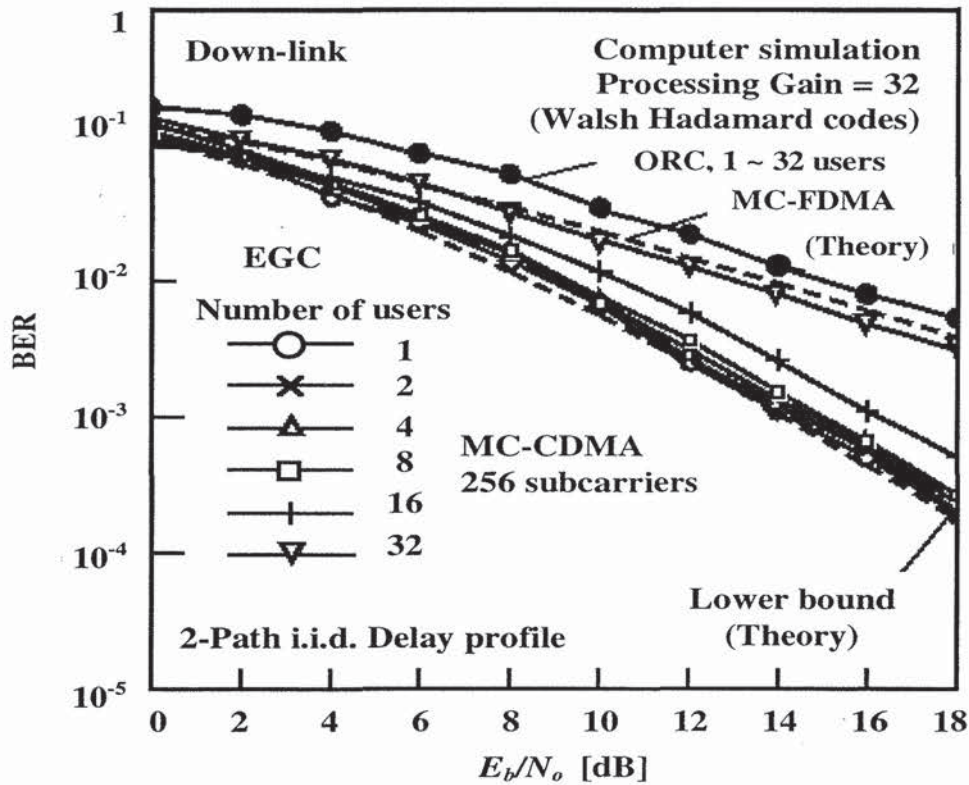


Figure 8.7 Down-link BER of MC-CDMA system with EGC.

BER performance of the ORC is independent of the number of users; however, it is worse than that of the MC-FDMA scheme. Therefore, we do not have to employ the ORC even when we can estimate the channel condition perfectly. The MRC can perform better when the number of users is less than eight. For the case of more users,

however, the performance abruptly becomes worse, because the interference resulting from distorted code orthogonality is multiplied in the combining process. On the other hand, as the interference is not multiplied in the EGC, it can perform better than the MRC for the cases of 16 and 32 users. The MMSEC can perform best among the four combining strategies, although it requires information on the number of total active users and the noise power, in addition to the channel condition. In the following downlink BER comparison, we select the MMSEC as the best combining strategy.

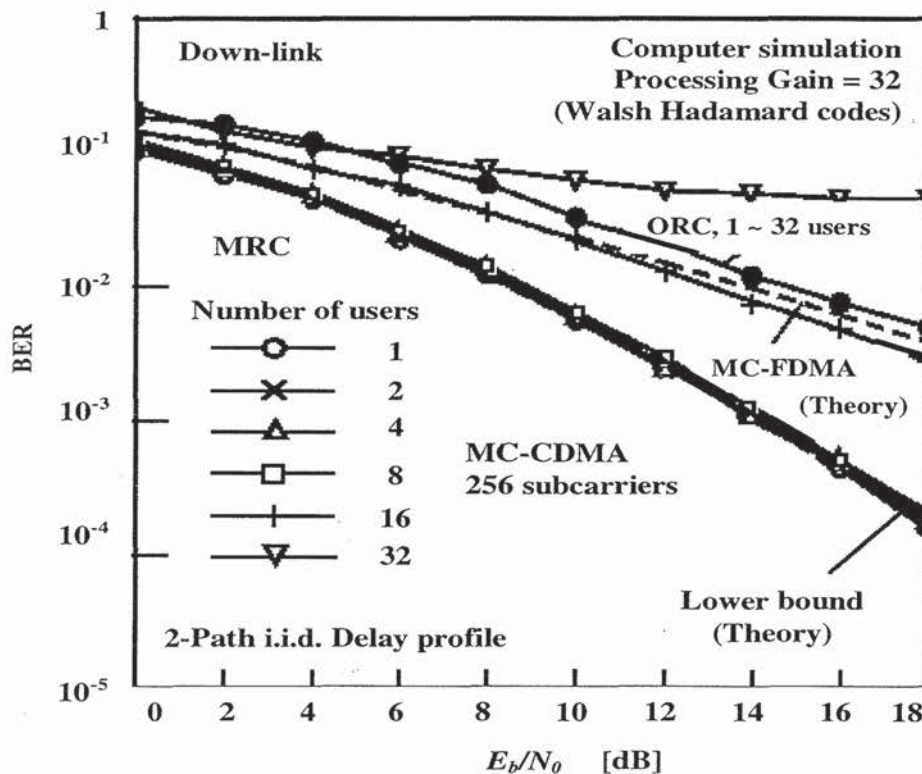


Figure 8.8 Downlink BER of MC-CDMA system with MRC.

Figure 8.10 shows the BER comparison between DS-CDMA and MC-CDMA schemes for the 2-path i.i.d. delay profile. For the DS-CDMA scheme, the BER of 2 (full)-finger RAKE combiner is a little worse than the lower bound even for the case of a single user because of the self-interference resulting from the imperfect auto-correlation characteristic of the Gold codes. Also, the BER of a 1-finger RAKE combiner, which selects the largest path, is worse than that of a 2-finger RAKE combiner, because it always misses a part of the received signal energy scattered in the time domain. On the other hand, for the MC-CDMA scheme, the MMSEC outperforms the full-finger DS-CDMA RAKE combiner. This is because the MMSEC-based MC-CDMA scheme can effectively combine all the received signal energy scattered in the frequency domain.

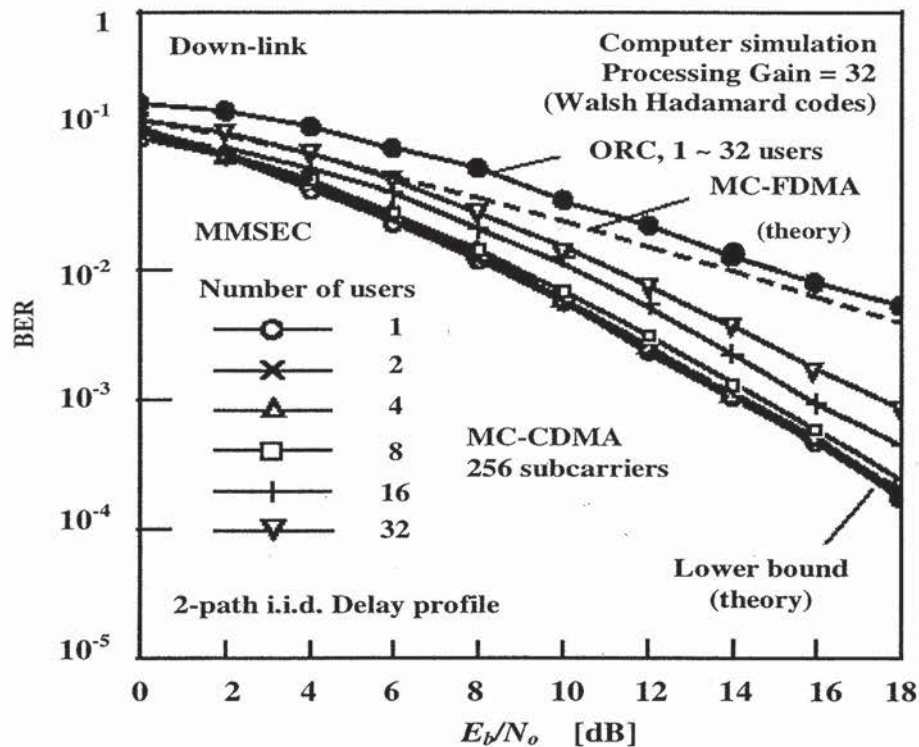


Figure 8.9 Downlink BER of MC-CDMA system with MMSEC.

Figure 8.11 shows the BER comparison for a 7-path exponential delay profile with a delay spread of 10 ns. We obtain  $[N_{opt}, \Delta_{opt}/T_s] = [1024, 0.018]$  as an optimal set for this particular channel, and the theoretical BER lower bound is given by (8.36) with  $I = 7$ .

For the DS-CDMA scheme, the BER performance depends on how many fingers the RAKE receiver employs. Usually, a 1-, 2-, 3- or 4-finger RAKE receiver is used, depending on hardware limitation. Therefore, if the received signal is composed of more paths than the number of RAKE fingers, the receiver misses a part of its energy. In these figures, the BERs of 1-finger, 2-finger, and 3-finger RAKE combiners are worse than that of seven (full)-finger RAKE combiners, because they always miss a larger part of the received signal energy scattered in the time domain. On the other hand, for the MC-CDMA scheme, the MMSEC outperforms the 3-finger DS-CDMA RAKE combiner, and for the case of eight users or more, it performs better than the full-finger DS-CDMA RAKE combiner.

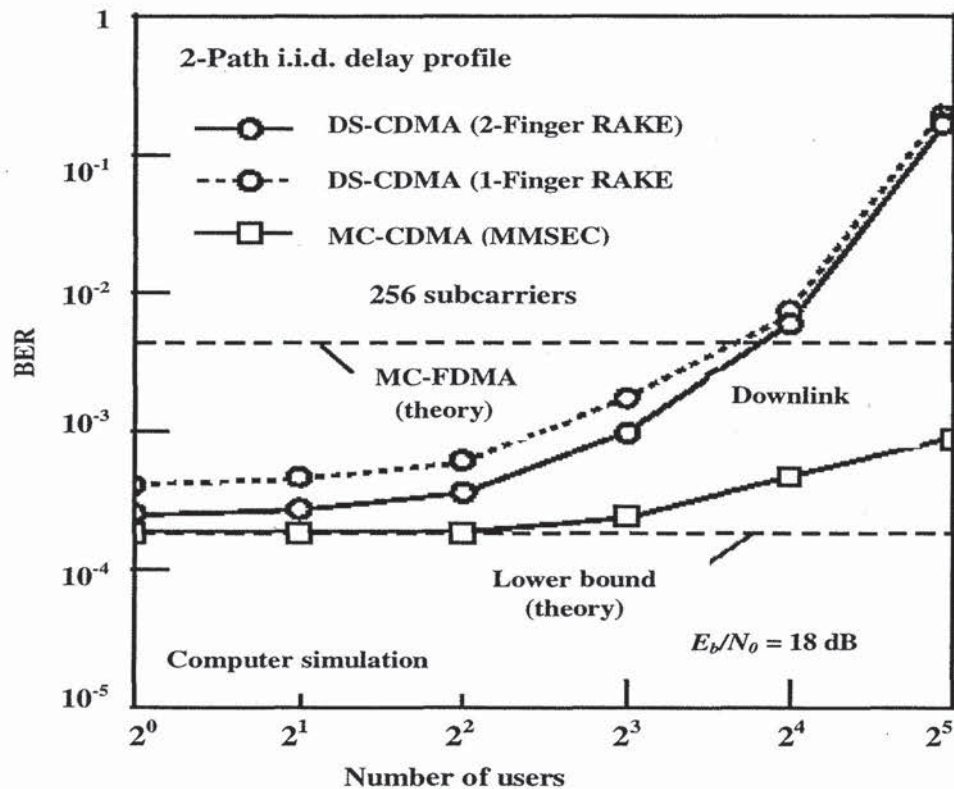


Figure 8.10 BER comparison in a downlink channel with 2-path i.i.d. multipath delay profile.

From all the results obtained in this subsection, we can conclude that it could be difficult for a DS-CDMA receiver to employ all the received signal energy scattered in the time domain, whereas an MC-CDMA receiver can effectively combine all the received signal energy scattered in the frequency domain. A DS-CDMA receiver needs to make efforts to select larger paths; on the other hand, MC-CDMA receiver does not care about where the received signal energy is. This is a significant advantage of the MC-CDMA scheme over a DS-CDMA scheme, and it makes the MMSEC-based MC-CDMA a promising access scheme in a downlink channel.



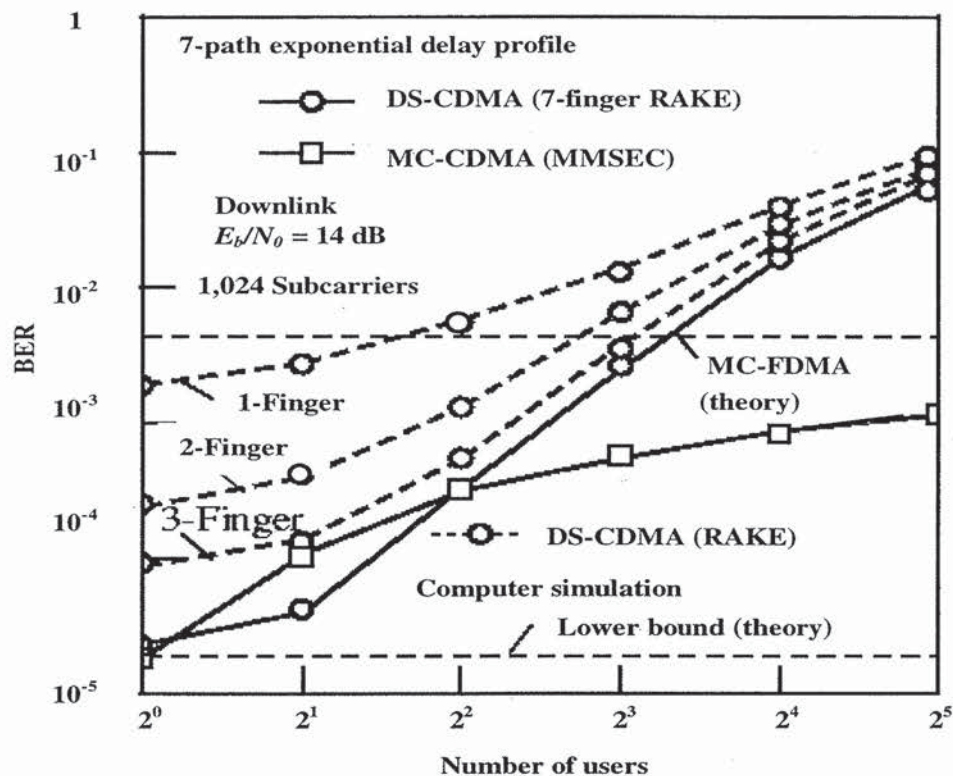


Figure 8.11 BER comparison in a downlink channel with 7-path exponential multipath delay profile.

### 8.6.3 Uplink BER Performance

Figures 8.12, 8.13, and 8.14 show the uplink BER performance of MC-CDMA system with EGC, MRC, and MMSEC for the 2-path i.i.d. delay profile, respectively. In these figures, the BER of an MC-FDMA scheme and the BER lower bound are also shown. The MMSEC can perform best among the three combining strategies, although there is no large difference in the attainable BER. Therefore, we select it as the best combining strategy.

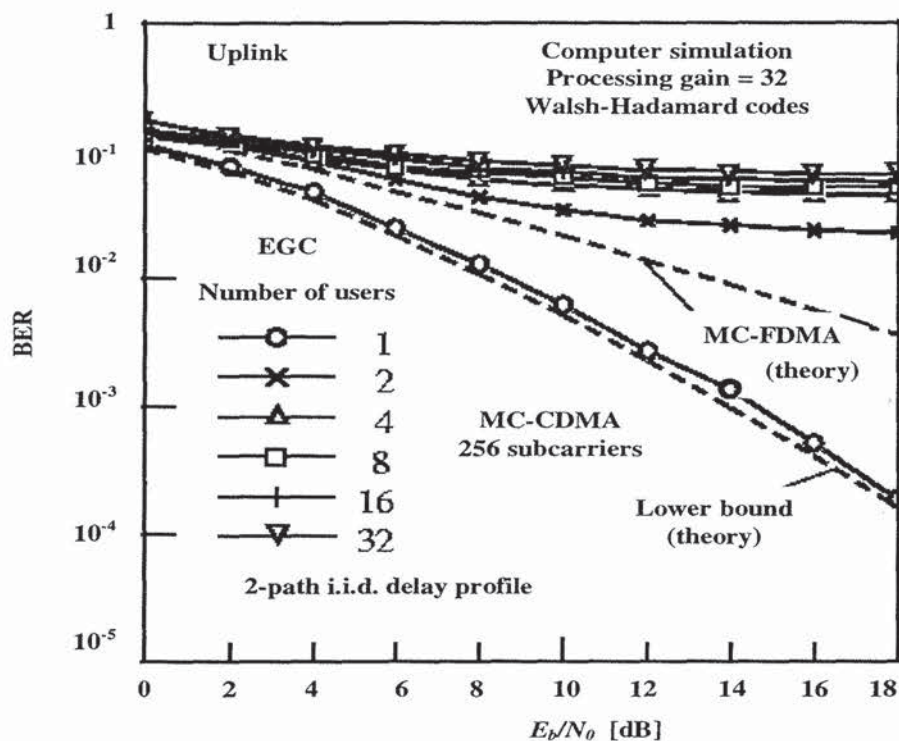


Figure 8.12 Uplink BER of MC-CDMA system with EGC.

Figures 8.15 and 8.16 show the BER comparison between DS-CDMA and MC-CDMA schemes for the 2-path i.i.d. and 7-path exponential delay profiles, respectively. As compared with the DS-CDMA scheme, the MMSEC performs well only for the case of a single user and otherwise performs poorly. This is because the code orthogonality among users is totally distorted by the instantaneous frequency response. Therefore, in the uplink application, a multiuser detection scheme is required, which jointly detects the signals to mitigate the nonorthogonal properties [27]. There are many other detectors reported in the literature [28, 29].

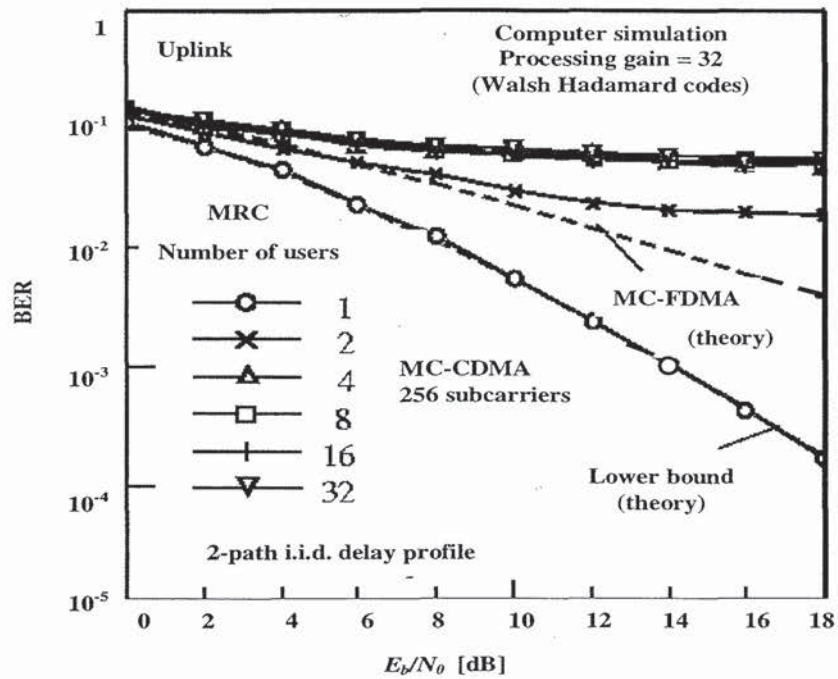


Figure 8.13 Uplink BER of MC-CDMA system with MRC.

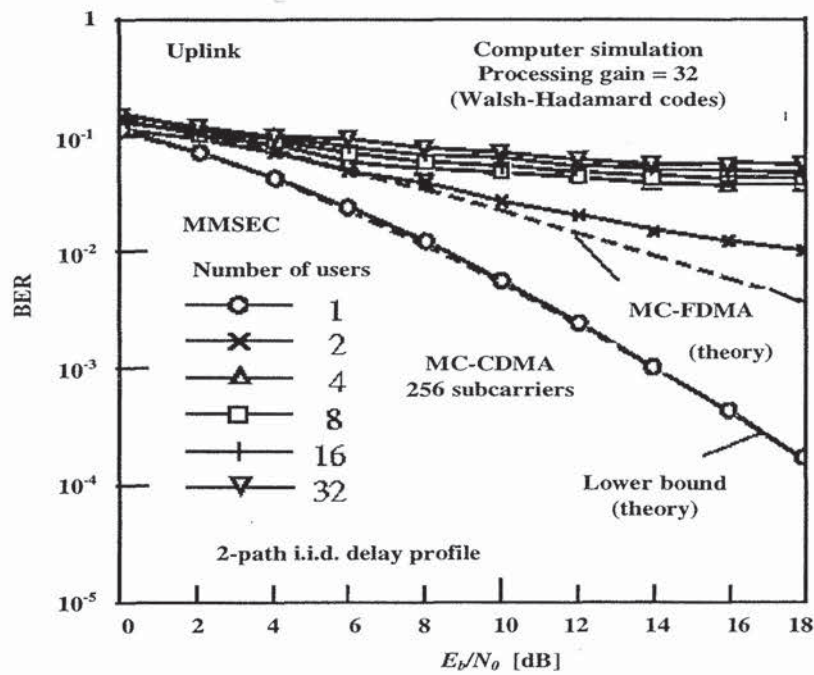


Figure 8.14 Uplink BER of MC-CDMA systems with MMSEC.

## 8.7 CONCLUSIONS

In this chapter, we discussed the advantages and disadvantages of the MC-CDMA system and have shown the BER performance by computer simulation.

An MC-CDMA system has no major advantage over a DS-CDMA system in terms of required bandwidth, because the bandwidth of the MC-CDMA signal spectrum is almost the same as that of a DS-CDMA signal spectrum. Also, in terms of transmission performance, the BER lower bound of an MC-CDMA system is the same as that of a DS-CDMA system. Therefore, if we make every effort to improve the BER in each system, there is no difference in the attainable BER as long as the same channel is used.

A DS-CDMA system cannot always employ all the received signal energy scattered in the time domain, whereas an MC-CDMA system can effectively combine all the received signal energy scattered in the frequency domain. The MMSEC-based MC-CDMA is a promising scheme in a downlink channel, although estimation of the noise power as well as the subcarrier reference values is required. On the other hand, in the uplink application, a multiuser detection is required because the code orthogonality among users is totally distorted by the channel frequency selectivity.

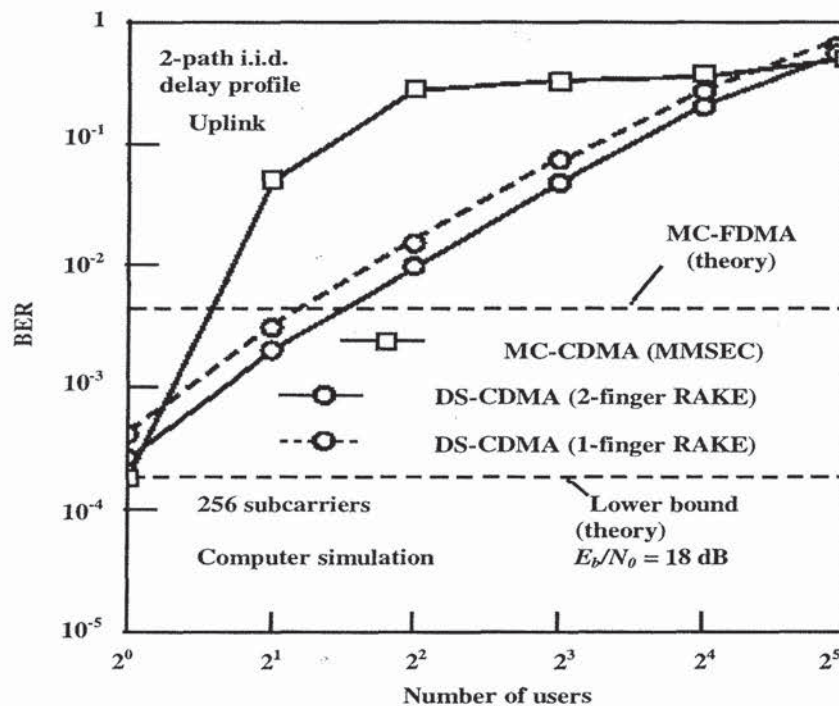
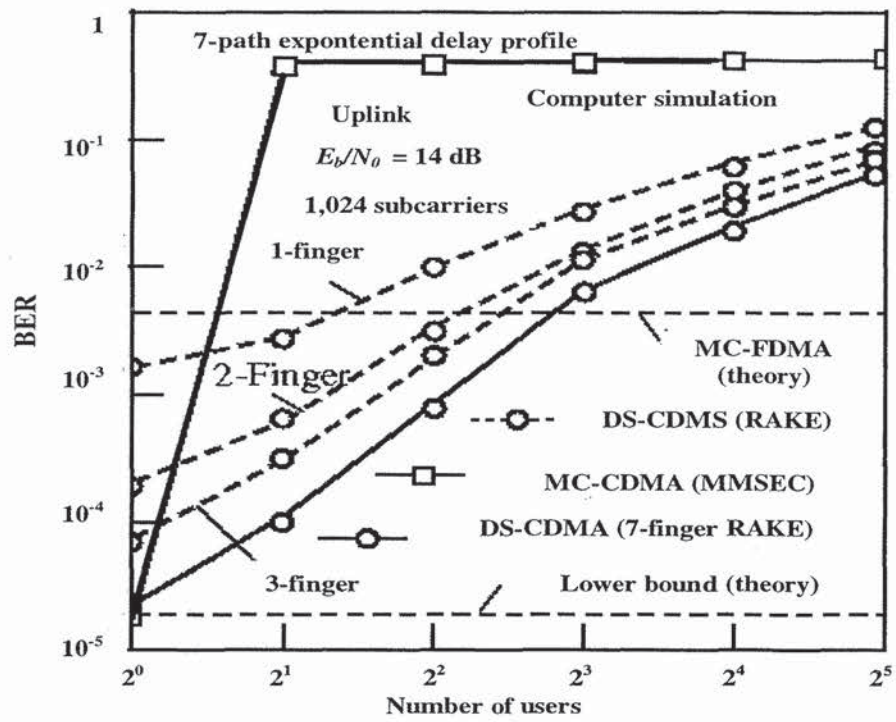


Figure 8.15 BER comparison in an uplink channel with 2-path i.i.d. multipath delay profile.



**Figure 8.16** BER comparison in an uplink channel with 7-path exponential multipath delay profile.

## APPENDIX 8A

(8.11) is written as

$$s_{MC}^j(t) = \sum_{i=-\infty}^{+\infty} \sum_{q=0}^{N-1} c_{j,q}(i) p_s(t - iT_s') e^{j2\pi\Delta f / P \cdot q(t - T_s')} \quad (8A.1)$$

$$c_{j,q=Pm+p}(i) = a_{j,p}(i) d_j(m) \quad (8A.2)$$

where  $c_{j,q}(i)$  has the following property:

$$E[c_{j,q}(i) \cdot c_{j,q'}(i)] = \begin{cases} 1 & (q = q') \\ 0 & (q \neq q') \end{cases} \quad (8A.3)$$

Substituting (8.1) and (8.26) into (8.28) leads to

$$\begin{aligned} r_{MC}^{j,q}(iT_s') = & \left\{ \sum_{l=1}^{L_1} \frac{1}{T_s' - \Delta} \int_{iT_s'}^{iT_s' + T_s' - \Delta} g_l^j(t) dt c_{j,q}(i) e^{-j2\pi q \Delta f' \tau_l} \right. \\ & + \left. \sum_{l=L_1+1}^{L_1+L_2} \frac{1}{T_s' - \Delta} \int_{iT_s' - \Delta + \tau_l}^{iT_s' + T_s' - \Delta} g_l^j(t) dt \cdot c_{j,q}(i) e^{-j2\pi q \Delta f' \tau_l} \right\} \\ & + \left\{ \sum_{l=1}^{L_1} \sum_{k=0, k \neq q}^{N-1} \frac{1}{T_s' - \Delta} \int_{iT_s'}^{iT_s' + T_s' - \Delta} g_l^j(t) e^{j2\pi(k-q)\Delta f'(t - iT_s')} dt \cdot c_{j,k}(i) e^{-j2\pi k \Delta f' \tau_l} \right. \\ & + \sum_{l=L_1+1}^{L_1+L_2} \sum_{k=0, k \neq q}^{N-1} \frac{1}{T_s' - \Delta} \int_{iT_s' - \Delta + \tau_l}^{iT_s' + T_s' - \Delta} g_l^j(t) e^{j2\pi(k-q)\Delta f'(t - iT_s')} dt \cdot c_{j,k}(i) e^{-j2\pi k \Delta f' \tau_l} \\ & + \left. \sum_{l=L_1+1}^{L_1+L_2} \sum_{k=0, k \neq q}^{N-1} \frac{1}{T_s' - \Delta} \int_{iT_s'}^{iT_s' - \Delta + \tau_l} g_l^j(t) e^{j2\pi(k-q)\Delta f'(t - iT_s')} dt \cdot c_{j,k}(i-1) e^{-j2\pi k \Delta f'(\tau_l - T_s')} \right\} \\ & + \sum_{l=L_1+1}^{L_1+L_2} \frac{1}{T_s' - \Delta} \int_{iT_s'}^{iT_s' - \Delta + \tau_l} g_l^j(t) dt \cdot c_{j,q}(i-1) e^{-j2\pi q \Delta f'(\tau_l - T_s')} + n_q(i) \quad (8A.4) \end{aligned}$$

where the first term of (8A.4) represents the desired signal component, the second and third terms represent ICI and ISI components, respectively, and  $n_q(i)$  is the Gaussian random noise component with zero mean and variance  $\sigma_n^2$ .

With (8A.4),  $E[r_{j,q}(iT_s') r_{j,q}^*((i-1)T_s')]$  and  $E[r_{j,q}(iT_s') r_{j,q}^*(iT_s')]$  in (8.29) written as

$$E[r_{MC}^{j,q}(iT_s') \cdot r_{MC}^{*j,q}((i-1)T_s')] = \sum_{l=1}^{L_1} \frac{1}{(T_s' - \Delta)^2} \int_0^{T_s' - \Delta} \int_{-T_s'}^{-\Delta} \rho_l(x-y) dx dy$$

$$+ \sum_{l=L_1+1}^{L_1+L_2} \frac{1}{(T_s' - \Delta)^2} \int_{-\Delta+\tau_l}^{T_s' - \Delta} \int_{-T_s' - \Delta + \tau_l}^{-\Delta} \rho_l(x-y) dx dy \quad (8A.5)$$

$$E[r_{MC}^{j,q}(iT_s') \cdot r_{MC}^{*j,q}(iT_s')] = \sum_{l=1}^{L_1} \frac{1}{(T_s' - \Delta)^2} \int_0^{T_s' - \Delta} \int_0^{T_s' - \Delta} \rho_l(x-y) dx dy$$

$$+ \sum_{l=L_1+1}^{L_1+L_2} \frac{1}{(T_s' - \Delta)^2} \int_{-\Delta+\tau_l}^{T_s' - \Delta} \int_{-\Delta+\tau_l}^{T_s' - \Delta} \rho_l(x-y) dx dy$$

$$+ \sum_{l=1}^{L_1} \sum_{k=0, k \neq q}^{N-1} \frac{1}{(T_s' - \Delta)^2} \int_0^{T_s' - \Delta} \int_0^{T_s' - \Delta} \rho_l(x-y) e^{j2\pi(k-q)\Delta f'(x-y)} dx dy$$

$$+ \sum_{l=L_1+1}^{L_1+L_2} \sum_{k=0, k \neq q}^{N-1} \frac{1}{(T_s' - \Delta)^2} \int_{-\Delta+\tau_l}^{T_s' - \Delta} \int_{-\Delta+\tau_l}^{T_s' - \Delta} \rho_l(x-y) e^{j2\pi(k-q)\Delta f'(x-y)} dx dy$$

$$+ \sum_{l=L_1+1}^{L_1+L_2} \sum_{k=0}^{N-1} \frac{1}{(T_s' - \Delta)^2} \int_{-\Delta+\tau_l}^{-\Delta+\tau_l} \int_{-\Delta+\tau_l}^{-\Delta+\tau_l} \rho_l(x-y) e^{j2\pi(k-q)\Delta f'(x-y)} dx dy + \sigma_n^2 \quad (8A.6)$$

Taking account of  $N = T_s' K_{MC} R$ , substituting (8.4) into (8A.5) and (8A.6) leads to (8.30), (8.31), and (8.32).

## REFERENCES

- [1] Prasad, R., *CDMA for Wireless Personal Communications*, Norwood, MA: Artech House, 1996.
- [2] Prasad, R., *Universal Wireless Personal Communications*, Norwood, MA: Artech House, 1998.
- [3] Ojanperä, T., and R. Prasad, *Wideband CDMA for Third Generation Wireless Personal Communications*, Norwood, MA: Artech House, 1998.
- [4] Yee, N., J-P. Linnartz and G. Fettweis, "Multi-Carrier CDMA in Indoor Wireless Radio Networks," *Proc. of IEEE PIMRC'93*, pp.109–113, Sept. 1993.
- [5] Fazel, K., and L. Papke, "On the performance of convolutionally-coded CDMA/OFDM for Mobile Communication System," *Proc. of IEEE PIMRC'93*, pp.468–472, Sept. 1993.

- 
- [6] Chouly, A., A. Brajal and S. Jourdan, "Orthogonal Multicarrier Techniques applied to Direct Sequence Spread Spectrum CDMA Systems," *Proc. of IEEE GLOBECOM'93*, pp.1723–1728, Nov. 1993.
- [7] Fazel, K., S. Kaiser and M. Schnell, "A Flexible and High Performance Cellular Mobile Communications System Based on Orthogonal Multi-Carrier SSMA," *Wireless Personal Communications*, Vol.2, No. 1 & 2, pp.121–144, Kluwer Academic Publishers, Nov. 1995.
- [8] Möller, T., H. Rohling and R. Grönheid, "Comparison of Different Detection Algorithms for OFDM-CDMA in Broadband Rayleigh Fading," *Proc. of IEEE VTC'95*, pp.835–838, July 1995.
- [9] Kaiser, S., "OFDM-CDMA versus DS-CDMA: Performance Evaluation for Fading Channels," *Proc. of IEEE ICC'95*, pp.1722–1726, June 1995.
- [10] Kaiser, S., "On the Performance of Different Detection Techniques for OFDM-CDMA in fading channels," *Proc. of IEEE GLOBECOM'95*, pp.2059–1063, Nov. 1995.
- [11] Hara, S., T-H. Lee and R. Prasad, "BER Comparison of DS-CDMA and MC-CDMA for Frequency Selective Fading Channels," *Proc. of 7th Tyrrhenian International Workshop on Digital Communications*, pp.3–14, Sept. 1995.
- [12] Hara, S., and R. Prasad, "DS-CDMA, MC-CDMA and MT-CDMA For Mobile Multi-media Communications," *Proc. of IEEE VTC'96*, pp.1106–1110, April 1996.
- [13] Prasad, R., and S. Hara, "An Overview of Multi-Carrier CDMA," *Proc. of the 4th IEEE International Symposium on Spread Spectrum Techniques and Applications (ISSSTA'96)*, pp.107–114, Sept. 1996.
- [14] Kleer, F., S. Hara and R. Prasad, "Detection Strategies and Cancellation Schemes in a MC-CDMA System," in *CDMA Techniques For Third Generation Mobile Systems* edited by F. Swarts, P. van Rooyan, I. Oppermann and M. P. Lötter, Kluwer Academic Publishers, Boston/Dordrecht/London, 1999.
- [15] Proakis, J. G., *Digital Communications, 3rd ed.* New York: Mc-Graw Hill, 1995, pp.758–785.
- [16] Lee, W.C.Y., *Mobile Communications Engineering*, New York: Mc-Graw Hill, 1995, pp.40–44.
- [17] Jakes Jr., W. C., *Microwave Mobile Communications*, New York: Wiley, 1974, pp.19–26.
- [18] Chen, Q., E. S. Sousa and S. Pasupathy, "Performance of a Coded Multi-Carrier DS-CDMA System in Multi-path Fading Channels," *Wireless Personal Communications*, Vol.2, Nos.1 & 2, pp.167–187, 1995.



- 
- [19] Da Silva, V. M., and E. S. Sousa, "Multicarrier orthogonal CDMA signals for quasi-synchronous communication systems," *IEEE J. Select. Areas in Commun.*, Vol. JSAC-12, No. 5, June 1994.
- [20] Dambacher, P., *Digital Broadcasting, The Institution of Electrical Engineers*, pp.97–114, 1996.
- [21] Hara, S., M. Mouri, M. Okada and N. Morinaga, "Transmission performance analysis of multi-carrier modulation in frequency selective fast Rayleigh fading channel," *Wireless Personal Communications*, Vol. 2, No. 4, pp.335–356, 1995/1996.
- [22] Mosen, P., "Digital transmission performance on fading dispersive diversity channels," *IEEE Trans. Commun.*, Vol. COM-21, pp.33–39, Jan. 1973.
- [23] Rappaport, T. S., *Wireless Communications, Principles and Practice*, Upper Saddle River, NJ, Prentice-Hall, pp.188 – 189, 1996.
- [24] Steele, R., *Mobile Radio Communications*, London: Prentech Press, pp. 727 – 729, 1992.
- [25] Cimini, L. J., "Analysis and Simulation of a Digital Mobile Channel Using Orthogonal Frequency Division Multiplexing," *IEEE Trans. on Commun.*, Vol. COM-33, No. 6, pp. 665–675, June 1985.
- [26] Sampei, S., *Applications of Digital Wireless Technologies to Global Wireless Communications*, Upper Saddle River, NJ: Prentice-Hall, pp. 315–332, 1997.
- [27] A. Duel-Hallen, J. Holtzman and Z. Zvonar, "Multiuser detection for CDMA system," *IEEE Personal Communications*, Vol. 2, No. 2, pp. 46–58.
- [28] Rohling, H., et al., "Performance comparison of different multiple access schemes for the downlink of an OFDM communication system," *VTC '97*, pp. 1365–1369, 1997.
- [29] Chuang, J. C-I, "An OFDM-based System with Dynamic Packet Assignment and Interference Suppression for Advanced Cellular Internet Service," *Globecom'98*, Sydney, Australia, 1998.



## CHAPTER 9

# Orthogonal Frequency Division Multiple Access

### 9.1 INTRODUCTION

The previous chapter described some ways in which OFDM could be used both as a modulation scheme and as part of the multiple access technique, by applying a spreading code in the frequency domain. In this chapter, a variation on this theme is described, namely orthogonal frequency division multiple access (OFDMA). In OFDMA, multiple access is realized by providing each user with a fraction of the available number of subcarriers. In this way, it is equal to ordinary frequency division multiple access (FDMA); however, OFDMA avoids the relatively large guard bands that are necessary in FDMA to separate different users. An example of an OFDMA time-frequency grid is shown in Figure 9.1, where seven users  $a$  to  $g$  each use a certain fraction—which may be different for each user—of the available subcarriers. This particular example in fact is a mixture of OFDMA and Time Division Multiple Access (TDMA), because each user only transmits in one out of every four timeslots, which may contain one or several OFDM symbols.

### 9.2 FREQUENCY-HOPPING OFDMA

In the previous example of OFDMA, every user had a fixed set of subcarriers. It is a relatively easy change to allow hopping of the subcarriers per timeslot, as depicted in Figure 9.2. Allowing hopping with different hopping patterns for each user actually transforms the OFDMA system in a frequency-hopping CDMA system. This has the benefit of an increased frequency diversity, because each user uses all of the available bandwidth, as well as the interference averaging benefit that is common for all CDMA variants. By using forward-error correction coding over multiple hops, the system can correct for subcarriers in deep fades or subcarriers that are interfered by other users. Because the interference and fading characteristics change for every hop, the system

performance depends on the average received signal power and interference, rather than on the worst case fading and interference power.

Frequency	a		d		a		d		a		d	
	a		d		a		d		a		d	
	a	c	e		a	c	e		a	c	e	
	a	c	e		a	c	e		a	c	e	
	b		e	g	b		e	g	b		e	g
	b		e	g	b		e	g	b		e	g
	b		f	g	b		f	g	b		f	g
	b		f	g	b		f	g	b		f	g
Time												

**Figure 9.1** Example of the time-frequency grid with seven OFDMA users, a to g, which all have a fixed set of subcarriers every four timeslots.

Frequency	a											b		
													c	
		c			b									
				a										
								b	c					
	b												a	
					c									
								a						
Time														

**Figure 9.2** Example of the time-frequency grid with three hopping users, a, b and c, which all have one hop every four time slots.

A major advantage of frequency-hopping CDMA systems over direct-sequence or multicarrier CDMA systems is that it is relatively easy to eliminate intracell interference by using orthogonal hopping patterns within a cell. An example of such an orthogonal hopping set is depicted in Figure 9.3. For  $N$  subcarriers, it is always possible to construct  $N$  orthogonal-hopping patterns. Some useful construction rules for generating hopping patterns can be found in [1].



so a large fading margin has to be taken into account, which reduces system capacity. In a CDMA system, the interference is a sum of a large number of interfering signals. Because all these signals fade independently, the fluctuation in the total interference power is much less than the power fluctuation of a single interfering signal. Hence, in a CDMA system the fading margin can be significantly smaller than the margin for a non-CDMA system. This improvement in margin largely determines the capacity gain of a CDMA system.

In OFDMA, interference averaging is obtained by having different hopping patterns within each cell. The hopping sequences are constructed in such a way that two users in different cells interfere with each other only during a small fraction of all hops. In a heavily loaded system, many hops will interfere, but the interference will be different for each hop. Hence, by forward-error correction across several hops, the OFDMA performance will be limited by the average amount of interference rather than the worst case interference. An additional advantage of OFDMA over DS-SS-SS and MC-SS-SS is that there are some relatively simple ways to reduce the amount of intercell interference. For instance, the receiver can estimate the signal quality of each hop and use this information to give heavily interfered hops a lower weight in the decoding process.

Another important feature of CDMA is the possibility to perform soft handover by transmitting two signals from different base stations simultaneously on the same channel to one mobile terminal. Combining the signals from different base stations gives a diversity gain that significantly reduces the fading margin, because the probability that two base stations are in a fade is much smaller than the probability that one base station is in a fade. Less fading means that less power has to be transmitted, and hence less interference is generated, which gives an improvement in the capacity of the system. A nice feature of CDMA soft handover is that it has no impact on the complexity of the mobile terminal; as far as the mobile terminal is concerned, the overlapping signals of different base stations have the same effect as overlapping signals caused by multipath propagation.

For OFDMA systems, two basic soft handover methods exist, applicable to both the uplink and the downlink. (base station-to-mobile, mobile-to-base station). A requirement for both methods is that the transmissions from and to the base stations are synchronized such that the delay differences at the two base stations are well within the guard time of the OFDM symbols.

The first technique is to use the same set of subcarriers and the same hopping sequence in two cells to connect to two base stations. Hence, in the downlink the mobile receives a sum of two signals with identical data content. The mobile is not able to distinguish between the two base stations; the effect of soft handover is similar to that of adding extra multipath components, increasing the diversity gain. This type of soft handover is similar to soft handover in DS-SS-SS networks.

The second way for soft handoff is to use different sets of subcarriers in two cells. In contrast to the first method, in the downlink the mobile has to distinguish now

between the two base stations. It has to demodulate the signals from the two base stations separately, after which they can be combined, preferably by using maximal ratio combining. This type of soft handover is similar to the one that could be used in a non-CDMA network.

Advantages of the second method over the first—in the downlink—are an increased SNR gain because of receiver diversity, and more freedom for the base stations to allocate available subcarriers. In the first method, base stations are forced to use the same subcarriers. A main advantage of the first method is its simpler implementation; no additional hardware is needed, only some extra protocol features to connect to two base stations simultaneously. The second method does require extra hardware, because it has to demodulate an extra set of subcarriers. Further, it has to perform extra processing for the maximal ratio combining of the signals from the different base stations.

#### 9.4 OFDMA SYSTEM DESCRIPTION

As an example of an OFDMA system, this section gives a description of a system that was proposed for the European UMTS [3, 4]. Table 9.1 summarizes the parameters and key technical characteristics of this OFDMA air interface.

**Table 9.1**  
Parameters of the Proposed OFDMA system

No.	Parameter	Value
1	Subcarrier spacing	4.1666 kHz
2	Symbol time	288.46 $\mu$ s
3	Number of subcarriers per bandslot of 100 kHz	24
4	Pre-guard time	38 $\mu$ s
5	Post-guard time	8 $\mu$ s
6	Modulation unit	1 bandslot and 1 time slot (= 1 symbol)
7	Modulation block	4 time slots and 1 bandslot

Figure 9.4 illustrates the time-frequency grid of the OFDMA system. The resources (time and frequency) are allocated based on the type of services and operational environment. The number of timeslots and bandslots per user is variable to realize variable data rates. The smallest data rate is obtained for one bandslot of 24 subcarriers per timeslot of 288.46  $\mu$ s.

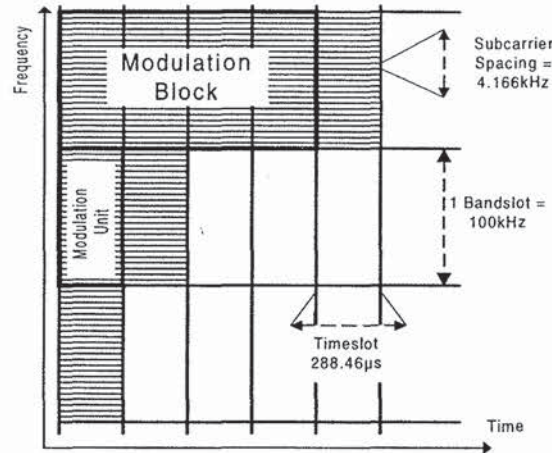


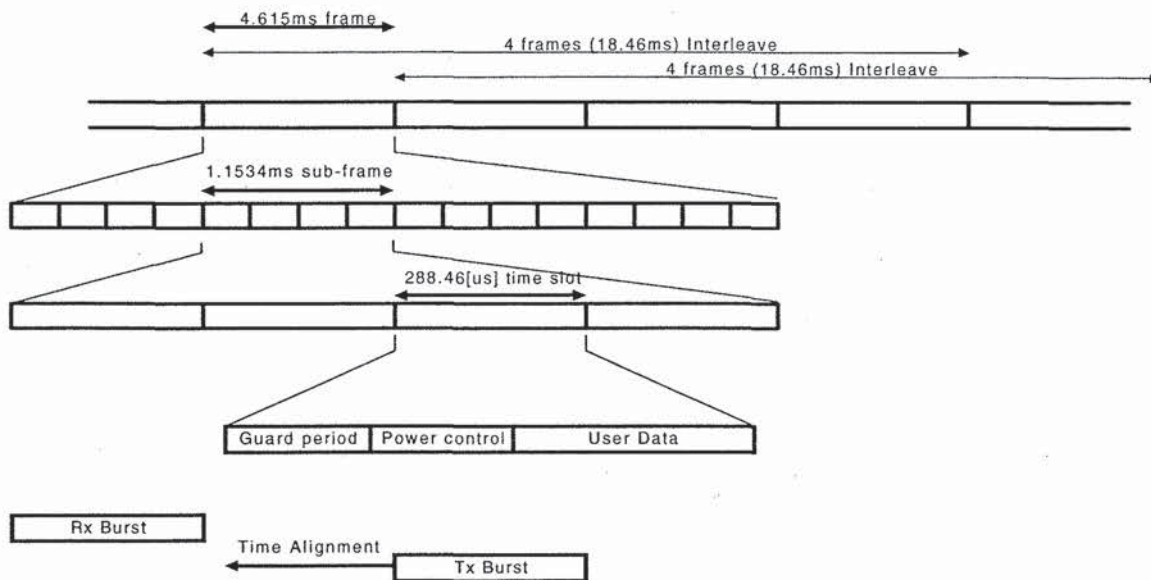
**Figure 9.4** Time-frequency grid.

The following summary shows some advantages of the proposed OFDMA system:

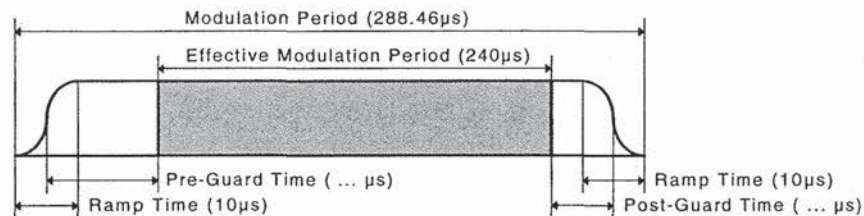
- Use of frequency-hopping OFDMA for interference averaging and frequency diversity;
- Time-division duplex MAC with dynamic channel allocation used for unpaired spectrum allocations, asymmetrical services, and unlicensed usage;
- Straightforward and efficient high bit rate support by allocating more subcarriers and/or timeslots;
- Small guard band requirements at approximately 100 kHz;
- No frequency planning option available; effective re-use factor of 1;
- GSM backwards compatibility; and
- Minimum bandwidth requirements for system deployment only 1.6 MHz (or less) and deployment possible in steps of 100kHz.

Figure 9.5 shows the TDMA frame structure. Each frame is of length 4.615 ms, which is divided into 4 subframes of length 1.1534 ms. A sub-frame contains 4 time-slots of duration 288.46  $\mu$ s. The timeslot contains a guard period, power control information and data. Every OFDM symbol is mapped onto one time-slot. The structure of an OFDMA symbol is depicted in Figure 9.6.





**Figure 9.5** Frame (TDMA) Structure.



**Figure 9.6** OFDM modulation burst.

The whole system frequency band is divided into small blocks (bandslots) with a fixed number of subcarriers. To maintain compatibility with GSM, a 100-kHz bandslot is chosen that consists of 24 subcarriers. Therefore, the subcarrier spacing is  $100/24 = 4.167$  kHz. Figure 9.7 shows the OFDMA frequency structure.

In each bandslot, the two subcarriers at the edge of the bandslot are left unmodulated to relax receiver blocking requirements. In addition, the interference of two adjacent blocks of subcarriers is reduced, which may occur when their orthogonality is compromised because of nonlinear PA effects. Adjacent bandslots can be concatenated to allow transmission of wideband services.

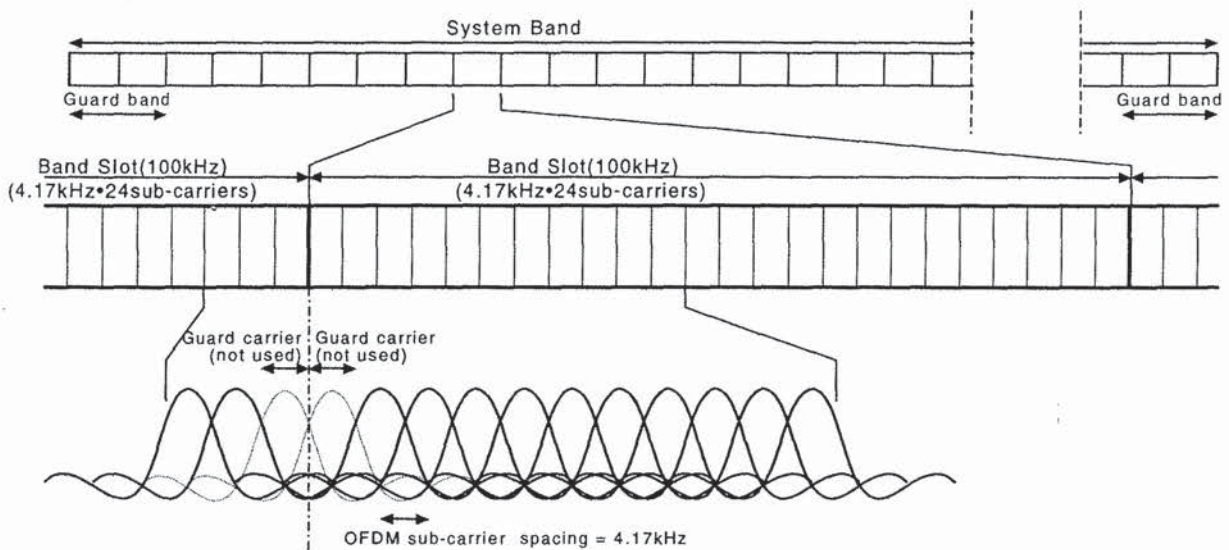


**Figure 9.7** OFDMA frequency structure.

### 9.4.1 Channel Coding

Convolutional encoding and soft-decision Viterbi decoding is used for the basic data transmission. The objective of this coding is to achieve good quality in the tough mobile radio channel. A constraint length of seven is used together with variable coderates in the range of  $1/4$  to  $3/4$ . To achieve very low bit-error rates (e.g.  $10^{-6}$ ) for video encoding or data transmission, a concatenated coding scheme is used with an inner convolutional code and an outer Reed-Solomon code.

### 9.4.2 Modulation

The modulation schemes of the OFDMA proposal are QPSK and 8-PSK with differential encoding in the frequency domain. An optional coherent mode with 16-QAM is available, which uses pilot subcarriers to obtain a channel estimate at the receiver. For differential encoding, each bandslot contains one known reference subcarrier value, as depicted in Figure 9.8.

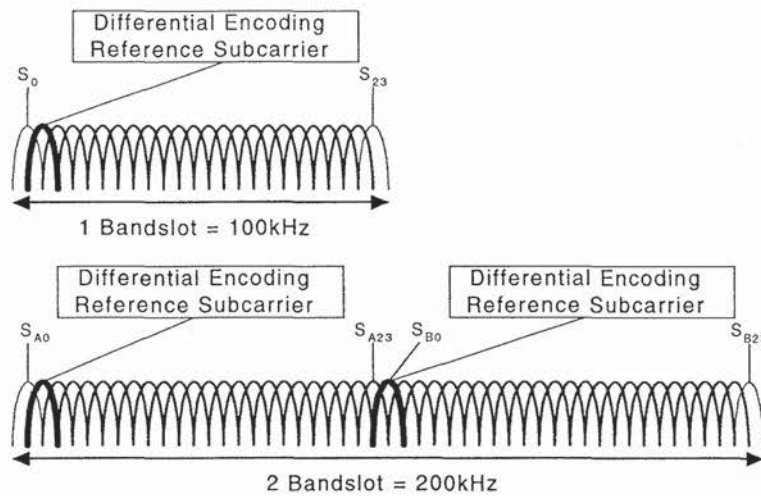


**Figure 9.8** Reference subcarrier allocation.

### 9.4.3 Time and Frequency Synchronization

Synchronization is an essential issue for the OFDMA system. The following aspects are considered for uplink and downlink: initial modulation timing synchronization, modulation timing tracking, initial frequency offset synchronization, and frequency tracking.

### 9.4.4 Initial Modulation Timing Synchronization

Initial timing synchronization is required to adjust the mobile station's internal timing to the base station's timeframe. After switching on, the mobile station monitors the initial acquisition channel (IACH) and the broadcast channel (BCCH).

After the mobile has detected the base station's timing, it sends a random access channel (RACH) packet to the base station. The base station measures the time offset for the received RACH packet and sends back the necessary timing advance to the mobile (similar to GSM). In the frame structure of the OFDMA system, reserved slots for reception of RACH packets exist.

Because of the time and frequency structure of the OFDMA system, the timing tracking is less critical compared with other OFDM systems where users are interleaved in the frequency domain. The base station can measure the position of the received OFDM burst within the allocated slot for each mobile station individually and send the according timing alignment information back to the mobile station. In addition, timing information can be refined and tracked after the transformation in the subcarrier domain, where a time shift is observed as a phase rotation.

In the mobile station, the timing information is obtained and adjusted by the above-mentioned correlation algorithm. Accurate timing information is required to determine the position of the useful data samples within each burst so the FFT window can be placed correctly. The guard samples relax the requirement for accurate timing because the position of the FFT window can be shifted within the guard time without performance degradation. Additional timing offset correction can be performed to cope with the FFT window misplacements.

#### **9.4.5 Initial Frequency Offset Synchronization**

After initial timing synchronization of the mobile station, the frequency offset can be measured by phase comparison of the (ideally) equal time samples within each burst. Equal samples are placed in the guard interval of the OFDM burst. A phase rotation indicates a frequency offset. Using this technique, a frequency error up to half the subcarrier spacing can be detected. The initial offset, however, can be larger, so it has to be detected using the specially designed symbols in the IACH channel.

#### **9.4.6 Synchronization Accuracy**

The proposed synchronization, acquisition, and tracking algorithm is independent of the modulation scheme (coherent or noncoherent). For coherent 16-QAM reception, further processing in the frequency (subcarrier domain) is possible to improve the performance. Frequency domain time tracking (or combined time-domain/frequency-domain tracking algorithms) can be based on observing phase shifts of the known pilots within the time-frequency grid on the subcarrier domain.

In the downlink, only an IACH is multiplexed to allow fast and precise initial timing and frequency synchronization. In the actual communication mode, timing and frequency tracking can be performed using a correlation-based synchronization algorithm. In the uplink, the rough timing offset is detected by the base station by measuring the arrival time of the RACH burst. This gives an initial time-advance value that is reported back to the mobile. During communication, the arrival time of the burst is detected by the base station using the proposed tracking algorithm (same as in the downlink) or a tracking algorithm in the frequency (subcarrier) domain, based on the detected constellation rotation.

Both algorithms can also be combined. The alignment values are calculated regularly and reported to the mobile station. Accuracy requirements are relaxed because the design of the burst allows some overlapping arrival (another advancing feature of the raised cosine pulse-shaping besides the reduction of out-of-band emission). In addition, the guard time helps to compensate timing misalignments. The OFDMA burst design provides a guard interval at the front and an additional guard interval at the back

of the OFDM symbol—see Figure 9.9—which provides robustness against a timing inaccuracy of  $\pm 10 \mu\text{s}$ .

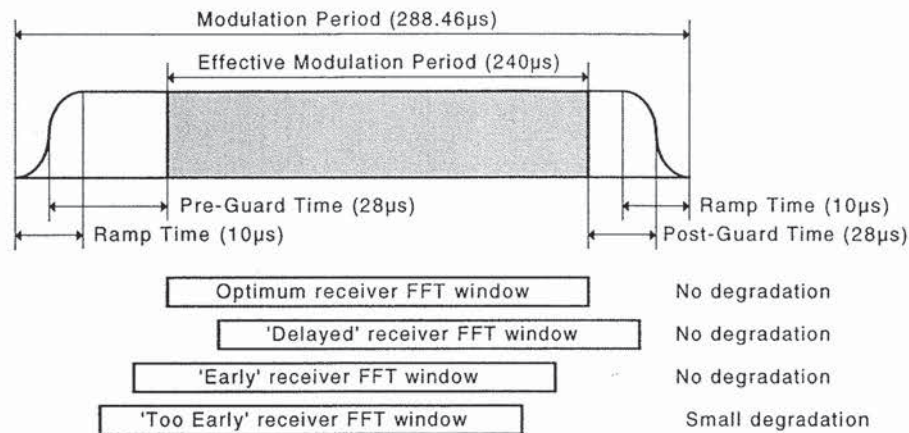


**Figure 9.9** OFMDA burst and synchronization requirements.

#### 9.4.7 Power Control

Power control in the uplink removes the unevenness of received signal strength at the base station side and decreases the total power to the minimum level required to support the specified quality of service (e.g. BER). The accuracy is less critical than CDMA because with OFDMA, orthogonality is always provided within one cell. A precise power control, however, not only improves the transmission performance but also minimizes the interference to other cells and therefore increases overall capacity.

The OFDMA concept uses both closed-loop and open-loop power control. Based on quality parameters, measured on a slot-by-slot basis, the power is adjusted in the mobile as well as in the base station transmitter. Each receiver measures the quality of the received burst ( $C/I$  ratio) and transmits in the next burst a request to the opposite transmitter to increase, keep, or decrease the power level in steps of 1 dB. For the fastest power control mode, one subcarrier is dedicated to carry power control information, and the power is then adjusted on a frame-by-frame basis (each 1.152 ms). Figure 9.10 depicts the power control operation.

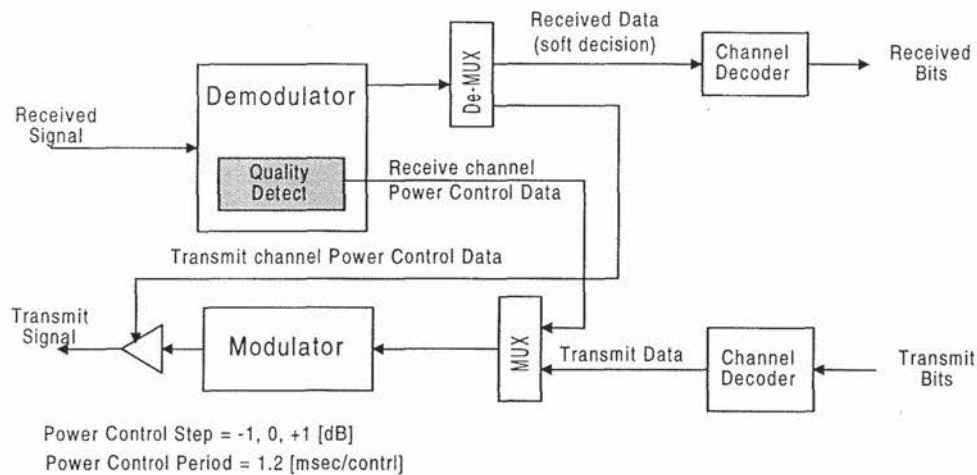


**Figure 9.10** Operation of power control in a mobile station.

#### 9.4.8 Random Frequency-Hopping Operation

Frequency hopping is very effective to achieve frequency diversity and interference diversity. Frequency diversity is useful to average the frequency-selective channel properties (fading dips). Interference diversity is one of the important techniques used in the OFDMA proposal and has been shown to improve capacity in slow frequency-hopping TDMA systems [8].

The random hopping pattern is designed to be orthogonal within one cell (no collisions in the time-frequency grid) and random between cells (this causes cochannel interference).

The frequency hopping pattern has to fulfill certain requirements:

- Orthogonality within one cell,
- Support of a variety of services by assigning different bandwidth (number of bandslots),
- Support of a variety of services by assigning timeslots (number of timeslots), and
- Support of a couple of timeslot structures (4-TDMA, 8-TDMA, 16-TDMA) within the pattern.

The hopping pattern is generated at the base station according to the expected service and traffic requirement and assigned to the cell. This assignment can be modified because of changes in the traffic characteristics. The base station can then support a set of services and a certain number of users for each service.

### 9.4.9 Dynamic Channel Allocation (Fast DCA)

Besides FH hopping mode, the system can also be operated in time division duplex (TDD) mode. Unlike the FH mode, the TDD mode does not separate the spectrum in an uplink and a downlink. Instead, it assigns bandslots individually to uplink or downlink connections. In TDD mode, a dynamic channel allocation algorithm is employed to avoid (rather than to average) excessive interference. The TDD mode is intended for pico-cellular, indoor use. The indoor environment is characterized by

- Short radio propagation delays (100m is traversed in  $0.3 \mu\text{s}$ , or 0.1% of the symbol duration),
- Greater demand for high rate services, reducing the interference averaging advantage of frequency-hopping mode,
- High-speed data traffic is often asymmetric, prompting flexible division of bandwidth between uplink and downlink, and
- Less severe propagation conditions than those outdoor; mobility-induced Doppler spread and delay spread are both lower.

In the TDD mode, the transmissions of mobile users are scheduled by the base station, which regularly transmits a frame map containing:

- Bandslot allocations for the next frame. Bandslots can be allocated to
  - The base station for downlink transmission to a single terminal,
  - The base station for downlink transmission to all terminals (broadcast),
  - A single terminal for an uplink transmission, and
  - All (or a group of) terminals for contention based access,
- Transmit power assignments for MTs,
- Acknowledgements for contention traffic received in the previous frame,
- Slots are allocated on a connection basis, so that connection-dependent QoS can be provisioned (a mobile can have one or more connections), and
- Control data and user data are transmitted on different connections.

Terminals can transmit requests for bandslots in contention slots designated by the base station in the FM. They can also piggyback requests onto uplink transmissions, which provides contention free access, particularly under heavy traffic conditions. The base station performs interference measurements in all bandslots, except at the timeslots in which it is transmitting. This information is used by the bandslot allocation algorithm to assign uplink transmissions to slots with minimal interference. Note that an uplink transmission in an interference free slot (as measured by the base station) may interfere with a simultaneous uplink transmission at a neighboring base station. No simultaneous uplink and downlink transmissions may be scheduled within a cell. Therefore, the inability of the base station to measure interference in slots in which it is transmitting, does not reduce capacity.

The frame layout is entirely decided by the DCA algorithm. Like the FH algorithm, the DCA algorithm is distributed and does not rely on communication by

way of the infrastructure. Also, as the FH algorithm, it is not part of the system specification, the algorithm may be vendor specific, allowing competitive positioning within a standardized system.

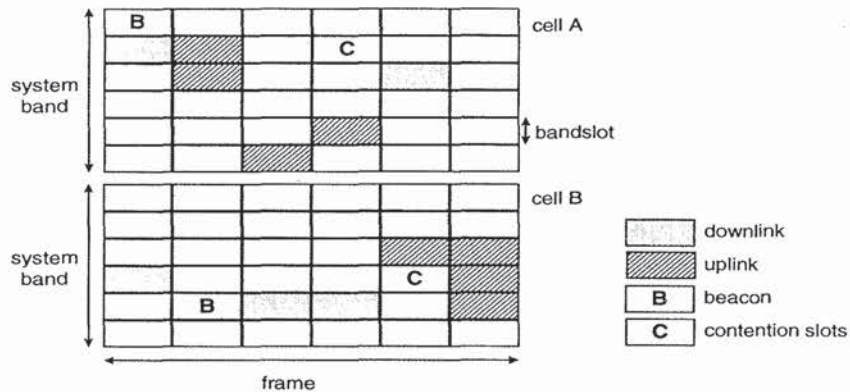


**Figure 9.11** Example of frame layout.

An example of a frame layout is shown in Figure 9.11. The figure is purely illustrative. The frame duration and system bandwidth have unrealistically small values. Also, the packets, such as the frame map—that is transmitted in the beacon—and user data packets, occupy more than one bandslot in practice.

In general, the applied DCA algorithm must strive to reduce intracell and intercell interference. Constant bit-rate traffic causes long-term interference that is highly predictive of the interference in the next slot. If traffic is bursty, the predictive value of interference measurements is limited. Because a base station is not aware whether bandslots in neighboring cells are allocated to circuit mode or packet mode connections, base stations and mobiles average measurements over longer periods of time. As a rule, busy slots (high average interference level) are avoided for any transmission. Quiet slots (low average interference level) are assigned to constant bit-rate connections, or to the guaranteed part of a variable bit-rate connection. Slots with medium average interference are assigned to connections with bursty traffic, which use contention mode access.

Initial association does not differ from the procedure in FH mode. When joining the base station, a mobile station first detects the location of the initial acquisition channel and the broadcast channel. The broadcast channel is used to convey the location of the frame map in the current frame to the mobile station. Once the frame map is located, it can be tracked because it advertises when it is moved to a different location.



#### 9.4.10 Simple Dynamic Channel Allocation

Simple DCA assigns a fixed resource (bandslots and timeslots) to a communication during setup. This assignment is kept for the whole duration of the communication. This scheme is very simple but cannot react on varying interference or channel conditions compared with fast DCA where the “actual best” channel (= timeslot and bandslot combination) is used for transmission. This scheme has a lower performance than the fast DCA operation but can be used for simple (uncoordinated) applications like cordless telephony.

#### 9.4.11 OFDMA Capacity

System-level simulations were conducted for various types of services and environments. The simulations were conducted in accordance with [7]. Table 9.2 lists the simulated capacities.

**Table 9.2**  
Capacities for various services and environments.

	Environment	Cell capacity (#Users/MHz/Cell) (uplink/downlink)	Spectrum efficiency (kbps/MHz/Cell) (uplink/downlink)
Data 384 kbps	Outdoor to indoor and pedestrian A		440/465
Data 2048 kbps	Indoor		240/240
Speech 8 kbps	Indoor office A	33.0/31.0	132/124
Speech 8 kbps	Outdoor to indoor and pedestrian A	30.75/32.25	123/129
Speech 8 kbps	Vehicular A	27.0/30.5	108/122

### 9.5 CONCLUSIONS

OFDMA is a very flexible multiple access scheme. In combination with frequency hopping, it offers all the benefits of direct-sequence CDMA or multicarrier CDMA systems, with the following additional advantages:

- OFDMA can achieve a larger system capacity because it is not affected by intracell interference, which is the dominant source of interference in DS-CDMA and MC-CDMA.
- OFDMA is flexible in terms of the required bandwidth; it can easily be scaled to fit in a certain available piece of spectrum simply by changing the number of used subcarriers. DS-CDMA and MC-CDMA require a fixed and relatively large chunk of spectrum because of the fixed spread-spectrum chip rate.

- OFDMA seems more suited than DS-CDMA and MC-CDMA for support of large data rates. When the data rates per user become larger, the spreading gain becomes lower, so the performance of a CDMA system converges to that of a nonspread system. In that case, OFDMA with dynamic channel allocation instead of frequency hopping makes more sense than multicode DS-CDMA or MC-CDMA.

## REFERENCES

- [1] Pottie, G. J., and A. R. Calderbank, "Channel Coding Strategies for Cellular Radio," *IEEE International Symposium on Information Theory*, San Antonio, TX, Jan. 1993.
- [2] Viterbi, A. J., "The Orthogonal-Random. Waveform Dichotomy for Digital Mobile Communication," *IEEE Personal Communications*, pp.18–24, First Quarter 1994.
- [3] OFDMA Evaluation Report, "The Multiple Access Scheme Proposal for the UMTS Terrestrial Radio Air Interface (UTRA) System, Part 1: System Description and Performance Evaluation," SMG2 Tdoc 362a/97, 1997.
- [4] Suzuki, M., R. Boehnke, and K. Sakoda, "BDMA - Band Division Multiple Access. new Air-Interface for 3<sup>rd</sup> Generation Mobile System, UMTS, in Europe," *Proceedings ACTS Mobile Communications Summit*, Aalborg, Denmark, pp. 482–488, Oct. 1997.
- [5] Rohling, H., and R. Grünheid, "Performance Comparison of Different Multiple Access Schemes for the Downlink of an OFDM Communication System," *Proceedings of IEEE VTC '97*, Phoenix, AZ, pp. 1365–1369, May 1997.
- [6] Chuang, J., "An OFDM Based System with Dynamic Packet Assignment and Interference Suppression for Advanced Internet Service," *Globecom '98*, Sydney, Australia, May 1998.
- [7] ETSI draft specification on the selection procedure for the choice of radio transmission technologies of the Universal Mobile Telecommunication System (UMTS), ETR/SMG-50402, Vers. 0.9.5.
- [8] Olofsson, H., J. Naslund, and J. Sköld, "Interference Diversity Gain in Frequency Hopping GSM," *Proceedings IEEE Vehicular Technology Conference*, Chicago, pp. 102–106, June 1995.

# CHAPTER 10

## Applications of OFDM

### 10.1 INTRODUCTION

This chapter describes four applications of OFDM in wireless systems. The first two are broadcasting applications for both audio and television. The Digital Audio Broadcasting (DAB) standard was in fact the first OFDM-based standard. The main reasons to choose OFDM for this system, which also applies to Digital Video Broadcasting (DVB), are the possibility to make a single frequency network and the efficient handling of multipath delay spread.

After DAB and DVB, two wireless LAN applications are described. The first one is an OFDM-based wireless ATM network, which was developed in the European Magic WAND project. The last section describes the OFDM-based IEEE, ETSI and MMAC wireless LAN standard for the 5-GHz band, providing data rates of 6 up to 54 Mbps. This new standard is the first to use OFDM in packet-based wireless communication, after projects like Magic WAND demonstrated the viability of OFDM for this type of application.

### 10.2 DIGITAL AUDIO BROADCASTING

DAB is the successor of current analog audio broadcasting based on AM and FM. DAB offers improved sound quality, comparable to that of a compact disc, new data services, and a higher spectrum efficiency. DAB was standardized in 1995 by the European Telecommunications Standards Institute (ETSI) as the first standard to use OFDM [1, 2]. The basis for this standard was the specification developed by the European Eureka 147 DAB project, which started in 1988.

DAB has four transmission modes using different sets of OFDM parameters, which are listed in Table 10.1. The parameters for modes I to III are optimized for use

in specific frequency bands, while mode IV was introduced to provide a better coverage range at the cost of an increased vulnerability to Doppler shift.

**Table 10.1**  
DAB OFDM Parameters.

	<b>Mode I</b>	<b>Mode II</b>	<b>Mode III</b>	<b>Mode IV</b>
Number of subcarriers	1,536	384	192	768
Subcarrier spacing	1 kHz	4 kHz	8 kHz	2 kHz
Symbol time	1.246 ms	311.5 $\mu$ s	155.8 $\mu$ s	623 $\mu$ s
Guard time	246 $\mu$ s	61.5 $\mu$ s	30.8 $\mu$ s	123 $\mu$ s
Carrier frequency	<375 MHz	<1.5 GHz	<3 GHz	<1.5 GHz
Transmitter separation	<96 km	<24 km	<12 km	<48 km

One important reason to use OFDM for DAB is the possibility to use a single frequency network, which greatly enhances the spectrum efficiency. In a single-frequency network, a user receives the same signal from several transmitters simultaneously. Because of the propagation differences among transmitters, there is some delay between the arrival of the signals. This is illustrated in Figure 10.1, where two DAB signals arrive at the user with a delay difference that is equal to the distance difference ( $d_1 - d_2$ ) divided by the speed of light. Basically, to the user this situation is equivalent to a two-ray multipath channel. Hence, as long as the propagation differences between the two signals are smaller than the guard time of the OFDM symbols, no ISI or ICI will occur. The addition of the two time-shifted signals creates a diversity advantage for the user; the probability that the sum of both signals has an unacceptably low power because of shadowing or flat fading is much lower than the probability that one of the individual signals is too weak.

The DAB transmitted data consists of a number of audio signals, sampled at 48 kHz with an input resolution up to 22 bits. The digital audio signal is compressed to a rate in the range of 32 to 384 kbps, depending on the desired quality. The signal is divided into frames of 24 ms. The start of a frame is indicated by a null symbol, which is a silence period that is slightly larger than the duration of a normal OFDM symbol. Then, a reference OFDM symbol is sent which serves as the starting point for the differential decoding of the QPSK-modulated subcarriers. Differential encoding is applied in the time domain, so in the receiver, the phase of each subcarrier is compared with the phase of the same subcarriers from the previous OFDM symbol.

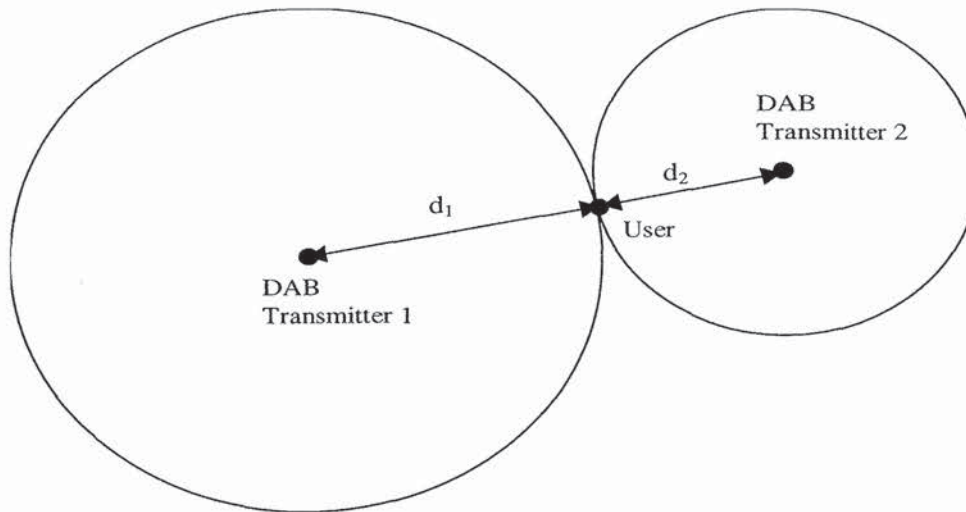


**Figure 10.1** User receiving two DAB transmitters.

The digital input data is encoded by a rate  $1/4$  convolutional code with constraint length 7 to provide protection against fading subcarriers. The coding rate can be increased up to  $8/9$  by puncturing. This gives a maximum total data rate of  $1,536 \times 2 \times 8/9 \times 1/1.246 \cdot 10^{-3}$ , which is approximately 2.2 Mbps. The coded data are interleaved to separate coded bits in the frequency domain as much as possible, which avoids large error bursts in case of a deep fade affecting a group of subcarriers.

### 10.3 TERRESTRIAL DIGITAL VIDEO BROADCASTING

Research on a digital system for television broadcasting has been carried out since the late 1980s. In 1993, a pan-broadcasting-industry group started the Digital Video Broadcasting (DVB) project. Within this project, a set of specifications was developed for the delivery of digital television over satellites, cable, and through terrestrial transmitters. This section describes the terrestrial DVB system, which was standardized in 1997 [3, 4].

Terrestrial DVB uses OFDM with two possible modes, using 1,705 and 6,817 subcarriers, respectively. These modes are referred to as 2k and 8k modes, respectively, as these are the sizes of the FFT/IFFT needed to generate and demodulate all subcarriers. The main reason to have two modes were doubts about the implementability of the 8k subcarrier system. Basically, the 2k system is a simplified version which requires an FFT/IFFT that is only a quarter of the size that is needed for the 8k system. Because the guard time is also four times smaller, the 2k system can handle less delay spread and less propagation delay differences among transmitters within a single-frequency network. The FFT interval duration for the 8k system is 896

$\mu\text{s}$ , while the guard time can have four different values from 28 to 224  $\mu\text{s}$ . The corresponding values for the 2k system are four times smaller.

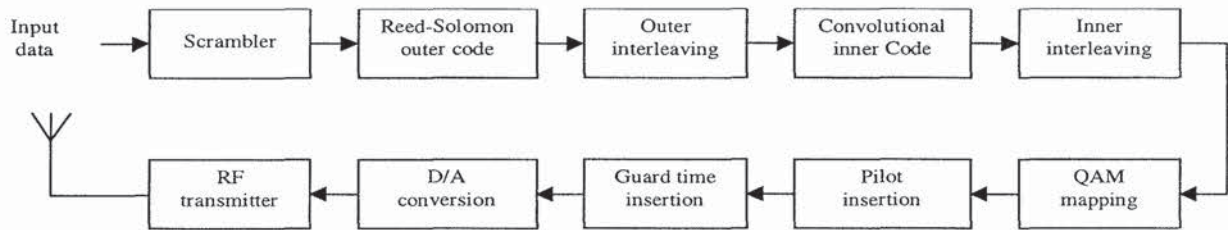


**Figure 10.2** Block diagram of a DVB-T transmitter.

Figure 10.2 shows a block diagram of a DVB-T transmitter. The input data are divided into groups of 188 bytes, which are scrambled and coded by an outer shortened Reed-Solomon code (204,188,  $t=8$ ). This code can correct up to eight erroneous bytes in a frame of 204 bytes. The coded bits are interleaved by a convolutional interleaver that interleaves byte-wise with a depth of 12 bytes and then again coded by a rate 1/2, constraint length 7 convolutional code with generator polynomials (171, 133 octal). The rate of this latter code can be increased by puncturing to 2/3, 3/4, 5/6, or 7/8. The convolutionally encoded bits are interleaved by an inner interleaver and then mapped onto QPSK, 16-QAM, or 64-QAM symbols.

For 16-QAM and 64-QAM, optional hierarchical coding can be applied. In this case, the constellation points are moved farther away from the origin so the quadrants can be detected more reliably than the position within each quadrant. This is illustrated in Figure 10.3 for a hierarchical 16-QAM constellation. For this constellation, the minimum distance between points from different quadrants is double the distance of a normal 16-QAM constellation, where the constellation points would have values of 1 and 3 instead of 2 and 4. Corrected for the increased power of the constellation, the detection of the quadrants has a 3-dB SNR advantage over the detection of points in a normal 16-QAM constellation. The advantage of this hierarchical coding is that users for which the SNR is just too low to decode all bits can at least decode the two most significant bits that determine the quadrant. These bits give them the same video signal, but at a lower resolution.

To obtain reference amplitudes and phases to perform coherent QAM demodulation, pilot subcarriers are transmitted. For the 8k mode, in each symbol there are 768 pilots, so 6,048 subcarriers remain for data. The 2k mode has 192 pilots and 1,512 data subcarriers. The position of the pilots varies from symbol to symbol with a pattern that repeats after four OFDM symbols. The pilots allow a receiver to estimate the channel both in frequency as well as in time, which is important as for mobile receivers there can be significant channel changes within a few OFDM symbols.

Techniques to do this type of two-dimensional channel estimation based on pilot subcarriers are described in Chapter 5.

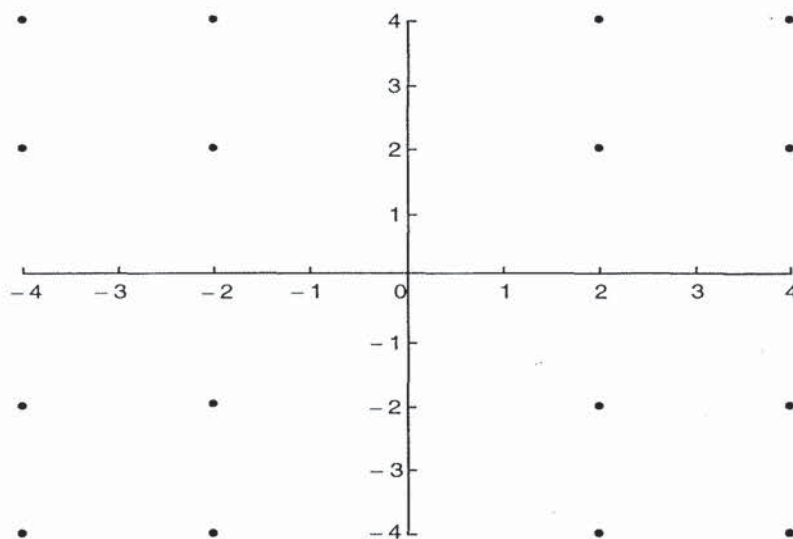
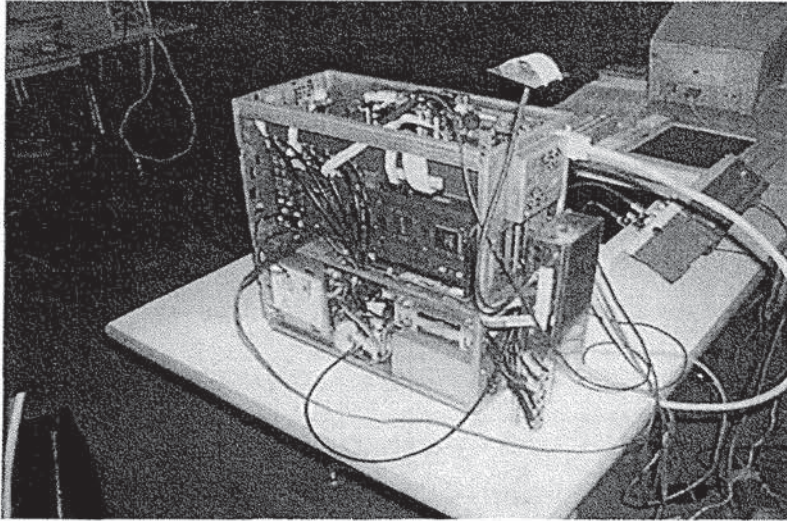


Figure 10.3 Hierarchical 16-QAM.

#### 10.4 MAGIC WAND

The Magic WAND (Wireless ATM Network Demonstrator) project was part of the European ACTS (Advanced Communications Technology and Server) program [5]. The Magic WAND consortium members implemented a prototype wireless ATM network based on OFDM modulation. This prototype had a large impact on standardization activities in the 5-GHz band. First, by employing OFDM-based modems, Magic WAND helped to gain acceptance for OFDM as a viable modulation type for high-rate wireless communications. Second, the wireless ATM-based approach of Magic WAND forms the basis for the standardization of the HIPERLAN type 2 Data Link Layer.

Figure 10.4 shows one of the prototype Magic WAND 5-GHz modems demonstrating wireless video playback and Web browsing applications at the Demo '98 exhibition in Berlin [6].



**Figure 10.4** Magic WAND prototype 5-GHz modem.

#### 10.4.1 Magic WAND Physical Layer

The main parameters of the WAND physical layer are listed in Table 10.2. OFDM with 16 subcarriers is used, the number of which was chosen to facilitate implementation. The 400-ns guard time provides a delay spread tolerance of about 50 ns. Because of a 240-ns rolloff time (see Chapter 2), the effective guard time is only 160 ns. While this is sufficient for most office buildings and the WAND trial site, a realistic product would require more delay spread robustness to also cover large office buildings and factory halls.

The OFDM subcarriers are 8-PSK modulated. At a symbol rate of 13.3 Msymbols/s, this gives a raw bit rate of 40 Mbps. The rate 1/2 complementary coding reduces the data rate to 20 Mbps. The subcarrier spacing is 1.25 MHz, which gives a total (3-dB) bandwidth of 20 MHz.

The packet preamble is 8.4  $\mu$ s in duration and consists of one OFDM symbol, repeated seven times. This preamble is used for packet detection, automatic gain control, frequency offset estimation, symbol timing, and channel estimation.

The PHY payload holds an odd number of half-slots. Each half-slot consists of 9 symbols or 27 bytes. This number was chosen so that a full slot, of 54 bytes, can hold an ATM cell (which is 52 bytes long), and is also a multiple of 3 bytes, which is imposed by the PHY's modulation scheme.



**Table 10.2**  
Main parameters of the WAND OFDM modem.

Number of subcarriers	16
Modulation	8-PSK
Coding	Two interleaved length 8 complementary codes, rate $\frac{1}{2}$
Bit rate (after decoding)	20 Mbps (24 bits per symbol)
Symbol time	1.2 $\mu$ s
Guard time	0.4 $\mu$ s
Windowing	Raised cosine, rolloff factor = 0.2
Subcarrier spacing	1.25 MHz
Training length	7 symbols
Carrier frequency	5.2 GHz
Peak output power	1W

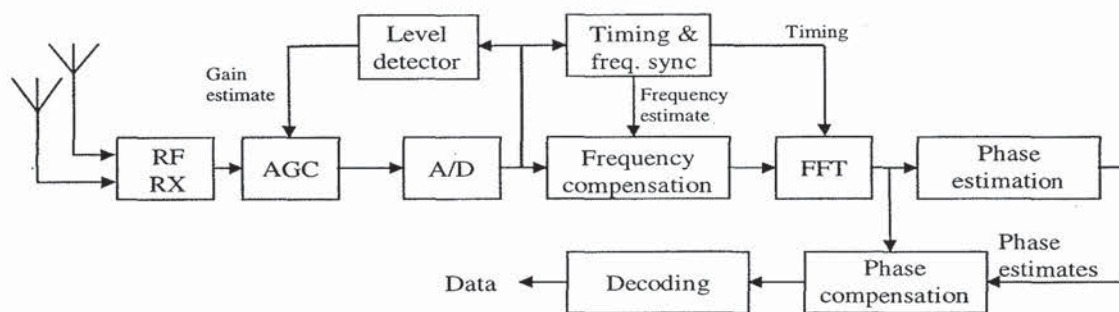


**Figure 10.5** OFDM receiver.

Figure 10.5 shows a block diagram of the OFDM receiver. The RF receiver takes care of amplifying and down-converting the signal. The automatic gain control (AGC) is one of the most difficult parts in the receiver, since the gain has to settle within 3  $\mu$ s after start of reception. After the analog-to-digital (A/D) conversion, the frequency of the signal has to be estimated and corrected for, because OFDM is sensitive to frequency errors (see Chapter 4).

By taking the FFT of groups of samples at the right time instants, the receiver obtains amplitude and phase estimates of the 16 subchannels. From the initial training sequence, the receiver has to acquire and track the reference phases for all subchannels. After phase compensation, finally the 24 information bits can be decoded from the 16 complex subcarrier values.

### 10.4.2 Coding

The WAND modem uses complementary codes for both forward-error correction coding and peak-to-average power (PAP) reduction. Length 8 complementary codes are used, with four input 8-PSK phases generating eight complex code outputs as described in Chapter 6. By taking the IFFT of these complex values, an OFDM signal with a low PAP ratio is obtained. To encode all 16 subcarriers, two length 8 codes are interleaved, which maximizes the benefits of frequency diversity. It is also possible to use length 16 complementary codes, but for that length, only five phases can be encoded into 16 subcarriers, reducing the coding rate from 1/2 to 5/16. The minimum distance of the length 8 code is four subsymbols. Hence, three arbitrary subchannels can be erased without causing errors, providing that the remaining subchannels are not in error.

### 10.4.3 Simulated Error Probabilities

Bit-error ratios (BER) and packet-error ratios (PER) for various delay spreads are depicted in Figure 10.6. For each mean  $E_b/N_o$  value, 40,000 ATM-cell transmissions have been simulated in Rayleigh fading channels, without antenna diversity. In all transmissions, a frequency offset of 40 kHz was simulated, which has to be estimated and compensated for by the receiver. Figure 10.6 clearly shows that the coded OFDM system is able to benefit from the frequency diversity, which is present for nonzero delay spreads.

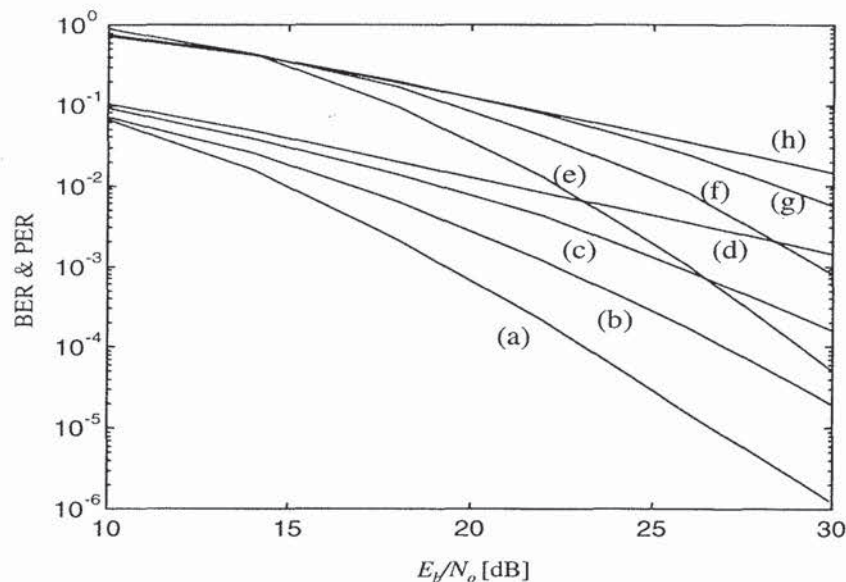


**Figure 10.6** BER (a–d) and PER (e–h) versus mean  $E_b/N_o$  for delay spreads of (a,e) 50 ns, (b,f) 20 ns, (c,g) 10 ns, (d,h) 0.

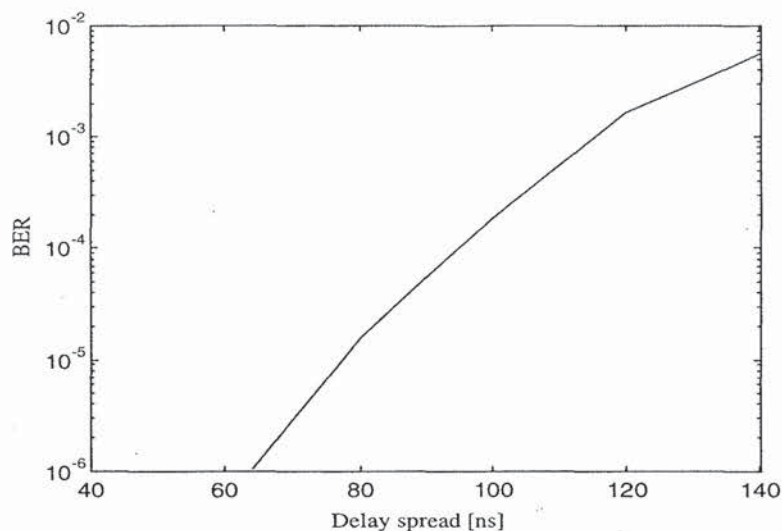


**Figure 10.7** Irreducible BER versus delay spread for an exponential power delay profile.

For delay spreads larger than 50 ns, the error curves converge to some irreducible error floor, caused by intersymbol and intercarrier interference of multipath signals with excess delays larger than the guard time. In Figure 10.7, this irreducible BER is plotted versus the delay spread. Notice that an exponential power-delay profile is used in the simulations. For a two-ray model, for instance, the irreducible error floor arises only for delay spreads larger than half of the guard time (i.e., 200 ns for the prototype WAND modem). Thus, the exponential power delay profile gives much more pessimistic results in this respect. Conversely, the two-ray model is known to give less diversity gain, because there are only two independent fading paths.

#### 10.4.4 Effects of Clipping

Despite the use of complementary coding in the WAND OFDM system, the transmitted signal still has a 6-dB PAP ratio. To make the efficiency of the transmitter power amplifier as high as possible, we have to accept a certain nonlinear distortion in the peaks of the OFDM signal. A crude analysis of this nonlinear distortion can be made by assuming a clipping transfer function. Figure 10.8 shows the BER in an AWGN channel for clipping levels of 0 to 4 dB below the maximum amplitude. It can be seen that significant degradation occurs only for a clipping level of more than 3 dB below the peak amplitude. Of course, such severe clipping is not allowed from a spectrum point of view, but the analysis at least shows that the OFDM transmission itself is relatively insensitive against clipping.

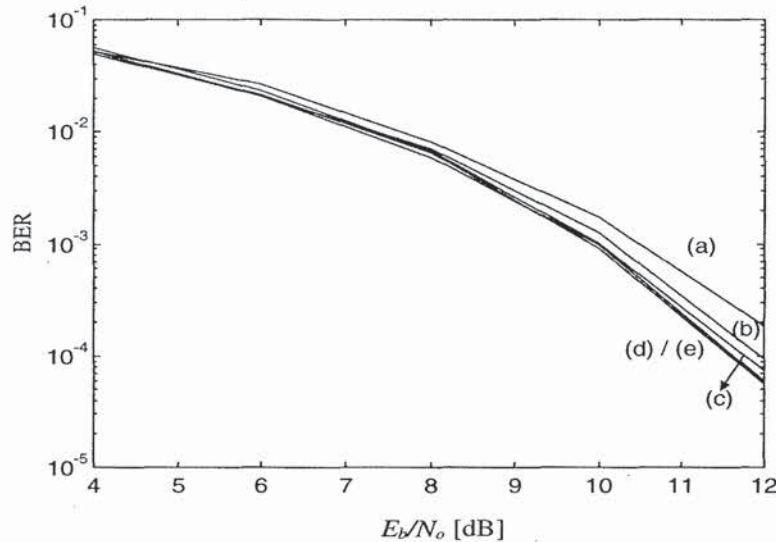


**Figure 10.8** BER in AWGN with the transmitted OFDM signals clipped at (a) 4 dB, (b) 3 dB, (c) 2 dB, (d) 1 dB and (e) 0 dB below the maximum amplitude.

Clipping at the receiver is different from clipping at the transmitter, because the receiver does not know in advance what the peak amplitude is, contrary to the transmitter. Even after the initial training symbols, when the receiver freezes its AGC, the receiver does not know what the peak amplitude will be in the rest of the packet. Except for noise, this is caused by two effects: first, multipath fading channels change the peak-to-average power ratio of the OFDM signal and second, different symbols have different PAP ratios.

An OFDM receiver must freeze its AGC based on the observed amplitude level during training. The peak amplitude during training is most probably not the largest amplitude of the entire packet. Thus, the question is how to set the AGC level such that clipping effects are negligible. Based on the results from Chapter 6, the ideal AGC setting is such that the clipping level is about 6 to 10 dB above the average input power level. In this case, the interference caused by clipping is relatively small compared with the average signal power. If the clipping level is more than 10 dB above the average power level, then the risk exists that quantization noise starts dominating over clipping noise, as the most significant bits of the A/D converter are hardly used in this case.

#### 10.4.5 Magic WAND Medium Access Control Layer

The MAC (Medium Access Control) and DLC (Data Link Control) layers of the WAND system have been combined in one layer, bearing the name MASCARA (Mobile Access Scheme based on Contention And Reservation for ATM). The underlying concept is based on the following set of ideas and requirements which are elaborated in the subsequent paragraphs.

- QoS-aware, reservation-based demand assigned protocol;
- Multiple virtual connections per terminal;
- Power efficiency;
- Cell transfer service for optimal interworking with ATM;
- Amortization of PHY overhead over multiple ATM cells;
- Contention-mode request and control channel; and
- ARQ (Automatic Repeat reQuest)-based cell loss recovery.

ATM is designed to offer service to wire-line users with a guaranteed quality of service. To extend ATM service to mobile terminals, the wireless access network needs to be QoS-aware as well. A centralized algorithm allotting transmission time to users on the basis of their explicit demands seems to be an obvious way to provide QoS and isolation among users' traffic streams. We note that the disadvantage over contention-based algorithms as used in wireless LANs and wireless PBXs is that they do not inherently support multicellular operation. To function correctly, they require a cellular frequency reuse topology, with perfect separation between radio cells with identical frequencies. As usual for wireless LANs, TDD between uplink and downlink is chosen, primarily to support traffic asymmetry.

As a multimedia terminal may have many simultaneous connections, most probably with different QoS requirements, the network must be able—besides addressing individual terminals—to distinguish separate connections of those terminals. Given the smaller number of users and the scarcity of bandwidth, the relatively large addressing overhead of ATM, being designed for large wire-line networks, must be avoided.

Mobile terminals draw power from batteries, and to extend battery-life the protocols need to be energy aware. A frame-based MAC, in which the access point notifies all associated terminals about their expected transmissions and receptions in the entire frame helps to conserve power: terminals switch on their radios only when necessary. From the energy perspective, the frame duration should be made as long as possible. QoS considerations, on the other hand, put a bound on the maximal frame length. For this scheme to work, a frame structure by itself is not sufficient. A common time base among terminals and access point is required as well. For practical reasons the granularity of time must be bounded. The unit of time in MASCARA is a timeslot, and all packet transmissions commence on a timeslot boundary.

To provide seamless interworking with the ATM backbone, and transparency to the user, packets must carry ATM cells. It makes sense to choose the slot duration equal to a cell's transmission time. The same length of time is imposed on the packet header (radio preamble and MAC header) as well. In the WAND system, the first half of the overhead slot is used for the preamble, the other half is used for the MAC header.

If each packet were to contain just one cell, the protocol efficiency would be merely 50%. To increase efficiency, a longer packet size can be adopted. On the other

hand, QoS-driven restrictions on cellization delay put an upper bound on packet length. In the case of 64 kbps speech traffic for instance, cellization delay is 6 ms per cell, which restricts the packet length to one or two cells. The logical decision is to allow packets of variable length, depending on the connection's delay requirements, with a payload of an integer number of cells.

Demand-assigned algorithms assign timeslots to terminals, based on terminal demand. Uplink packets contain fields in which a terminal can put its request. If a terminal cannot piggyback its request, because no timeslots were assigned to it (a deadlock situation), or because it cannot afford to wait for the next packet, the terminal can transmit its request in an unreserved timeslot. A contention period is scheduled at the end of every frame. Contention slots can be used for incidental control packets as well.

Adverse radio propagation conditions affect the cell loss ratio (CLR) QoS. By its nature, a radio network cannot provide the same QoS consistently. To sustain a negotiated CLR QoS as long as possible, the DLC layer adds ARQ capability to the system. ARQ can help to retain the agreed-on cell loss rate, at the cost of an increase in delay and data overhead.

Figure 10.9 depicts an example frame. Two mobile terminals (MT) and one access point (AP) are engaged in the exchange of packets. For instruction purposes, the frame duration is shorter than typically encountered in practice. The access point initiates every frame by broadcasting a frame header (FH), containing the slot map to all associated mobile terminals. The FH has a long preamble, allowing mobile terminals to synchronize to the access point. Subsequently, the access point sends its downlink data, one packet in this example. The channel remains idle for one slot to allow the access point to turn around its radio from transmitting to receiving. Then the mobile terminals are allowed to transmit their packets. In this example each mobile terminal transmits one. After the uplink period, a contention period is scheduled, which in this example is used by both terminals. Terminal 1 is transmitting two request packets and terminal 2 is transmitting a two-slot control packet. In the example, two packets collide, resulting in the loss of the control packet and one of the request packets. The second request packet is transmitted successfully in the third slot. After the contention period, and before the next frame, an idle slot is inserted to allow the mobile terminal radios to turn around.

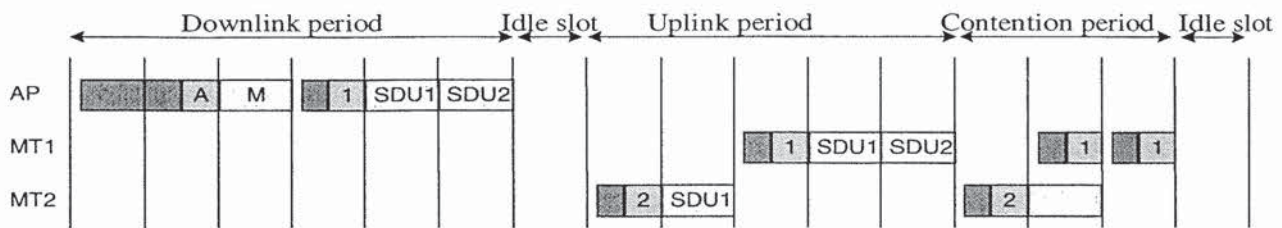


Figure 10.9 Magic WAND MAC frame.

The master scheduler, which must be able to schedule the transmissions of any mix of ATM traffic classes, employs a leaky-bucket-based scheme where the highest priority is given to constant bit-rate traffic, the second priority to variable bit rate, and so on. Tokens, which are generated at a constant rate, fill a bucket. The scheduler takes tokens from the bucket, and translates them in the allocation of slots in the slot map according to the connections' delay requirements. A traffic source can request slots (access points directly, mobile terminals use piggy-backed and contention requests) in excess of the mean rate. Depending on the negotiated burstiness of the source, which is reflected in a commensurate bucket depth, the scheduler grants the request. Effectively, the scheduler polices and shapes the traffic on the wireless link, to guarantee delay QoS compliance for all connections. See [7] for an extensive discussion of scheduling.

The second important measure of QoS, besides delay and delay jitter, is the connection's error performance over the wireless ATM link. In WAND, the radio physical layer provides a constant service that can meet typical real-time service requirements (e.g., for a voice service). TCP/IP-based data connections cannot tolerate high cell loss ( $> 10^{-2}$ ) and these are protected by ARQ. Third, there are services such as video requiring real-time service with low error probability. The solution applied in WAND is to apply ARQ with a limited number of retransmissions.

## 10.5 IEEE 802.11, HIPERLAN/2 AND MMAC WIRELESS LAN STANDARDS

Since the beginning of the nineties, wireless local area networks (WLAN) for the 900-MHz, 2.4-GHz, and 5-GHz ISM (Industrial, Scientific, & Medical) bands have been available, based on a range of proprietary techniques. In June 1997, the Institute of Electrical and Electronics Engineers (IEEE) approved an international interoperability standard [8]. The standard specifies both medium access control (MAC) procedures and three different physical layers (PHY). There are two radio-based PHYs using the 2.4-GHz band. The third PHY uses infrared light. All PHYs support a data rate of 1 Mbps and optionally 2 Mbps. The 2.4-GHz frequency band is available for license-exempt use in Europe, the United States, and Japan. Table 10.3

lists the available frequency band and the restrictions to devices which use this band for communications.

**Table 10.3**  
International 2.4-GHz ISM bands.

Location	Regulatory range	Maximum output power
North America	2.400–2.4835 GHz	1,000 mW
Europe	2.400–2.4835 GHz	100 mW (EIRP*)
Japan	2.471–2.497 GHz	10 mW

\* EIRP = effective isotropic radiated power.

User demand for higher bit rates and the international availability of the 2.4-GHz band has spurred the development of a higher speed extension to the 802.11 standard. In July 1998, a proposal was selected for standardization, which describes a PHY providing a basic rate of 11 Mbps and a fall back rate of 5.5 Mbps. This PHY can be seen as a fourth option, to be used in conjunction with the MAC that is already standardized. Practical products, however, are expected to support both the high-speed 11- and 5.5-Mbit/s rates mode as well as the 1- and 2-Mbps modes.

A second IEEE 802.11 working group has moved on to standardize yet another PHY option, which offers higher bit rates in the 5.2-GHz band. This development was motivated by the adoption, in January 1997, by the U.S. Federal Communications Commission, of an amendment to Part 15 of its rules. The amendment makes available 300 MHz of spectrum in the 5.2-GHz band, intended for use by a new category of unlicensed equipment called Unlicensed National Information Infrastructure (UNII) devices [9]. Table 10.4 lists the frequency bands and the corresponding power restrictions. Notice that the maximum permitted output power depends on the emission bandwidth; for a bandwidth of 20 MHz, you are allowed to transmit at the maximum power levels listed in the middle column of Table 10.4. For a bandwidth smaller than 20 MHz the power limit reduces to the value specified in the right column.

**Table 10.4**  
United States 5.2 GHz U-NII band.

Location	Maximum output power	
	minimum of	
5.150–5.250 GHz	50 mW	4 dBm + $10\log_{10}B^*$
5.250–5.350 GHz	250 mW	11 dBm + $10\log_{10}B$
5.725–5.825 GHz	1,000 mW	17 dBm + $10\log_{10}B$

\* B is the –26-dB emission bandwidth in MHz.

Like the IEEE 802.11 standard, the European ETSI HIPERLAN type 1 standard [10] specifies both MAC and PHY. Unlike IEEE 802.11, however, no HIPERLAN type 1 compliant products are available in the market place. A newly formed ETSI working group called Broadband Radio Access Networks (BRAN) is now working on



---

extensions to the HIPERLAN standard. Three extensions are under development: HIPERLAN/2, a wireless indoor LAN with a QoS provision; HiperLink, a wireless indoor backbone; and HiperAccess, an outdoor, fixed wireless network providing access to a wired infrastructure.

In Japan, equipment manufacturers, service providers and the Ministry of Post and Telecommunications are cooperating in the Multimedia Mobile Access Communication (MMAC) project to define new wireless standards similar to those of IEEE 802.11 and ETSI BRAN. Additionally, MMAC is also looking into the possibility for ultra-high-speed wireless indoor LANs supporting large-volume data transmission at speeds up to 156 Mbps using frequencies in the 30- to 300- GHz band.

In July 1998, the IEEE 802.11 standardization group decided to select OFDM as the basis for their new 5-GHz standard, targeting a range of data rates from 6 up to 54 Mbps [12, 13]. This new standard is the first one to use OFDM in packet-based communications, while the use of OFDM until now was limited to continuous transmission systems like DAB and DVB. Following the IEEE 802.11 decision, ETSI BRAN and MMAC also adopted OFDM for their physical layer standards. The three bodies have worked in close cooperation since then to make sure that differences among the various standards are kept to a minimum, thereby enabling the manufacturing of equipment that can be used worldwide.

The focus of this section is on the physical layer side. In the case of the IEEE 802.11 standard, the MAC layer for the higher data rates remains the same as for the currently supported 1- and 2- Mbps rates. A description of this MAC can be found in [11].

### 10.5.1 OFDM Parameters

Table 10.5 lists the main parameters of the draft OFDM standard. A key parameter that largely determined the choice of the other parameters is the guard interval of 800 ns. This guard interval provides robustness to rms delay spreads up to several hundreds of nanoseconds, depending on the coding rate and modulation used. In practice, this means that the modulation is robust enough to be used in any indoor environment, including large factory buildings. It can also be used in outdoor environments, although directional antennas may be needed in this case to reduce the delay spread to an acceptable amount and increase the range.

**Table 10.5**  
Main parameters of the OFDM standard.

Data rate	6, 9, 12, 18, 24, 36, 48, 54 Mbps
Modulation	BPSK, QPSK, 16-QAM, 64-QAM
Coding rate	1/2, 2/3, 3/4
Number of subcarriers	52
Number of pilots	4
OFDM symbol duration	4 $\mu$ s
Guard interval	800 ns
Subcarrier spacing	312.5 kHz
-3-dB Bandwidth	16.56 MHz
Channel spacing	20 MHz

To limit the relative amount of power and time spent on the guard time to 1 dB, the symbol duration chosen is 4  $\mu$ s. This also determines the subcarrier spacing at 312.5 kHz, which is the inverse of the symbol duration minus the guard time. By using 48 data subcarriers, uncoded data rates of 12 to 72 Mbps can be achieved by using variable modulation types from BPSK to 64-QAM. In addition to the 48 data subcarriers, each OFDM symbol contains an additional four pilot subcarriers, which can be used to track the residual carrier frequency offset that remains after an initial frequency correction during the training phase of the packet.

To correct for subcarriers in deep fades, forward-error correction across the subcarriers is used with variable coding rates, giving coded data rates from 6 up to 54 Mbps. Convolutional coding is used with the industry standard rate 1/2, constraint length 7 code with generator polynomials (133,171). Higher coding rates of 2/3 and 3/4 are obtained by puncturing the rate 1/2 code. The 2/3-rate is used together with 64-QAM only to obtain a data rate of 48 Mbps. The 1/2-rate is used with BPSK, QPSK, and 16-QAM to give rates of 6, 12, and 24 Mbps, respectively. Finally, the 3/4-rate is used with BPSK, QPSK, 16-QAM, and 64-QAM to give rates of 9, 18, 36, and 54 Mbps, respectively.

### 10.5.2 Channelization

Figure 10.10 shows the channelization for the lower and middle UNII bands. Eight channels are available with a channel spacing of 20 MHz and guard spacings of 30 MHz at the band edges in order to meet the stringent FCC-restricted band spectral density requirements. The FCC also defined an upper UNII band from 5.725 to 5.825 GHz, which carries another four OFDM channels. For this upper band, the guard spacing from the band edges is only 20 MHz, as the out-of-band spectral requirements for the upper band are less severe than those of the lower and middle UNII bands. In Europe, a total of 455 MHz is available in two bands, one from 5.15 to 5.35 GHz and

another from 5.470 to 5.725 GHz. In Japan, a 100 MHz wide band is available from 5.15 to 5.25 GHz, carrying four OFDM channels.

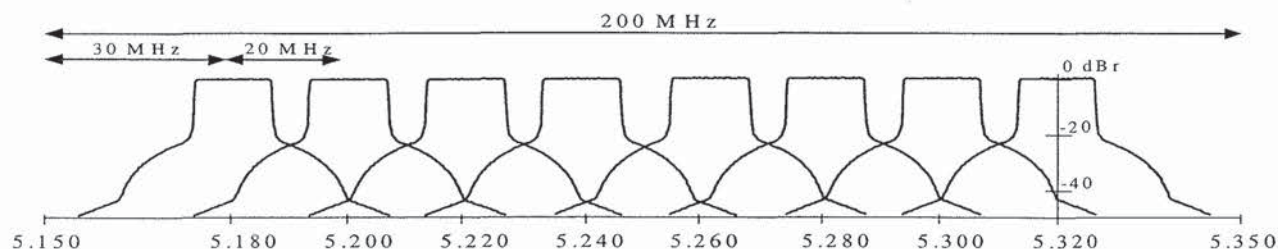


**Figure 10.10** Channelization in lower and middle UNII band.

### 10.5.3 OFDM Signal Processing

The general block diagram of the baseband processing of an OFDM transceiver is shown in Figure 10.11. In the transmitter path, binary input data is encoded by a standard rate  $1/2$  convolutional encoder. The rate may be increased to  $2/3$  or  $3/4$  by puncturing the coded output bits. After interleaving, the binary values are converted into QAM values. To facilitate coherent reception, four pilot values are added to each 48 data values, so a total of 52-QAM values is reached per OFDM symbol, which are modulated onto 52 subcarriers by applying the IFFT. To make the system robust to multipath propagation, a cyclic prefix is added. Further, windowing is applied to attain a narrower output spectrum. After this step, the digital output signals can be converted to analog signals, which are then up-converted to the 5-GHz band, amplified and transmitted through an antenna.

The OFDM receiver basically performs the reverse operations of the transmitter, together with additional training tasks. First, the receiver has to estimate frequency offset and symbol timing, using special training symbols in the preamble. Then, it can do an FFT for every symbol to recover the 52-QAM values of all subcarriers. The training symbols and pilot subcarriers are used to correct for the channel response as well as remaining phase drift. The QAM values are then demapped into binary values, after which a Viterbi decoder can decode the information bits.

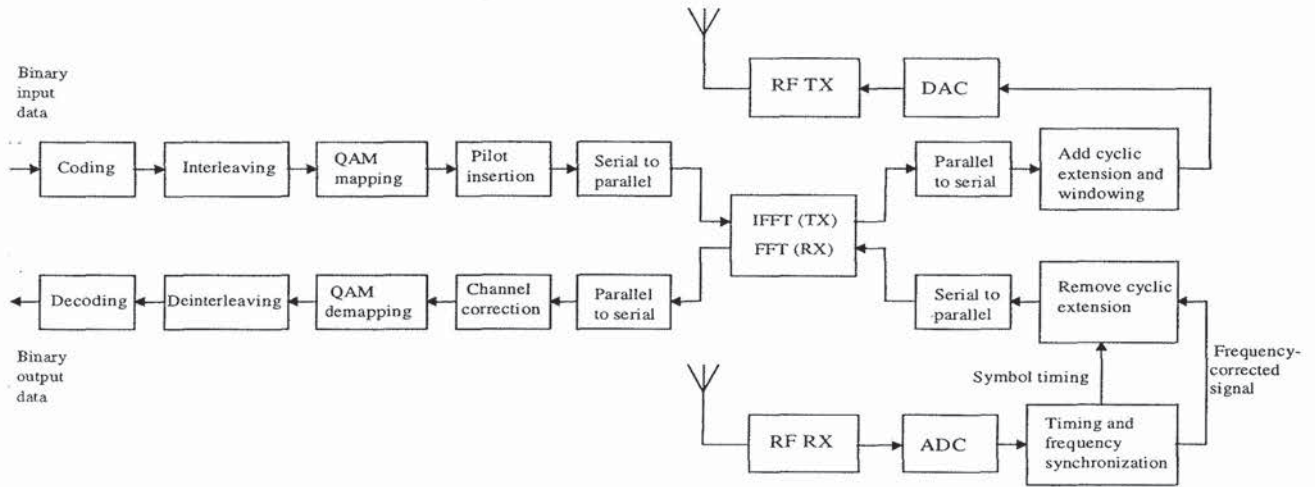


Figure 10.11 Block diagram of OFDM transceiver.

### 10.5.4 Training

Figure 10.12 shows the structure of the preamble that precedes every OFDM packet. This preamble is essential to perform start-of-packet detection, automatic gain control, symbol timing, frequency estimation, and channel estimation. All of these training tasks have to be performed before the actual data bits can be successfully decoded.

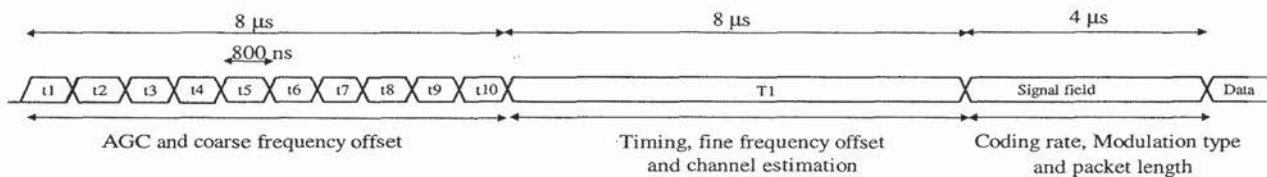


Figure 10.12 OFDM preamble.

The first part of the preamble consists of 10 repetitions of a training symbol with a duration of 800 ns each, which is only a quarter of the FFT duration of a normal data symbol. These short symbols are produced by using only nonzero subcarrier values for subcarrier numbers that are a multiple of 4. Hence, of all possible subcarrier numbers from  $-26$  to  $+26$ , only the subset  $\{-24, -20, -16, -12, -8, -4, 4, 8, 12, 16, 20, 24\}$  is used. There are two reasons for using relatively short symbols in this part of the training; first, the short symbol period makes it possible to do a coarse frequency offset estimation with a large unambiguous range. For a repetitive signal with a duration of  $T$ , the maximum measurable unambiguous frequency offset is equal to  $1/(2T)$ , as higher frequency offsets result in a phase change exceeding  $\pi$  from one symbol to another. Hence, by measuring the phase drift between two consecutive short symbols with a

duration of 800 ns, frequency offsets up to 625 kHz can be estimated. If training symbols with a duration equal to the FFT interval of 3.2  $\mu$ s were used, then the maximum frequency offset of only 156 kHz could be measured, corresponding to a relative frequency error of about 26 ppm at a carrier frequency of 5.8 GHz. The IEEE 802.11 standard specifies a maximum offset *per user* of 20 ppm, which means that the worst case offset as seen by a receiver can be up to 40 ppm, as it experiences the sum of the frequency offsets from both transmitter and receiver.

The second reason for using short symbols at the start of the training is that they provide a convenient way of performing AGC and frame detection. Detection of the presence of a packet can be done by correlating a short symbol with the next and detecting if the correlation magnitude exceeds some threshold. After each interval equal to two short symbol durations, the receiver gain can be adjusted after which detection and gain measuring can continue. Of course, this AGC algorithm could also be applied to long training symbols, but the advantage of short symbols is that we have more repetitions in the same amount of time, which makes it easier to do several measurements and gain adjustments during the training.

The short training symbols are followed by a long training symbol (T1) that contains 52 QPSK-modulated subcarriers like a normal data symbol. The length of this training symbol is twice that of a data symbol, however, which is done for two reasons. First, it makes it possible to do a precise frequency estimation on the long symbol. The long symbol is formed by cyclically extending the IFFT output signal to a length of 8  $\mu$ s. Thus, it contains two and a half times the original IFFT duration. The first 1.6  $\mu$ s serves as a guard interval, containing a copy of the last 1.6  $\mu$ s of the IFFT output. The long training symbol makes it possible to do a fine frequency offset estimation by measuring the phase drift between samples that are 3.2  $\mu$ s apart within the long training symbol. The second reason for having the long symbol is to obtain reference amplitudes and phases for doing coherent demodulation. By averaging the two identical parts of the long training symbol, coherent references can be obtained with a noise level that is 3 dB lower than the noise level of data symbols.

Both the long and short symbols are designed in such a way that the PAP ratio is approximately 3 dB, which is significantly lower than the PAP ratio of random OFDM data symbols. This guarantees the training degradation caused by nonlinear amplifier distortion to be smaller than the distortion of the data symbols. It also allows the use of a simple correlator implementation at the receiver as explained in Section 4.6.

After the preamble, there is still one training task left, which is tracking the reference phase. There will always be some remaining frequency offset that causes a common phase drift on all subcarriers. To track this phase drift, 4 of the 52 subcarriers contain known pilot values. The pilots are scrambled by a length 127 pseudonoise sequence to avoid spectral lines exceeding the average power density of the OFDM spectrum.

Figure 10.13 shows the time-frequency structure of an OFDM packet, where all known training values are marked in gray. It clearly illustrates how the packet starts with 10 short training symbols, using only 12 subcarriers, followed by the long training symbol and data symbols, with each data symbol containing four known pilot subcarriers.

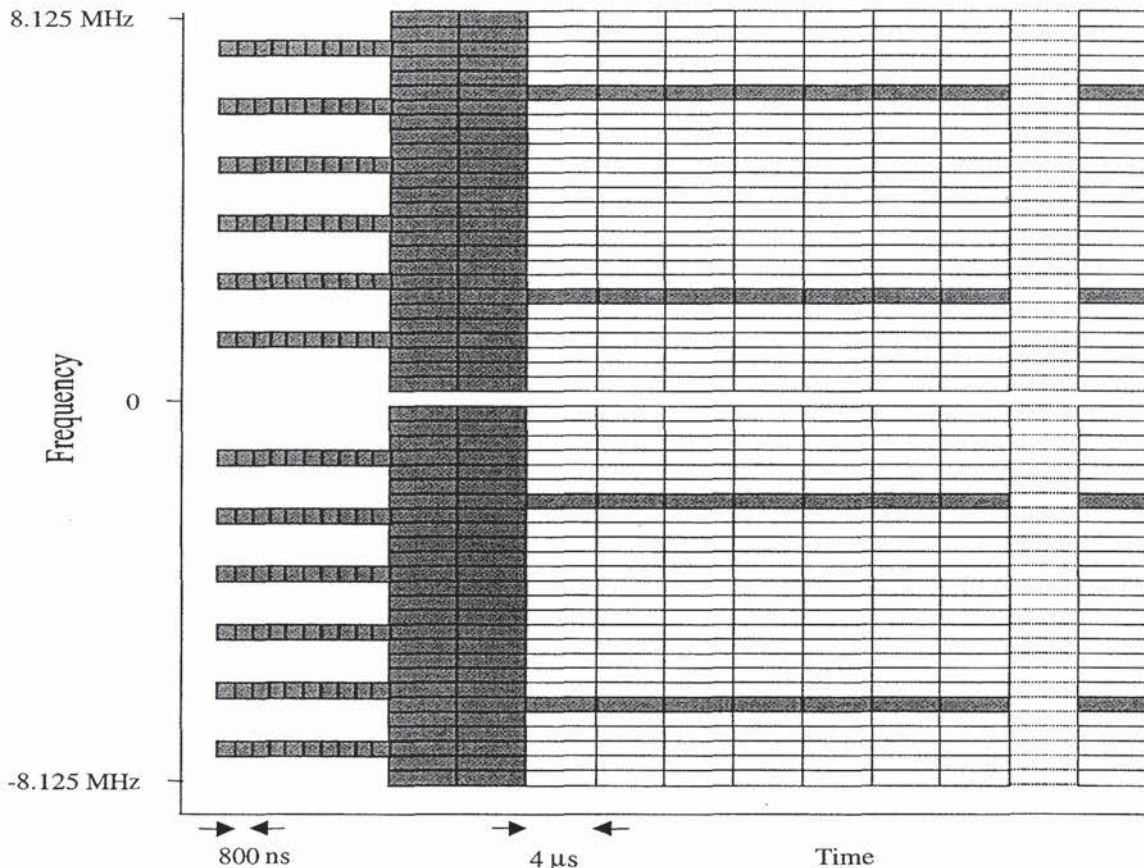


**Figure 10.13** Time-frequency structure of an OFDM packet. Gray subcarriers contain known training values.

In the case of the IEEE 802.11 standard, at the end of the preamble a special OFDM data symbol at the lowest 6-Mbps rate is sent, which contains information about the length, modulation type, and coding rate of the rest of the packet. Sending this information at the lowest possible rate ensures that the dynamic rate selection is at least as reliable as the most reliable data rate of 6 Mbps. Further, it makes it possible for all users to decode the duration of a certain packet, even though they may not be able to decode the data content. This is important for the IEEE 802.11 MAC protocol, which specifies that a user has to wait until the end of any packet already in the air before trying to compete for the channel.

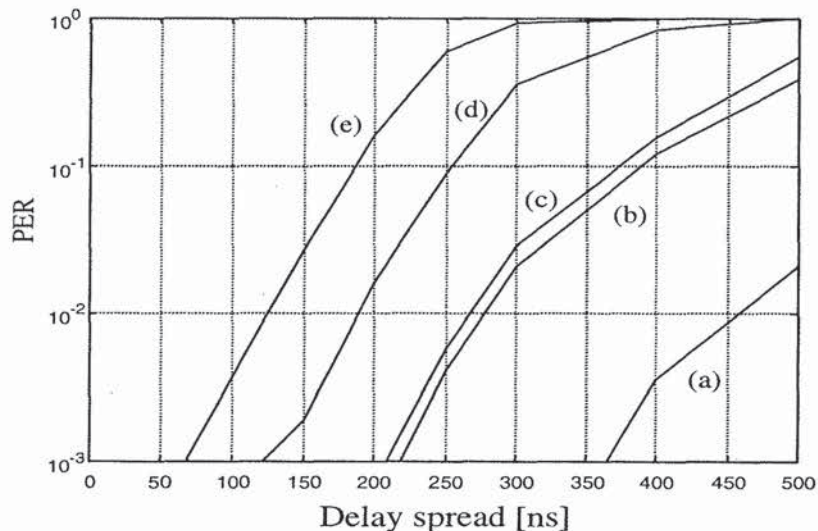
### 10.5.5 Differences Between IEEE 802.11, HIPERLAN/2 and MMAC

The main differences between IEEE 802.11 and HIPERLAN/2—which is standardized by ETSI BRAN [14]—are in the Medium Access Control (MAC). IEEE 802.11 uses a distributed MAC based on Carrier Sense Multiple Access with Collision Avoidance, (CSMA/CA), while HIPERLAN/2 uses a centralized and scheduled MAC, based on wireless ATM. MMAC supports both of these MACs. As far as the physical layer is concerned, there are a few relatively minor differences between IEEE 802.11 and HIPERLAN/2 which are summarized below:

- HIPERLAN uses different training sequences. The long training symbol is the same as for IEEE 802.11, but the preceding sequence of short training symbols is different. A downlink transmission starts with 10 short symbols as IEEE 802.11, but the first 5 symbols are different in order to detect the start of the downlink frame. The rest of the packets in the downlink frame do not use short symbols, only the long training symbol. Uplink packets may use 5 or 10 identical short symbols, with the last short symbol being inverted.
- HIPERLAN uses extra puncturing to accommodate the tail bits to keep an integer number of OFDM symbols in 54 byte packets. This extra puncturing operation punctures 12 bits out of the first 156 bits of a packet.
- In the case of 16-QAM, HIPERLAN uses a coding rate of 9/16 instead of 1/2—giving a bit rate of 27 instead of 24 Mbps—to get an integer number of OFDM symbols for packets of 54 bytes. The rate 9/16 is made by puncturing 2 out of every 18 encoded bits.
- Both IEEE 802.11 and HIPERLAN scramble the input data with a length 127 pseudo random sequence, but the initialization is different. IEEE 802.11 initializes with 7 random bits which are inserted as the first 7 bits of each packet. In HIPERLAN, the scrambler is initialized by {1, 1, 1} plus the first 4 bits of the Broadcast Channel at the beginning of a MAC frame. The initialization is identical for all packets in a MAC frame.
- HIPERLAN devices have to support power control in the range of -15 to 30 dBm with a step size of 3 dB.
- Dynamic frequency selection is mandatory in Europe over a range of at least 330 MHz for indoor products and 255 MHz (upper band only) for outdoor products. This means that indoor products have to support a frequency range from 5.15 to at least 5.6 GHz, covering the entire lower band and a part of the European upper band. Dynamic frequency selection was included to avoid the need for frequency planning and to provide coexistence with radar systems that operate in the upper part of the European 5 GHz band.

### 10.5.6 Simulation Results

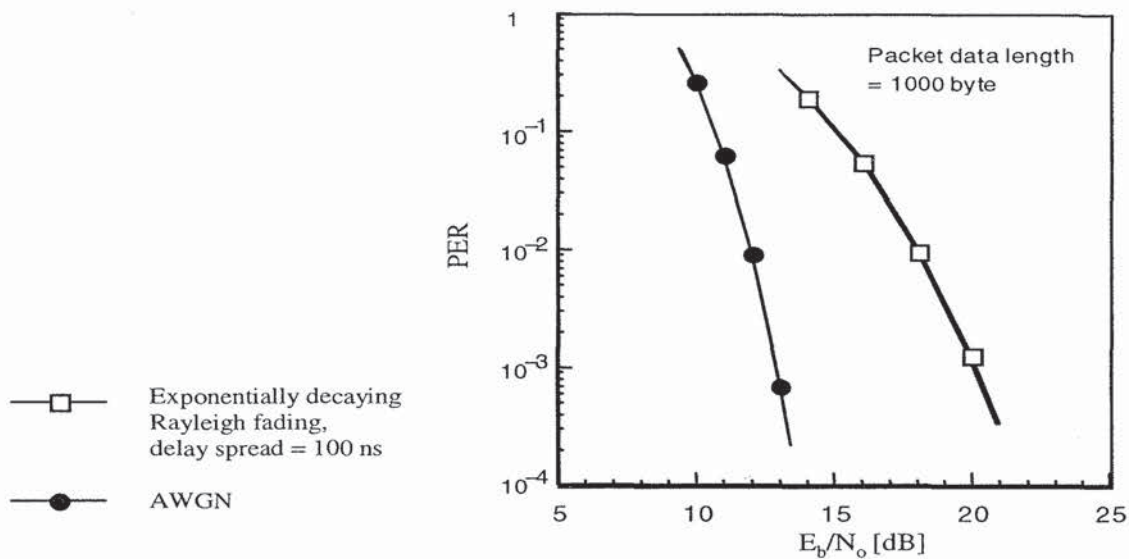
Figure 10.14 shows the irreducible PER versus delay spread for a few different data rates. This is the minimum possible PER for a certain delay spread, for which all packet errors are caused by intersymbol interference because of path delays exceeding the guard time of the OFDM symbols. Hence, Figure 10.14 demonstrates the delay spread robustness for several data rates. For a 1% PER, the tolerable delay spread is close to 200 ns at 36 Mbps, while at 12 Mbps a delay spread of 450 ns can be tolerated. In practice, this means that the 36-Mbps rate can be used in most indoor environments, except some large factory buildings. The 54 Mbps rate can tolerate delay spreads up to about 120 ns, which is sufficient for most office buildings. The 12-Mbps rate can work in any indoor and even in outdoor environments. This is also true for the lowest rate of 6 Mbps, that is not included in Figure 10.14.



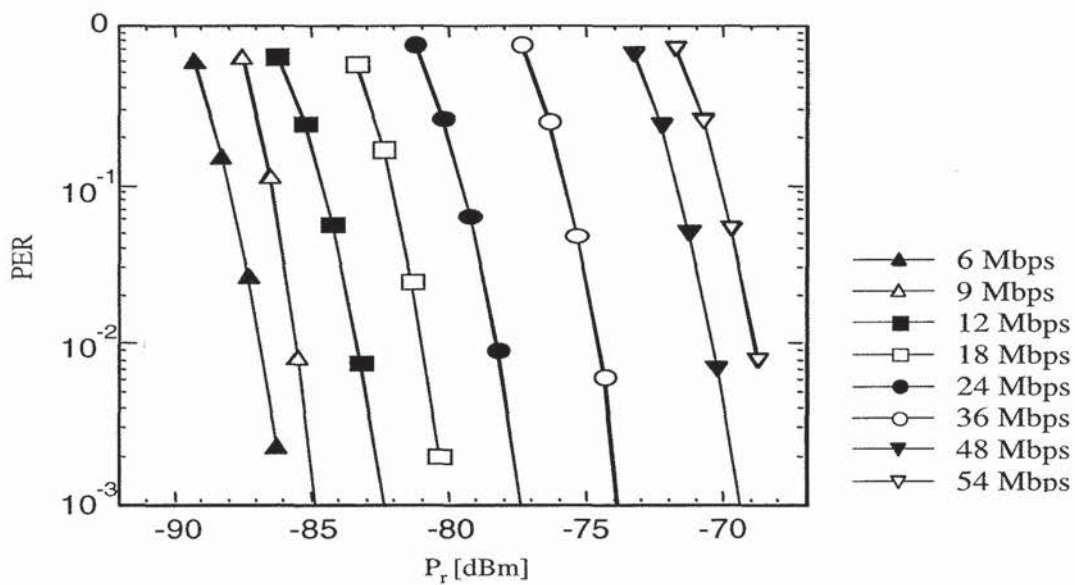
**Figure 10.14** PER versus rms delay spread (no noise) for Rayleigh fading paths with an exponentially decaying power delay profile. Packet size is 64 bytes with data rates of (a) 12, (b) 18, (c) 24, (d) 36, and (e) 54 Mbps.

Figure 10.15 shows the PER versus  $E_b/N_o$  for a data rate of 24 Mbps in case of an AWGN channel and a Rayleigh fading channel with a delay spread of 100 ns. An  $E_b/N_o$  of about 18 dB is required to achieve a 1% PER in the fading channel, which is approximately 6 dB more than what is needed for an ideal Gaussian noise channel. Of course, other data rates have different requirements. Figure 10.16 shows the PER for various data rates as a function of the input power. We can see a difference of almost 18 dB in the signal power requirements of the lowest and highest data rates. This illustrates the importance of fallback rates; users who cannot use the highest rate because they are too far away or are in a bad multipath situation can at least obtain a data link at a lower rate.





**Figure 10.15** PER versus mean  $E_b/N_0$  for AWGN and Rayleigh fading with a 100-ns delay spread and a bit rate of 24 Mbps.



**Figure 10.16** PER versus received power level for AWGN and various bit rates.

Figure 10.17 shows simulated spectra of an OFDM signal that is distorted by a nonlinear power amplifier with different backoff values. This is an important subject, because the susceptibility to nonlinear distortion and the need for large backoff values is often mentioned as a disadvantage of OFDM. As shown in [15], however, the effects of nonlinear distortion on the BER are negligible for backoff values of 6 dB or more, where the backoff is defined as the difference between the maximum (saturation) output power and the average output power in dB. The effects on the transmitted spectrum are illustrated in Figure 10.17. We can see that for a 7-dB backoff, the spectrum falls down very steeply after about 8 MHz, and only around 25 dB below the in-band density the spectrum starts to deviate significantly from an ideal undistorted OFDM signal. When the backoff is decreased to 5 dB, the out-of-band spectrum quickly grows toward the outer spectrum mask defined by IEEE 802.11.

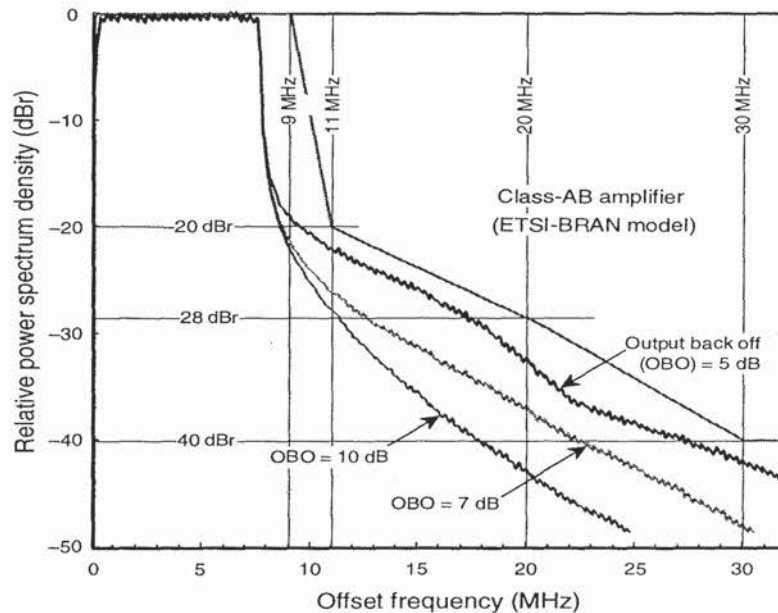


**Figure 10.17** OFDM spectrum after a nonlinear power amplifier.

## REFERENCES

- [1] ETSI, "Radio Broadcasting Systems: Digital Audio Broadcasting to Mobile, Portable and Fixed Receivers," European Telecommunication Standard, ETS 300-401, Feb. 1995.
- [2] Tuttlebee, W. H. W., and D. A. Hawkins, "Consumer Digital Radio: From Concept to Reality," *Electronics and Communication Engineering Journal*, Vol. 10, No. 6, pp. 263–276, Dec. 1998.

- 
- [3] ETSI, "Digital Video Broadcasting: Framing Structure, Channel Coding, and Modulation for Digital Terrestrial Television," European Telecommunication Standard, EN 300-744, Aug. 1997.
  - [4] Reimers, U., "DVB-T: The COFDM-Based System for Terrestrial Television," *Electronics and Communication Engineering Journal*, Vol. 9, No. 1, pp. 28-32, Feb. 1997.
  - [5] Mikkonen, J., J. P. Aldis, G. A. Awater, A. Lunn, and D. Hutchinson, "The Magic WAND—Functional Overview," *IEEE JSAC*, Vol. 16, No. 6, pp. 953-972, Aug. 1998.
  - [6] Awater, G. A., and J. Ala-Laurila, "Wireless ATM Network Demonstrator," Presentation and Demonstration, *Demo '98 conference*, Berlin, Germany, Oct. 15, 1998.
  - [7] Passas, N., S. Paskalis, D. Vali, L. Merakis, "Quality-of-Service-Oriented Medium Access Control for Wireless ATM Networks," *IEEE Communications Magazine*, Vol. 35, No. 11, Nov. 1997.
  - [8] IEEE. 802.11, IEEE Standard for Wireless LAN Medium Access Control (MAC) and Physical Layer (PHY) specifications, Nov. 1997.
  - [9] FCC, "Amendment of the Commission's Rules to Provide for Operation of Unlicensed NII Devices in the 5-GHz Frequency Range," Memorandum Opinion and Order, ET Docket No. 96-102, June 24, 1998.
  - [10] ETSI, "Radio Equipment and Systems, High Performance Radio Local Area Network (HIPERLAN) Type 1," European Telecommunication Standard, ETS 300-652, Oct. 1996.
  - [11] Crow, B. P., I. Widjada, J. G. Kim, and P. T. Sakai, "IEEE 802.11 Wireless Local Area Networks," *IEEE Communications Magazine*, pp. 116-126, Sept. 1997.
  - [12] Takanashi, H., and R. van Nee, "Merged Physical Layer Specification for the 5-GHz Band," IEEE P802.11-98/72-r1, Mar. 1998.
  - [13] IEEE, "Supplement to Standard for Telecommunications and Information Exchange Between Systems—LAN/MAN Specific Requirements—Part 11: Wireless MAC and PHY Specifications: High Speed Physical Layer in the 5-GHz Band," P802.11a/D7.0, July 1999.
  - [14] ETSI, "Broadband Radio Access Networks (BRAN); HIPERLAN Type 2 Technical Specification Part 1—Physical Layer," DTS/BRAN030003-1, Oct. 1999.
  - [15] Nee, R. van, "OFDM for High Speed Wireless Networks," IEEE P 802.11-97/123, Nov. 1997.



## About the Authors

**Richard D. J. van Nee** was born in Schoonoord, the Netherlands, on January 17, 1967. He received an M.Sc. degree (cum laude) from Twente University of Technology, Enschede, the Netherlands, and a Ph.D. degree (cum laude) from Delft University of Technology, Delft, The Netherlands, in 1990 and 1995, respectively.

From December 1994, he worked as a private consultant to NovAtel Communications, Calgary, working on the design of multipath-robust GPS receivers, which were used in the reference stations of the United States Wide Area Augmentation System. In March 1995, he joined AT&T—now Lucent Technologies—Bell Labs in Utrecht, The Netherlands, where he is working in the area of high speed wireless communications. He was involved in the design of the OFDM modems for the European Magic WAND project. Together with NTT, he made the original OFDM-based proposal which lead to the IEEE 802.11 wireless LAN high-rate extension for the 5 GHz band. He was also one of the original proposers of the 11 Mbps IEEE 802.11 extension for the 2.4 GHz band. He holds several patents and published over 40 papers in the area of spread-spectrum tracking systems and OFDM.

**Ramjee Prasad** was born in Babhaur (Gaya), Bihar, India, on July 1, 1946. He is now a Dutch Citizen. He received a B.Sc. (Eng) degree from Bihar Institute of Technology, Sindri, India and M.Sc. (Eng) and Ph. D. degrees from Birla Institute of Technology (BIT), Ranchi, India, in 1968, 1970 and 1979, respectively.

He joined BIT as a Senior Research Fellow in 1970 and became associate professor in 1980. While he was with BIT, he supervised a number of research projects in the areas of microwave communications and plasma engineering. During 1983 to 1988, he was with the University of Dar es Salaam (UDSM), Tanzania, where he rose to the level of professor of telecommunications at the Department of Electrical Engineering in 1986. At UDSM, he was responsible for the collaborative project “Satellite Communications for Rural Zones” with Eindhoven University of Technology, The Netherlands. From February 1988 to June 1999, he was with the Telecommunications and Traffic-Control Systems Group, Delft University of Technology (DUT), The Netherlands, where he was actively involved in the area of wireless personal and multimedia communications (WPMC). He was the Head of